Dynamics of a Space Elevator

Stephen S. Cohen

Department of Mechanical Engineering

McGill University, Montreal

August 2006

A thesis submitted to the Faculty of Graduate Studies and Research in partial fulfillment of the requirements of the degree of Master of Engineering

Your file Votre référence
ISBN: 978-0-494-32581-0
Our file Notre référence
ISBN: 978-0-494-32581-0

Acknowledgements

I would like to thank Professor Misra for supervising my thesis, and for having suggested such an interesting topic to study. His knowledge of mechanical engineering in general and dynamics in particular has been very helpful. In addition to supervising this thesis, he also helped to make me a much more able engineer and researcher.

Thank you to the Fonds Québécois de Recherche en Nature et Technologies (FQRNT) for funding this work.

I would also like to thank all of the members of Lab B23 for their company and help over the past two years. In particular, thank you to Brian Wong, who took time to brainstorm and generate ideas about my project, without asking for anything in return.

Finally, thank you to my family for their support throughout my education. Also, thanks to my loving wife Valerie. She may be the only Medical Doctor in the world who, through no choice of her own, is now able to explain the complex nature of space elevator dynamics.

Abstract

The space elevator offers an alternate and very efficient method for space travel. It will have two main components. The first component is the tether (or the ribbon), which extends from the Earth to an equatorial satellite at an altitude of about 100,000 kilometres, and is fixed to a base on the surface of the Earth at its lower end. The second component is the climber, which scales the ribbon, transporting payloads to space. An important issue for effective operation of the space elevator will be to understand its dynamics. This thesis attempts to develop a realistic and yet simple planar model for this. Both rigid and elastic ribbon models are considered. Their response to ascending climbers and to aerodynamic loads is studied. Specific climbing procedures are devised based on these results. The effect of the space elevator's motion on the orbit of a launched satellite is also examined.

Resumé

L'ascenseur spatial offre une option différente et très efficace pour le voyage dans l'espace. Il consiste en deux composantes principales. La première composante est le câble (ou ruban), qui s'étend de la Terre à un satellite équatorial à une altitude d'environ 100,000 kilomètres, et est fixée à une base terrestre à son extrémité inférieure. La deuxième composante est le grimpeur, qui monte le ruban, transportant des charges utiles dans l'espace. Un aspect important pour le fonctionnement efficace de l'ascenseur spatial dépend sur la compréhension de sa dynamique. Cette thèse tente de développer un modèle planaire simple, mais réaliste, pour étudier ce système. Des modèles de ruban rigide et de ruban élastique sont considérés et leurs réponses aux grimpeurs montants et aux charges aérodynamiques sont étudiées. En se basant sur ces résultats, des procédures spécifiques pour l'escalade de la corde sont conçues. L'effet du mouvement de l'ascenseur spatial sur l'orbite d'un satellite lancé est également examiné.

Table of Contents

Table of Symbols

A	Cross-sectional area of ribbon
$A_i(t)$	Non-dimensional generalized coordinates associated with assumed longitudinal modes
A_m	Maximum cross-sectional area of ribbon
$B_i(t)$	Non-dimensional generalized coordinates associated with sinusoidal lateral motion
$C(t)$	Generalized coordinate associated with V_a
C_D	Coefficient of aerodynamic drag
C_{SE}	Cost per unit kg of payload lifted to the geosynchronous altitude using the space elevator
C_b	Non-dimensional damping constant for base
C_e	Cost per MJ of electricity
D_b	Non-dimensional position of base
D_e	Non-dimensional position of elevator along reference line
$\bar{D}_e$	Non-dimensional position of elevator along reference line with respect to radius of the Earth
D_i	Non-dimensional initial position of climber
D_f	Non-dimensional final position of climber
E	Modulus of elasticity of ribbon material
$F(r)$	Taper function in terms of radius from Earth
$F(s)$	Taper function in terms of position along ribbon
$F(\xi)$	Taper function in terms of non-dimensional position along ribbon
F_D	Aerodynamic drag force
F_h	Component of aerodynamic force acting in local horizontal direction
F_L	Aerodynamic lift force
F_T	Thrust of motor acting on elevator
F_v	Component of aerodynamic force acting in local vertical direction
K	Kinetic energy expression
K_b	Non-dimensional spring constant for base
K_t	Non-dimensional torsional spring constant for ribbon

L	Nominally stretched length of ribbon
L_0	Nominal length of ribbon
M	Number of assumed sinusoidal modes for lateral motion
M_b	Non-dimensional mass of base
M_c	Non-dimensional mass of counterweight (ballast)
M_e	Non-dimensional mass of elevator (climber)
$\bar{M}_e$	Mass ratio (twice the climber mass to the rotational inertia of the space elevator)
M_p	Non-dimensional measure of mass of tether (ribbon)
$\bar{M}_p$	Mass ratio (payload to climber including payload)
N	Number of assumed modes for longitudinal extension
P	Potential energy expression
Q_i	Generalized Forces
R	Radius of the Earth
R_L	Length ratio (Earth radius to nominal ribbon length)
R_G	Synchronous orbit radius of the Earth
T	Tension in ribbon
T_R	Climber time ratio (acceleration to cruise)
U	Non-dimensional longitudinal extension of tether along reference line
V	Non-dimensional lateral extension of tether along reference line
V_a	Non-dimensional basis function for lateral displacement associated with aerodynamic loading
V_c	Non-dimensional cruise velocity of climber
W	Non-dimensional natural frequency of libration angle
W_T	Work done by the applied thrust of climber's motor
a	Semi-major axis of orbit
$a_i(t)$	Generalized coordinates associated with assumed longitudinal modes
b_{eff}	Effective width of ribbon
$b_i(t)$	Generalized coordinates associated with lateral motion
c_b	Damping constant for base
$c(t)$	Generalized coordinate associated with v_a
d_b	Position of base

d_e	Position of elevator along reference line
d_f	Final position of climber
d_0	Nominal position on ribbon at time of launch
e	Eccentricity of orbit
$\boldsymbol{e_v}$, $\boldsymbol{e_h}$	Unit vectors coinciding with local vertical and horizontal
g_0	Surface gravity of the Earth
h	Base displacement parameter
$\bar{h}$	Characteristic height of ribbon
h_L	Length ratio (Base displacement parameter to nominal ribbon length)
$\boldsymbol{i}, \boldsymbol{j}$	Unit vectors rotating with reference line
k_b	Spring constant for base
k_t	Torsional spring constant for ribbon
m_b	Mass of base
m_c	Mass of counterweight (ballast)
m_e	Mass of elevator (climber)
m_t	Mass of tether (ribbon)
m_{tot}	Total mass of system
p	Number of climbers for a given simulation
q	Dynamic pressure
q_i	Generalized coordinates
$\mathbf{r_B}$	Position vector of base
$\mathbf{r_C}$	Position vector of counterweight (ballast)
$\mathbf{r_E}$	Position vector of elevator (climber)
$\mathbf{r_T}(s)$	Position vector of point on tether (ribbon)
r_0	Radial position of climber at time of launch
s	Position on ribbon
t	Time
u	Longitudinal extension of tether along reference line
v	Lateral extension of tether along reference line
v_a	Basis function for lateral displacement associated with aerodynamic loading
$\mathbf{v_B}$	Velocity vector of base

$\mathbf{v_C}$	Velocity vector of counterweight (ballast)
$\mathbf{v_E}$	Velocity vector of elevator (climber)
$\mathbf{v_T}(s)$	Velocity vector of point on tether (ribbon)
v_w	Magnitude of wind velocity
v_0	Velocity of climber at time of launch
Ω	Spin rate of the Earth
$\bar{\Omega}_a$	Natural frequency ratio (axial frequency of ribbon to rotation of the Earth)
α	Angle between local vertical and reference line (libration angle)
α_{res}	Residual libration angle
β_0	Flight path angle of climber at time of launch
γ	Bulk density of ribbon material
ε_0	Nominal strain in ribbon
η	Overall efficiency of the space elevator's energy conversion process
λ	Natural frequency ratio (circular orbit with $r = R$ to spin rate of the Earth)
μ	Gravitational constant of the Earth
ν	Maximum allowable percent increase in ribbon stress due to climber
ξ	Non-dimensional position on ribbon
ρ_{air}	Air density
ρ_m	Maximum lineal density of ribbon
σ_0	Nominal stress in unoccupied ribbon
τ	Non-dimensional time
ϕ	Angle from unit normal of ribbon to relative velocity of air
ψ	Phase shift associated with rotational oscillation

Table of Figures

Chapter 1: Introduction

1.1 Motivation for a Space Elevator

In the 1950s, when the challenge of exploring space was taken on, the only method that current technology could provide was the use of rockets. However, this method of space travel is very inefficient. Since the method of propulsion uses fuel, this fuel must travel with the rocket. In order to escape the pull of the Earth, more than ninety percent of a rocket's original mass must consist of fuel. Another loss of efficiency occurs in the energy conversion process itself. The rocket must travel at several kilometres per second in order to escape the pull of the Earth, and engines operate very inefficiently at such high velocities. Finally, traveling at such high velocities within the atmosphere causes large drag forces, and high rates of heat transfer must be imposed upon the rocket.

As the number of satellite launches increases, the implementation of an alternative, more efficient method of space travel becomes very desirable. One alternative method to escape the pull of the Earth that has been proposed is the use of a 'canon-like' launch providing a single, very substantial impulse. However, the successor to rockets as the main method of space travel employed by man will most likely be the space elevator. The space elevator provides a much more elegant avenue to space than do rockets. The climber ascending the ribbon carries no excess mass, is powered by an electric motor, and can ascend (or descend) the ribbon however slowly it desires. By not having any of the aforementioned constraints of rockets, missions using the space elevator would cost around one hundredth of those using rockets. Its usefulness extends beyond transporting payloads efficiently to various positions along the ribbon. The space elevator could be used to retrieve disabled satellites from past missions that are currently cluttering the space surrounding the Earth. A conceptual drawing of the space elevator is shown in Figure 1.1. The principal parameters of the space elevator are displayed in Figure 1.2.

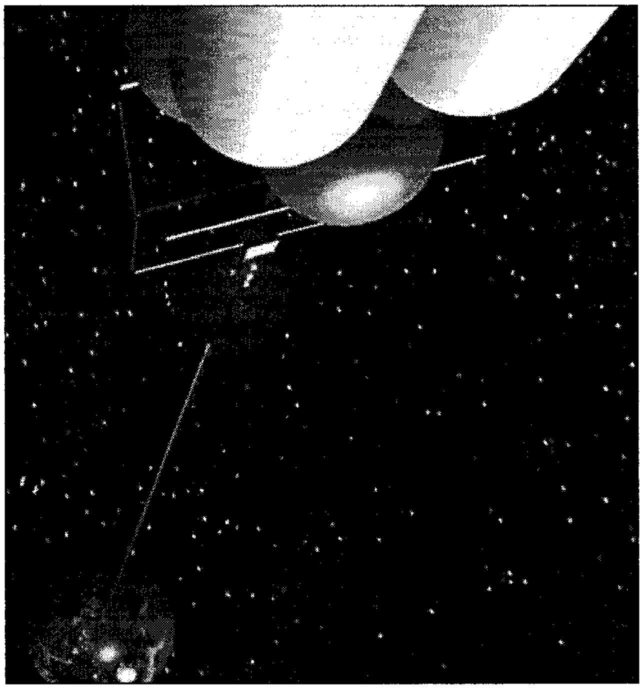

Figure 1.1: The space elevator (http://www.isr.us/SEGallery.asp?m=6)

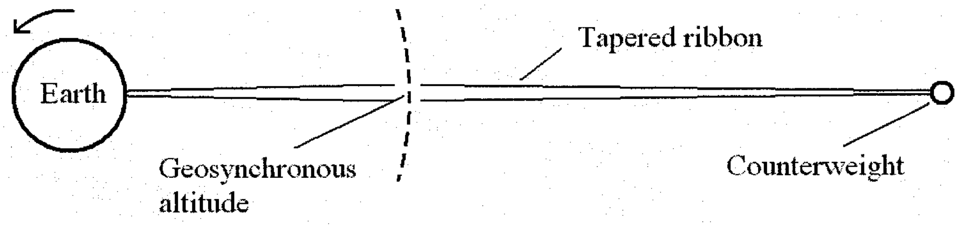

Figure 1.2: Schematic diagram of the space elevator in the equatorial plane

1.2 History of the Space Elevator

The concept of the space elevator originated in the late nineteenth century. Konstantin Tsiolkovsky was the first to document it (1895). The first modern ideas of the space elevator came from Yuri Artsutanov (1960). However, not much attention was paid to the subject until Jerome Pearson (1975) published his paper about the 'orbital tower'. Nearly all papers about the space elevator written since 1975 refer to Pearson's paper. It also inspired engineer and author, Arthur C. Clarke, to write "Fountains of Paradise" (1978); this novel about space elevators introduced the futuristic concept to the general population. Clarke (1979) also published a paper summarizing the work that had been done on the subject until then.

Still, it was made clear in Pearson's paper that for the space elevator to ever become a reality, the use of a material having a much higher strength to density ratio than that of steel would be necessary. So, although Pearson laid the foundation for the properties of a space elevator, there was little continuation of this research for many years, until Sumio Iijima (1991) discovered a new material composed of hexagonal arrays of carbon atoms. The material is known as carbon nanotube. The discovery of carbon nanotubes, which might be a suitable material for the space elevator, has increased the likelihood that a space elevator will be constructed in the foreseeable future, and has thus prompted much more research in this area. Brad Edwards (2000) performed an overall analysis of the space elevator and proposed a detailed design and a method of deployment. He concluded that the space elevator's construction and operation required no new technology, only progression in our ability to synthesize carbon nanotubes. So, although there are still many challenges facing the implementation of a space elevator, the major challenge is to develop a carbon nanotube lattice, having a sufficient material strength to density ratio, with which to construct the ribbon. With the progression of this technology, studying other aspects of the space elevator, such as its dynamics, becomes appropriate.

1.3 Review of Literature on the Space Elevator

1.3.1 Review of Literature on General Concepts of the Space Elevator

In a paper by Pearson (1975), many useful properties of the space elevator were derived. Pearson showed that the 'orbital tower' would not buckle because it would be built under tension and would remain so. In fact, the counteracting gravitational and centripetal loads would cause a great deal of tension to manifest within the ribbon. Pearson derived the taper function for the cross-sectional area of the ribbon that would minimize its maximum stress by making it constant throughout. The taper was found to depend on only one parameter, which he referred to as the characteristic height, which is proportional to the nominal strength to density ratio of the ribbon. The maximum cross-sectional area of the ribbon would be located at the geosynchronous altitude, and the minimum, at the surface of the Earth. The taper ratio, which is the quotient of these two values, is a function of the characteristic height of the ribbon material. The taper ratio was used as a design parameter throughout the paper. Pearson showed that for the taper ratio to be in a reasonable range, the characteristic height of the material used to construct the ribbon would have to be thousands of kilometres. Steel has a value of about 50 km; a steel ribbon would require the impossibly high taper ratio of exp(99) to have constant stress throughout it.

Pearson examined the longitudinal modes of the ribbon excited by the tidal forces of the Moon. He noted that for a taper ratio as small as three, the first longitudinal mode of the ribbon would have the same vibration period as that of the Moon (12.5 hours). He concluded that for this reason, such a low taper ratio should not be used. He also speculated that such a taper ratio was not feasible due to the high characteristic height it would require. Pearson also examined the transverse modes excited by climbers traversing the ribbon at a constant cruise speed. He found that for any taper ratio, no transverse modes would resonate due to the motion of a climber as long as its cruise velocity was less than 1 km/s.

Finally, Pearson showed that the deployment of the space elevator would be very difficult due to the immense volume of material that would need to be transported to geostationary orbit. The total transport effort would require thousands of separate rocket-powered trips. In the analysis, Pearson assumed that the deployed ribbon would not be altered over time, and thus needed to be reasonably thick to enable it to support the additional weight of reasonably large climbers.

About twenty-five years after the publication of Pearson's paper, Edwards (2000) published the next significant work on the space elevator. This paper examined many aspects of the space elevator's design and deployment in a much more detailed sense than had ever been done before. It was an in-depth feasibility analysis of the space elevator. Problems facing the space elevator such as environmental hazards and rupture due to space debris were dealt with. The overall conclusion was that none of these secondary problems were unsolvable using current or near-future technology. The primary problem was still, of course, the development of a material suitable for the ribbon.

The most important point in this paper was made in discussing the deployment of the space elevator. Edwards explained that the initial ribbon could be very thin, requiring just one single rocket for transport of the original ribbon mass. Then, lightweight climbers could gradually thicken this ribbon proportionally over time. This method of construction tackled the issue of deployment raised by Pearson, where *thousands* of rockets would be required to transport material to space. Instead, the space elevator is 'used' hundreds of times for its own construction. The fact that the space elevator could only be constructed feasibly using *itself* as a means of transporting mass into space illustrates why it would be such a useful tool. It should be mentioned that Artsutanov (1960) proposed this solution in his paper about forty years earlier. Pearson (1975) did not know of this solution when he wrote his paper, perhaps because it was published in Russia.

Edwards followed up this paper with a book (2002), which elaborates on all of the elements discussed in the paper. The book also discusses the space elevator's possible construction schedule, deployment costs and ability to generate profits. Finally, it describes the various impacts the space elevator would have on society.

1.3.2 Literature Review of Space Elevator Dynamics

Only a few dynamical studies of the space elevator exist. McInnes (2005) obtained analytical results for the simplest case of a space elevator: a climber traversing a stationary ribbon. The resulting non-linear equation of motion describing this scenario was reduced to a first order equation. It was clear that this simple model had one equilibrium position. The position, which was unstable, occurred at the geosynchronous altitude. Also, a phase plane diagram was obtained. The effect of friction between the climber and the ribbon was also examined.

Patamia (2005a, 2005b) developed an analytical model for studying the lateral displacement of the tether. With some approximation, he obtained the mode shapes of its lateral displacement. The mode shapes were sinusoidal in nature. Patamia used this model to determine how these transverse modes would be excited by solar radiation pressure (2005a) and magnetospheric forces (2005b). He determined that such forces could cause the tether to deviate by tens of kilometres. While this is small compared to the length of the tether, deviations of this order would further complicate the task of removing the tether from the path of orbital debris using the mobile base.

Lang (2005a, 2005b) used tether simulation software to obtain numerical results for the motion and internal stress of the ribbon in response to ascending climbers in the first paper, and aerodynamic loads in the second. The space elevator model he used differs from the conventional model where the climber has a motor that propels it along the ribbon. In Lang's model, the climbers are fixed to the ribbon, which functions like a conveyer belt. Though the mechanism used to move the climbers is different, the system behaves much like the conventional model (which is considered in this thesis), and thus, some of the results obtained in this thesis may be compared to those found in his work.

In the first of Lang's papers (2005a), which studied the response of the system to ascending climbers, the main conclusion was that the principal operational effect of a climber transit was due to the Coriolis force. The Coriolis effect caused the ribbon to rotate in the direction opposite to that of the spin of the Earth. This angle of rotation was referred to as the libration angle. In general, higher climber cruise velocities resulted in greater libration angles. Upon climber arrest, the ribbon oscillated about its final libration angle. Lang proposed that with proper speed modulation, a climber might be able to induce no residual libration angle when ascending from point A to B. He also found that longitudinal string modes of the ribbon were easily excited by climber acceleration and deceleration. Finally, he showed that sudden climber arrest could cause enough stress to rupture the ribbon, and concluded that the possibility of such an event must be eliminated.

In Lang's second paper (2005b), which studied the response of the system to aerodynamic loading, he showed that the ribbon was not very resistant to being driven out horizontally. Doubling the effective aerodynamic width exposed to winds resulted in the more than tripling of the lateral deflection of the ribbon. More disturbingly, doubling the wind velocity caused the lateral deflection of the ribbon to increase one hundredfold. Another important result was that when a climber was stationed at a low-Earth orbit, the effect of aerodynamics was amplified twenty five times from that of the unoccupied tether case. He concluded that the degree to which the system was susceptible to horizontal displacement was dependant upon the presence and location of a climber. A final conclusion was that a strong wind could potentially create near horizontal ribbon departure angles at the base. It was recommended that the space elevator be anchored in a location where very strong winds do not typically occur.

1.4 Objectives of the Thesis

There are three primary objectives of this thesis. The first objective is to understand the basic dynamic behaviour of the space elevator. This entails finding the equations of motion for the system, developing accurate closed form solutions to its response to climber transit and verifying these solutions using numerical tools. This is carried out first by ignoring the structural deformation of the ribbon, and then it is repeated with its inclusion. The space elevator's response to aerodynamic loading is to be analyzed in a similar fashion.

The second objective is to develop climber motion guidelines to minimize the deviation of the space elevator from its nominal state. This is accomplished through analysis of the closed form solutions.

The third objective is to examine the dynamics associated with satellite placement via the space elevator. This is realized by analyzing the launch from both a static ribbon and a dynamic one.

1.5 Outline of the Thesis

Throughout the thesis, only the planar motion of the space elevator is considered. In Chapter 2, the fundamentals of the mechanics associated with the space elevator are introduced. Key space elevator properties are derived in terms of the design parameters, and some of its basic dynamic properties are outlined. In Chapter 3, equations of motion are developed for the space elevator model where the ribbon is assumed to be rigid, and the base is given the freedom to translate. In Chapter 4, the basic dynamic behaviour of the space elevator is explored through simplification of the equations. From these analytical results, climbing procedures to avoid inducing oscillatory libration angles and to eliminate residual ones are proposed. The accuracy of the closed form solutions is determined through comparison with the results obtained numerically. Also, order of magnitude effects of aerodynamic forces are obtained. For the space elevator model considered in Chapter 5, the ribbon is assumed to be elastic, undergoing longitudinal and lateral deformations. Here, to simplify the analysis, the small movement of the base is ignored. Analytical and numerical results are obtained for this depiction of the space elevator, which is a more accurate one than that considered in Chapter 3. Chapter 6 deals with launch dynamics, and the effect that the space elevator's motion will have on the orbit of launched satellites. Finally, Chapter 7 contains a summary of the findings of the thesis, and suggestions for future work in this area.

Chapter 2: Fundamentals of the Space Elevator

2.1 Fundamentals of Space Elevator Design

2.1.1 The Ribbon

The main component of the space elevator is a very long tether. The cross-section of the tether will be rectangular, with one dimension much greater than the other (Edwards, 2000). For this reason, the tether is referred to as the *ribbon*. This particular choice of cross-section will be used to facilitate climbing and to avoid complete rupture when inevitable collisions with small space debris occur. This ribbon is attached to the base on the Earth. The base, located on the equator, may sit on land or water. It is likely that the base will be placed in an ocean, and will resemble an anchored oil tanker. One reason for this is that a mobile base would offer a means of control for the space elevator. For example, translation of the base could be used to remove the ribbon from the path of satellites or large space debris detected via radar.

The first criterion that the space elevator must satisfy is that its net load in the vertical direction should be zero without the presence of a climber (unoccupied state). As shown by Pearson (1975), this may be accomplished by using a nominally stretched ribbon length L, of about 144,000 km. It would be self-balanced. The ribbon is nominally stretched because, in its unoccupied state, the ribbon experiences a nominal strain due to gravitational and centripetal forces acting in opposite directions. The value of L is found by forcing the net load on the ribbon to be equal to zero. The net load on the ribbon is the integral of the two loads acting on it. The gravitational force per unit mass acting on a ribbon element in the vertical direction is given by $-\mu/r^2$, where μ is the gravitational constant of the Earth, and r is its radial position. The centripetal force per unit mass acting on the ribbon element in the vertical direction is given by $\Omega^2 r$, where Ω is the spin rate of the Earth. Figure 2.1 shows how these and the net force per unit mass vary with radial position.

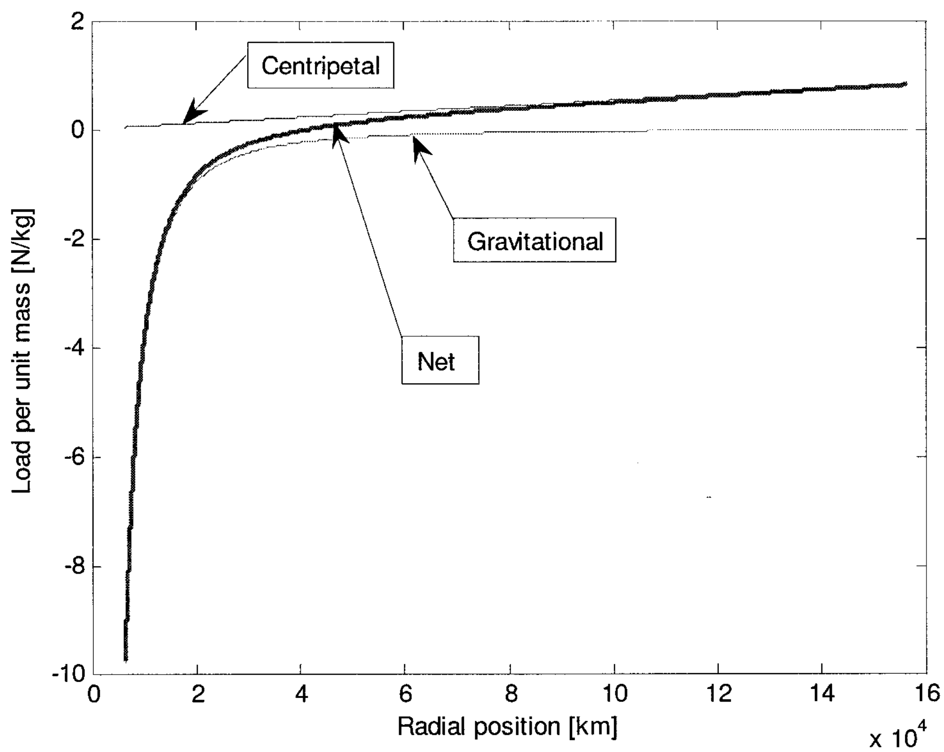

Figure 2.1: Centripetal, gravitational and net load per unit mass vs. radial position

The net load is zero at the geosynchronous radius of about 42,200 km. Below this radial position, the gravitational load dominates heavily, whereas the centripetal one begins to dominate beyond it. A ribbon with uniform bulk density and cross-sectional area along its stretched length L must satisfy

$$\int_R^{R+L} \left(\mu / r^2 - \Omega^2 r\right) dr = 0\,, \tag{2.1}$$

or

$$\mu\left(\frac{1}{R} - \frac{1}{R+L}\right) - \frac{\Omega^2}{2}\left[(R+L)^2 - R^2\right] = 0\,, \tag{2.2}$$

where R is the radius of the Earth. The value of L satisfying Eq. (2.2) is given by

$$L = (R/2)\left(\sqrt{1+8\left(R_G/R\right)^3} - 3\right), \tag{2.3}$$

where R_G is the geosynchronous orbit radius of the Earth. It is the radial position at which the orbital period is equal to the period of the Earth's rotation and is given by

$$R_G = \left(\mu/\Omega^2\right)^{\frac{1}{3}}. \tag{2.4}$$

At this altitude, the magnitudes of the gravitational and centripetal loads are equal. For a space elevator built on Earth, the nominally stretched length of a self-balanced ribbon is $L = 144{,}206$ km, or $L + R = 3.565 R_G$.

Since the aforementioned loads act in opposite directions, the static ribbon is in tension. The tension varies throughout the ribbon's length with the highest value occurring at the geosynchronous radius. For this reason, Pearson (1975) suggested tapering the cross-sectional area appropriately to ensure constant stress throughout the static unoccupied ribbon of the space elevator.

When Pearson (1975) developed the tapering function that ensures constant stress across the ribbon, he did not take the longitudinal extension caused by the tension in the static ribbon into account. The tension in the static ribbon will cause it to extend longitudinally from its unstressed state by $u(s)$, where s is a measure of the position of a ribbon element. Letting ε denote the strain in the ribbon,

$$\varepsilon(s) = \frac{du}{ds} = \frac{\sigma(s)}{E(s)}, \tag{2.5}$$

where $\sigma(s)$ and $E(s)$ are the stress and modulus of elasticity of the ribbon, respectively. The modulus of elasticity is assumed constant throughout the ribbon. Recalling that the static ribbon has constant stress throughout it, the strain of the static ribbon is a constant, $\varepsilon_0 = \sigma_0 / E$. Using zero deformation at the base as a boundary condition, the deformation of the static ribbon from its nominal, unstressed state is given by

$$u(s) = \varepsilon_0 s. \tag{2.6}$$

Thus, if the nominally stretched ribbon is to have length L, its original length L_0 must be given by

$$L_0 = L/(1+\varepsilon_0). \tag{2.7}$$

L_0 is the nominal length of the ribbon. It is noted that even for a small nominal strain, the difference between the ribbon length before and after deployment would be thousands of kilometres.

Consider an element dm at a distance r from the center of the Earth. Assume that the ribbon is designed such that the stress is uniform throughout and is given by σ_0. The forces acting on the element are shown in Figure 2.2.

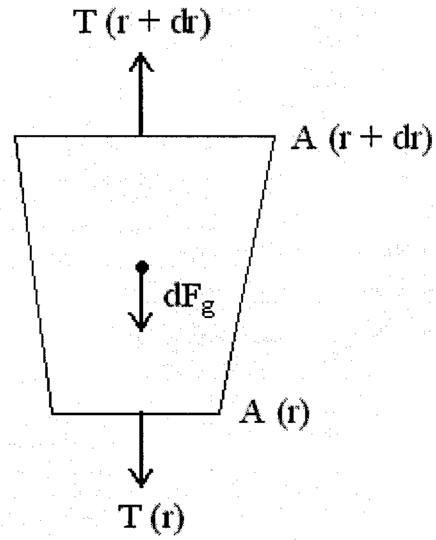

Figure 2.2: Free body diagram of a ribbon element

T is the tension in the ribbon, A is its cross-sectional area, and dF_g is the gravitational force acting on the element. From Newton's second law,

$$dma_r = \sum F_r = (T + dT) - T - dF_g \; . \tag{2.8}$$

Substituting values for tension, gravitational force and acceleration,

$$dm\left(-\Omega^2 r\right) = \sigma_0 A(r + dr) - \sigma_0 A(r) - dm\left(\mu / r^2\right). \tag{2.9}$$

dm is the product of the bulk density, γ, and the infinitesimal volume given by Ads, where s is a ribbon coordinate. The spatial coordinate r and the ribbon coordinate s are related by

$$r = R + s + u(s)\,, \tag{2.10}$$

where $u(s)$ is the longitudinal displacement of a ribbon element located at s. As a result, $dr = ds\left(1 + du/ds\right)$. As the ribbon taper will be designed to have constant stress, it will also have constant strain, such that $du/ds = \varepsilon_0$. Therefore, for the derivation of the cross-sectional area, the following substitution is made:

$$ds = dr/(1+\varepsilon_0). \tag{2.11}$$

The bulk density is assumed constant throughout the ribbon. Making the above substitutions and simplifying,

$$\left[\frac{\gamma A(r)dr}{(1+\varepsilon_0)}\right]\left(-\Omega^2 r + \mu/r^2\right) = \sigma_0 dA, \tag{2.12}$$

or,

$$\frac{dA}{dr} = \frac{\gamma}{\sigma_0(1+\varepsilon_0)} A(r)\left(\mu/r^2 - \Omega^2 r\right). \tag{2.13}$$

It is now useful to introduce the characteristic height of the ribbon, which is given by

$$\bar{h} = \sigma_0 / \gamma g_0. \tag{2.14}$$

g_0 is the surface gravity of the Earth, and is given by

$$g_0 = \mu/R^2. \tag{2.15}$$

The characteristic height is the strength to density ratio of the ribbon material, with a built-in safety factor, which is scaled with respect to the surface gravity of the Earth to be a measure of length. Clearly, materials with higher strength to density ratios have higher characteristic heights. The characteristic height is essentially a measure of the feasibility of constructing a space elevator out of a given material. If the nominal stress is equal to the maximum stress (no safety factor), Pearson (1975) defines $\bar{h}$ as "...the height to which a constant-cross-section ribbon of the material could be built in a uniform one-g field without exceeding the stress limit of the material at the base." Substituting

$\Omega^2 = \mu / R_G^3$, $\mu = g_0 R^2$, and $\sigma_0 = \bar{h}\gamma g_0$ into Eq. (2.13) and then simplifying, one arrives at

$$\frac{dA}{A} = \frac{R^2}{\bar{h}(1+\varepsilon_0)}\left(\frac{1}{r^2} - \frac{r}{R_G^3}\right)dr. \tag{2.16}$$

Integrating Eq. (2.16) results in

$$A(r) = c\exp\left[-\frac{R^2}{\bar{h}(1+\varepsilon_0)}\left(\frac{1}{r} + \frac{r^2}{2R_G^3}\right)\right], \tag{2.17}$$

where c is a constant of integration. The boundary condition for the ribbon is that the net force acting on its free end must be equal to the tension in it at that point. As there is no force acting at that point, this boundary condition could be satisfied by having the cross-sectional area equal zero at the tip (this would ensure zero tension). However, from Eq. (2.17), it is apparent that the cross-sectional area of the ribbon cannot be zero at any location if it is to have constant stress. Thus, in order to satisfy the boundary condition at the tip of the ribbon, a mass m_c, called the counterweight, must be attached there. The forces acting on the counterweight can be made equal to the tension at the tip by forcing

$$m_c\left\{\Omega^2(R+L) - \mu/(R+L)^2\right\} = \sigma_0 A(r)\big|_{r=R+L}. \tag{2.18}$$

Through differentiation of Eq. (2.17), it may be shown that the maximum value of cross-sectional area occurs at the radial position $r = R_G$. Therefore, $A(R_G)$ may be set to the useful design parameter A_m, which is the maximum cross-sectional area of the ribbon. Then, after some manipulation, the cross-sectional area profile may be expressed as

$$A(r) = A_m \exp\left[F(r)\right], \tag{2.19}$$

where

$$F(r)=\frac{R^2}{\bar{h}R_G\left(1+\varepsilon_0\right)}\left(\frac{3}{2}-\frac{R_G}{r}-\frac{r^2}{2R_G^2}\right). \tag{2.20}$$

An almost identical solution was obtained by Pearson (1975). The only difference is that the $\left(1+\varepsilon_0\right)$ term did not appear in his solution. This is because the nominal longitudinal extension was not considered in his taper function derivation. Also, in his derivation, the boundary condition at the tip of the ribbon was not satisfied. It is essential that there be a counterweight placed at the free end, and it is given by

$$m_c=\frac{\sigma_0 A_m \exp\left[F(r)\right]\Big|_{r=R+L}}{\left\{\Omega^2\left(R+L\right)-\mu/\left(R+L\right)^2\right\}}. \tag{2.21}$$

Including a counterweight in the design does not affect the taper function of the ribbon.

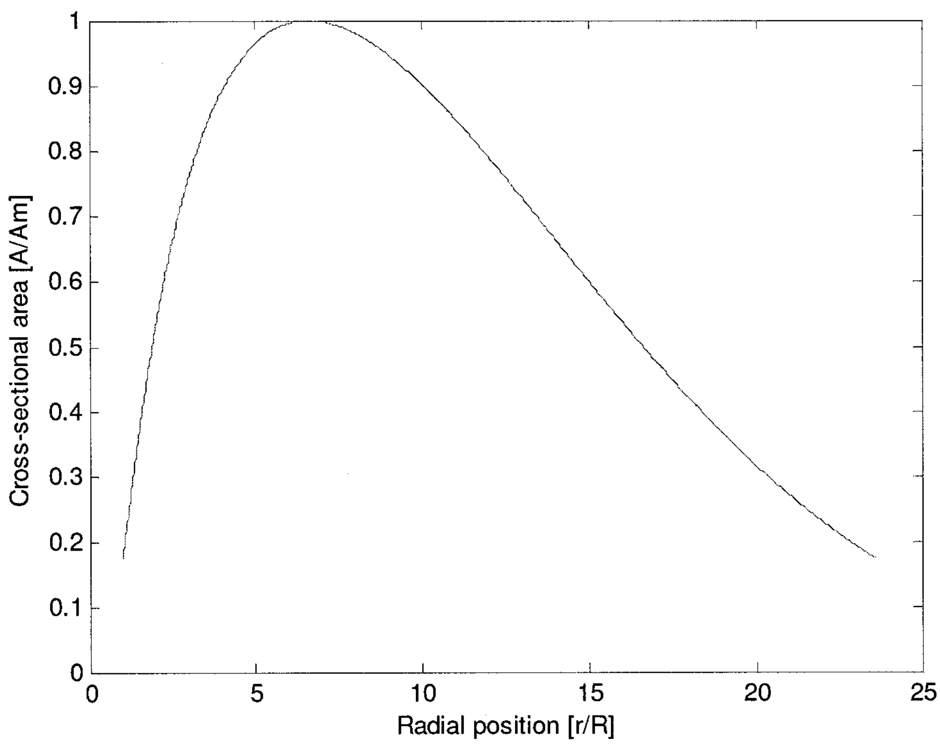

Figure 2.3: Cross-sectional area of ribbon vs. radial position for $\bar{h}$ = 2,750 km

The resulting taper ratio of the ribbon, which is the quotient of A_m, and the cross-sectional area at the Earth's surface, A_0, is given by

$$A_m / A_0 = \exp\left[\frac{R}{\bar{h}\,(1+\varepsilon_0)}\left(1-\frac{R}{R_G}\right)^2\left(1+\frac{R}{2R_G}\right)\right]. \tag{2.22}$$

Inputting values for R and R_G, the taper ratio is given by about $\exp\left(0.776R/\bar{h}\right)$. For a material with $\bar{h}$ = 2,750 km, the taper ratio is about 6. The taper function of a material having this characteristic height is plotted in Figure 2.3. The density of carbon nanotubes is 1,300 kg/m^3 and the theoretical value for its maximum tensile strength is 130 GPa (Yacobson *et al*, 1997). However, this strength property has yet to be attained in practice. Still, if the maximum strength of the ribbon material were only 70 GPa, its characteristic height would be 2,750 km using a safety factor of two (i.e., σ_0 = 35 GPa), and its cross-sectional area variation would be as plotted in Figure 2.3.

The nominal tension in the ribbon may now be expressed as:

$$T_0(r) = \sigma_0 A(r) = \sigma_0 A_m \exp\left[F(r)\right]. \tag{2.23}$$

The taper has no effect on the required stretched length of a self-balanced ribbon, since it can be shown numerically that the solution to

$$\int_R^{R+L} \exp\left[F(r)\right]\left(1/r^2 - r/R_G^3\right)dr = 0 \tag{2.24}$$

is also given in Eq. (2.3). However, it has been shown that for a ribbon of *any* length (even a self-balanced one) to have uniform stress, it must have a counterweight attached at its free end. The mass of the ribbon m_t, is given by

$$m_t = \gamma A_m \int_0^{L_0} \exp[F(s)]\,ds, \tag{2.25}$$

where

$$F(s) = \frac{R^2}{\bar{h}R_G(1+\varepsilon_0)}\left\{\frac{3}{2} - \frac{R_G}{(R+s+\varepsilon_0)} - \frac{(R+s+\varepsilon_0)^2}{2R_G^2}\right\}. \tag{2.26}$$

2.1.2 The Counterweight

As shown in Section 2.1.1, a counterweight is a necessary component of the space elevator, as without one, the ribbon could not satisfy the boundary condition at the free end. Through manipulation of Eq. (2.21), the equation for the required counterweight may be expressed as

$$m_c = \gamma A_m \bar{h} \frac{\exp\left[F(s)\big|_{s=L_0}\right]}{\left(\dfrac{R}{R_G}\right)^2\left[\dfrac{R+L}{R_G} - \left(\dfrac{R_G}{R+L}\right)^2\right]}. \tag{2.27}$$

Clearly, the required counterweight is proportional to the maximum cross-sectional area of the ribbon, and also depends on the ribbon's other design and material parameters.

Placing a counterweight at the space end of the ribbon allows the stretched ribbon length L to be a design parameter, which must only satisfy $L+R>R_G$ in order to have a balanced ribbon. However, if $L>144{,}206\,\text{km}$, unnecessary additional tension will manifest at the base of the ribbon. The freedom to choose a nominally stretched length of ribbon is useful from a design standpoint. It is clear from Eq. (2.27) that as L approaches its minimum acceptable value of $R_G - R$, the required value of m_c approaches infinity.

As will be seen in Chapter 6, it is desirable to have a ribbon that extends far beyond the geosynchronous altitude so that payloads may be sent to planets other than the Earth.

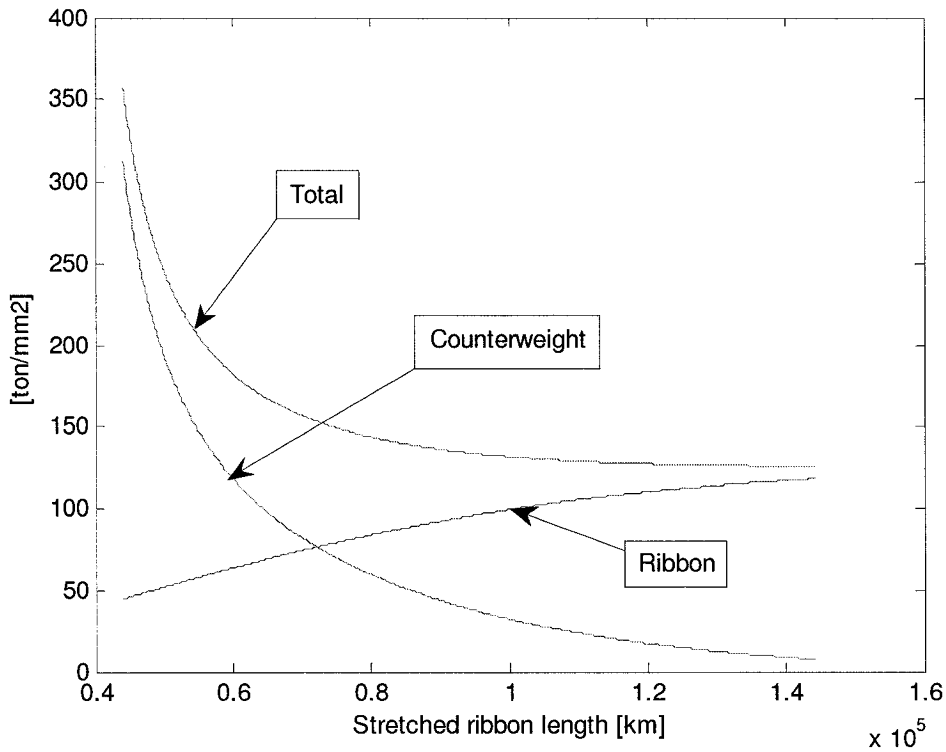

Figure 2.4: Ribbon, counterweight and total mass per unit area (A_m) of ribbon vs. stretched ribbon length; taper ratio = 6

Figure 2.4 illustrates how massive the space elevator will be. The ribbon's bulk density and modulus of elasticity are assumed to be 1,300 kg/m^3 and 1 TPa, respectively. If the ribbon were to have a taper ratio of about 6 ($\sigma_0 = 35$ GPa) and a stretched ribbon length of 100,000 km, and if its maximum cross-sectional area were only 10 mm^2, its mass would be about 990 tons. The corresponding counterweight mass would be about 330 tons. A lower taper ratio does not affect the counterweight mass by much, but does increase the ribbon mass slightly for the same value of A_m. The advantage of a ribbon having a lower taper ratio is seen in its lifting capability; this is discussed later.

A counterweight is also a necessary component of the design because it will consist initially of the original spacecraft that transported the wound ribbon to the geosynchronous altitude for earthward and spaceward deployment (Edwards, 2000). Equations (2.25) and (2.27) are important to consider when planning for the deployment of the space elevator. Furthermore, early operation of the space elevator will involve sending climbers that gradually thicken the ribbon to increase the maximum climber mass that it can support (Edwards, 2000). These climbers will end their trajectories at the space end of the ribbon, becoming part of the counterweight. The mass of these climbers will be such that their presence at the space end of the ribbon balances the offset caused by the additional material they added to it. It follows that if a climber is to thicken the tapered ribbon during its ascension by a certain percentage, the mass of the climber must be the same percentage of the mass of the current counterweight.

2.1.3 The Climber

As the balanced, tapered ribbon is deployed from the geosynchronous altitude in both the Earthward and spaceward directions, the transport spacecraft will concurrently ascend the ribbon to become the counterweight of the space elevator. Then, the ribbon may be connected to the base on the surface of the Earth. This will complete the deployment phase of the space elevator. At this point, climbers may move to any position along the ribbon, and launch their payload in its desired trajectory, be it to an Earth orbit, or to another destination in the solar system.

The presence of a climber will cause an additional tension gradient across the ribbon. The magnitude of this additional tension gradient is related to the position and acceleration of the climber. Assuming that the acceleration of the climber is not too large, the rise in tension will be mainly due to the gravitational and centripetal forces acting on the climber. Letting m_e be the mass of the climber (elevator), the increase in stress caused by the climber, σ_e, as a function of radial position r is given by

$$\sigma_e(r) = m_e\left\{\mu / r^2 - \Omega^2 r\right\} \big/ A(r). \tag{2.28}$$

The maximum increase in stress occurs at the base ($r = R$), where the load acting on the climber is the highest (see Figure 2.1), and the cross-sectional area of the ribbon is the lowest, due to the taper. Letting the maximum allowable increase in stress due to the climber's load be a fraction, ν, of the nominal stress, σ_0, the maximum permissible climber mass is given by

$$m_{e,\max} = \nu \frac{A_0 \sigma_0}{\left\{\mu / R^2 - \Omega^2 R\right\}}. \tag{2.29}$$

If the constraint given by Eq. (2.29) is not respected, the ribbon will rupture. It is therefore useful to minimize the taper ratio, because for a given A_m, both the cross-sectional area at the base A_0 and the nominal stress σ_0 would increase as a result, thereby increasing the maximum allowable climber mass. It can be shown that as the taper ratio decreases, the percentage increase in $m_{e,\max}$ is much greater than that of the ribbon mass. Of course, the minimum allowable taper ratio is related to the strength limitations of the ribbon material. Also, as stated by Pearson (1975), a taper ratio in the neighbourhood of three should be avoided due to resonance with the frequency of the moon.

For a space elevator having the numerical values, $\gamma = 1{,}300$ kg/m^3, $A_m = 10$ mm^2, and $\sigma_0 = 35$ GPa (taper ratio of about six), the maximum climber mass is roughly 5.9ν tons. If the stress in the ribbon is only allowed to increase from its nominal amount by 10% due to the presence of a climber, then the climber must satisfy $m_e \leq 0.59$ tons. As previously stated, a nominally stretched ribbon measuring 100,000 km having the aforementioned properties will have a mass of about 990 tons, and will require a 330-ton counterweight connected to its free end. Clearly, if the constraint given by Eq. (2.29) is to be satisfied, the mass of the climber will be very small compared to that of the ribbon and counterweight. This fact will be used while deriving closed-form solutions.

2.2 Comparison with Typical Tethered Satellite Systems

The dynamics of a space elevator resemble those of a standard two-satellite space tethered system, but with several major differences. A standard tethered satellite system consists of two satellites connected by a long tether pointing in the radial direction, with one point of the tether (not necessarily the center of mass of the system) in a circular orbit. The most notable difference between this system and that of the space elevator is the length of the tether. Long tethers in space are of the order of 100 km end to end; the space elevator will be roughly one thousand times this length.

Often, with tethered satellite systems, the dynamics can be well modeled by neglecting the mass of the tether, as it is small with respect to the two end masses. For the space elevator, the tether is in fact much more massive than the climbers it will support (as shown in Section 2.1.3), and is of the same order as the end mass. Therefore, in parts of the analysis in this thesis, the mass of the climber will actually be neglected. The long tether causes other differences to arise. Climbers traversing the entire ribbon will do so in weeks rather than hours. Also, because the radius of the Earth is actually much smaller than the length of the tether, the gravitational potential energy expressions for the space elevator may not be approximated using a binomial expansion as is usually done.

Another major difference between the two systems is the fact that the space elevator ribbon/tether is connected to a base on the surface of the Earth (not a second satellite). One consequence of this difference is that other than structural deformation, the nominal length of the tether will not change. For tethered satellites, the deployment and retrieval of a satellite involves deploying and retrieving the tether itself. These types of dynamics will occur only during the deployment of the space elevator, and not during general operation, which is what this thesis aims to examine.

Like typical tethered satellite dynamic models, the libration angle of the space elevator is its most important degree of freedom. However, for these typical models, this angle refers to the rotation of the tether about its center of mass. For the space elevator, the libration angle refers to the rotation of the ribbon at the base located on the surface of the Earth.

Although there appear to be many factors distinguishing the space elevator from a typical tethered two-satellite system, it will be observed that the governing dynamics of the two systems are quite similar.

2.3 Operational Costs

From a business standpoint, the primary motivation for the implementation of a space elevator is that it would drastically reduce the cost of satellite placement and space missions. Its construction costs, which are heavily dependent upon the cost of carbon nanotube synthesis, have been approximated in the tens of billions of dollars (USD) (Edwards *et al*, 2002). While this may seem expensive, with frequent use, the savings incurred during the space elevator's operation could be enough to recover these setup costs rather quickly.

The case where a payload is carried inside a climber from the surface of the Earth to some altitude, d_f, below the geosynchronous orbit is examined. The climb beyond this altitude is propelled by the spin of the Earth, the effect of which is greater than that of the gravitational force beyond the geosynchronous altitude. If the climb is done at a constant speed, and the ribbon remains in its nominal position, the required thrust by the climber, F_T, is given by

$$F_T = m_e\left\{\mu/\left(d_e+R\right)^2 - \Omega^2\left(d_e+R\right)\right\}, \tag{2.30}$$

where d_e is the position of the climber. The work done by the climber, W_T, is found by integrating the product of climber thrust and differential climber position:

$$W_T = \int F_T dd_e \,. \tag{2.31}$$

The work per unit mass done by the motor to move the climber from the surface of the Earth to some altitude below the geosynchronous orbit, d_f, is then given by

$$\frac{W_T}{m_e} = \frac{\mu}{R}\left(\frac{d_f}{d_f + R}\right) - \frac{\Omega^2}{2}\left[\left(R + d_f\right)^2 - R^2\right]. \tag{2.32}$$

Therefore, the work per unit mass done by the motor to move the climber from the surface of the Earth to the geosynchronous altitude is about 48.5 MJ/kg. An apparent anomaly occurs when examining the change in the energy per unit mass of the climber before and after transit, $E_{1\rightarrow 2}$, given by

$$\frac{E_{1\rightarrow 2}}{m_e} = \left[\frac{\Omega^2}{2}\left(R + d_f\right)^2 - \frac{\mu}{\left(R + d_f\right)}\right] - \left[\frac{\Omega^2}{2}R^2 - \frac{\mu}{R}\right], \tag{2.33}$$

or

$$\frac{E_{1\rightarrow 2}}{m_e} = \frac{\mu}{R}\left(\frac{d_f}{d_f + R}\right) + \frac{\Omega^2}{2}\left[\left(R + d_f\right)^2 - R^2\right]. \tag{2.34}$$

The increase in the total energy per unit of mass of the climber in moving from the surface of the Earth to the geosynchronous altitude is about 57.7 MJ/kg. This result begs the questions, "How did the climber gain more energy than the work the motor put into it?" and "Where did this free energy come from?" The *free* energy came from the spin of the Earth. For a transit to the altitude d_f, the energy per unit mass extracted from the Earth is given by $\Omega^2\left[\left(d_f + R\right)^2 - R^2\right]$; for this particular case, it is $\Omega^2\left(R_G^2 - R^2\right)$. The slowing of the spin of the Earth due to this energy extraction is negligible. The situation is analogous to that of gravity assist. This result implies that even if a rocket were made to function with the same overall efficiency as that of the space elevator, it would still be less efficient, as it could not extract this free energy. It is however somewhat of a moot point, as these savings are small compared to those incurred due to the actual difference in the overall efficiency between the two methods of space travel.

The fuel cost for a typical shuttle launch to the geosynchronous orbit is around \$210 per kilogram of payload (Edwards *et al*, 2002). The required energy cost in order to accomplish this same feat with the space elevator, C_{SE}, is given by

$$C_{SE} = 48.5 \frac{C_e}{\eta \bar{M}_p}. \tag{2.35}$$

C_e is the cost of electricity per MJ, and η is the overall efficiency of the energy conversion process, which includes that of the transmission from Earth via laser (which is quite low) and that of the climber's motor. $\bar{M}_p$ is the ratio of the payload mass to that of the entire mass being lifted, m_e. If reasonable values are assumed for these parameters ($C_e = 0.012$ \$/MJ, $\eta = 0.3$ and $\bar{M}_p = 0.65$), the cost for transport to the geosynchronous orbit using the space elevator is around \$3 per kilogram of payload.

It is clear that the space elevator could bring space travel costs down by two orders of magnitude. If power-beaming technology were to progress greatly, this decrease in operational costs would be even greater. Also of interest is the fact that climbers ascending the ribbon at constant speed beyond the geosynchronous altitude would be required to brake, and could actually generate energy in doing so. A more detailed cost analysis of the space elevator is provided by Edwards (2002).

Chapter 3: Rigid Tether, Mobile Base Model

3.1 Description of the System

The physical model used to describe the space elevator is in the equatorial plane. The model, seen in Figure 3.1, is simplified in this chapter (and the next) by assuming the ribbon to be rigid. To depict this mathematically, the modulus of elasticity of the ribbon material is set to infinity. As such, the ribbon experiences no strain, and its unloaded length L_0 and deployed length L are identical.

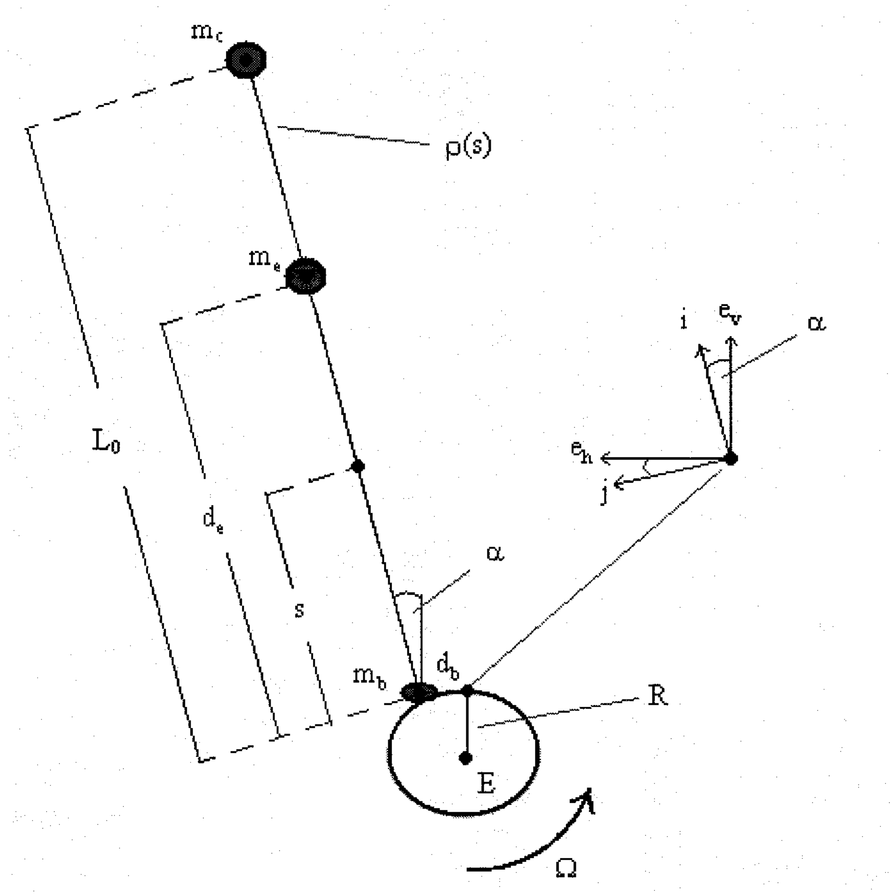

Figure 3.1: Space elevator components and degrees of freedom

The base is allowed to move to include the scenario of the space elevator floating in the ocean. The Earth has a uniform radius R, and rotates with angular velocity Ω. The center of the Earth is assumed to be inertially fixed. The origin of the inertial frame coincides with this point. The rotating unit vectors $\mathbf{e_v}$ and $\mathbf{e_h}$ point in the local vertical and horizontal directions, respectively. Unit vector $\mathbf{i}$ is along the ribbon. The unit vectors $\mathbf{i}$ and $\mathbf{j}$ are obtained by rotating $\mathbf{e_v}$ and $\mathbf{e_h}$ through an angle α. s is the coordinate measured along the ribbon. As shown in Section 2.1.1, the relationship between radial position r and ribbon coordinate s is given by $r = R + s + u(s)$, where $u(s)$ is the longitudinal elastic displacement of an element at s. For all derivation and analysis in Chapters 3 and 4, the longitudinal extension, $u(s)$, is zero, because there is zero strain. Non-zero $u(s)$ is considered in Chapter 5.

The base, having mass m_b, is free to translate horizontally; the translational displacement is denoted by d_b. The translation of the base from its nominal position is likely to be small compared to the radius of the Earth, and hence allowing it to slide only in the $\mathbf{e_h}$ direction is a good assumption. The ribbon, extending from the base to the counterweight, rotates in the vertical plane by an angle α; this is defined as the libration angle. The elevator, having mass m_e, can move along the ribbon; its distance from the base is denoted by d_e. Generalized co-ordinates d_b, α, and d_e describe the three-degree-of-freedom system.

The counterweight has mass m_c, and the ribbon's lineal density, $\rho(s)$, varies across its length, as $\rho(s)=\rho_m \exp[F(s)]$. ρ_m is the maximum lineal density and corresponds to the density at the geosynchronous altitude. It is the product of the ribbon's bulk density, γ, and its maximum cross-sectional area, A_m. The ribbon's taper function defined by $F(s)$ was given in Chapter 2 (Eq. (2.26)).

Items not shown in Figure 3.1 are spring and damping constants k_b and c_b, which emulate an anchor restricting the motion of the base. There is also a torsional spring constant k_t, restricting the rotation of the ribbon.

3.2 Energy Expressions and Equations of Motion

Equations governing the motion of the system are derived using the Lagrange approach. In order to use this approach, expressions for the kinetic and potential energy of the system are needed.

The position vectors for the various space elevator components are given by

$$
\begin{aligned}
&\mathbf{r_B} = d_b\mathbf{e_h} + R\mathbf{e_v}, \\
&\mathbf{r_E} = \mathbf{r_B} + d_e\mathbf{i}, \\
&\mathbf{r_R}(s) = \mathbf{r_B} + s\mathbf{i}, \text{ and} \\
&\mathbf{r_C} = \mathbf{r_B} + L_0\mathbf{i}.
\end{aligned}
\tag{3.1}
$$

Here, the subscripts B, E, R and C stand for the base, elevator, ribbon and counterweight, respectively. The velocity vectors are given by

$$
\begin{aligned}
\mathbf{v_B} &= \left(\dot{d}_b \sin\alpha + R\Omega\sin\alpha - d_b\Omega\cos\alpha\right)\mathbf{i} \\
&\quad + \left(\dot{d}_b \cos\alpha + R\Omega\cos\alpha + d_b\Omega\sin\alpha\right)\mathbf{j}, \\
\mathbf{v_E} &= \mathbf{v_B} + \dot{d}_e\mathbf{i} + \left[(\Omega+\dot{\alpha})d_e\right]\mathbf{j}, \\
\mathbf{v_R}(s) &= \mathbf{v_B} + \left[(\Omega+\dot{\alpha})s\right]\mathbf{j}, \text{ and} \\
\mathbf{v_C} &= \mathbf{v_B} + \left[(\Omega+\dot{\alpha})L_0\right]\mathbf{j}.
\end{aligned}
\tag{3.2}
$$

The total kinetic energy of the system can be written as

$$K = K_B + K_E + K_R + K_C,$$

where

$$
\begin{aligned}
K_B &= \frac{1}{2}m_b\left(\mathbf{v_B}\bullet\mathbf{v_B}\right), \\
K_E &= \frac{1}{2}m_e\left(\mathbf{v_E}\bullet\mathbf{v_E}\right), \\
K_R &= \frac{1}{2}\int_0^{L_0}\rho(s)\left[\mathbf{v_R}(s)\bullet\mathbf{v_R}(s)\right]ds, \text{ and} \\
K_C &= \frac{1}{2}m_c\left(\mathbf{v_C}\bullet\mathbf{v_C}\right).
\end{aligned}
\tag{3.3}
$$

The total potential energy of the system is

$$P = P_B + P_E + P_R + P_C + P_{EL},$$

where

$$
\begin{aligned}
P_B &= \frac{-\mu m_b}{\sqrt{\mathbf{r_B}\bullet\mathbf{r_B}}}, \\
P_E &= \frac{-\mu m_e}{\sqrt{\mathbf{r_E}\bullet\mathbf{r_E}}}, \\
P_R &= -\mu\int_0^{L_0}\frac{\rho(s)}{\sqrt{\mathbf{r_R}(s)\bullet\mathbf{r_R}(s)}}ds, \\
P_C &= \frac{-\mu m_c}{\sqrt{\mathbf{r_C}\bullet\mathbf{r_C}}}, \text{ and} \\
P_{EL} &= \frac{1}{2}k_b d_b^2 + \frac{1}{2}k_t\alpha^2.
\end{aligned}
\tag{3.4}
$$

P_{EL} is the elastic potential energy associated with the anchor of the base and the ribbon attachment system, respectively.

Lagrange's equations can be written as

$$\frac{d}{dt}\left[\frac{\partial K}{\partial \dot{q}_i}\right]-\frac{\partial K}{\partial q_i}+\frac{\partial P}{\partial q_i}=Q_i, \quad q_i=d_e,d_b,\alpha. \tag{3.5}$$

In Eq. (3.5), q_i is a generalized coordinate, and Q_i is the corresponding generalized force. By substituting the energy expressions from Eqs. (3.3) and (3.4) into Eq. (3.5), one obtains, after considerable algebra,

$$\begin{aligned}&\ddot{d}_e-(\Omega+\dot{\alpha})^2 d_e+\left(\ddot{d}_b-\Omega^2 d_b\right)\sin\alpha-\Omega\left(2\dot{d}_b+R\Omega\right)\cos\alpha\\&+\frac{\mu\left(d_e+R\cos\alpha+d_b\sin\alpha\right)}{\left(R^2+d_b^2+d_e^2+2Rd_e\cos\alpha+2d_bd_e\sin\alpha\right)^{\frac{3}{2}}}=\frac{Q_{de}}{m_e},\end{aligned} \tag{3.6}$$

$$\begin{aligned}&m_{tot}\left(\ddot{d}_b-\Omega^2 d_b\right)+\left(I_2+m_cL_0+m_ed_e\right)\left\{\ddot{\alpha}\cos\alpha-(\Omega+\dot{\alpha})^2\sin\alpha\right\}\\&+2m_e\dot{d}_e(\Omega+\dot{\alpha})\cos\alpha+m_e\ddot{d}_e\sin\alpha\\&+\frac{\mu m_b d_b}{\left(R^2+d_b^2\right)^{\frac{3}{2}}}+\mu\int_0^{L_0}\frac{\rho(s)\left(d_b+s\sin\alpha\right)}{\left(R^2+d_b^2+s^2+2Rs\cos\alpha+2d_bs\sin\alpha\right)^{\frac{3}{2}}}ds\\&+\frac{\mu m_c\left(d_b+L_0\sin\alpha\right)}{\left(R^2+d_b^2+L_0^2+2RL_0\cos\alpha+2d_bL_0\sin\alpha\right)^{\frac{3}{2}}}\\&+\frac{\mu m_e\left(d_b+d_e\sin\alpha\right)}{\left(R^2+d_b^2+d_e^2+2Rd_e\cos\alpha+2d_bd_e\sin\alpha\right)^{\frac{3}{2}}}+k_bd_b+c_b\dot{d}_b=Q_{db},\end{aligned} \tag{3.7}$$

and

$$
\begin{aligned}
&\ddot{\alpha}\left(m_c L_0^2 + m_e d_e^2 + I_3\right) + 2m_e d_e \dot{d}_e \left(\Omega + \dot{\alpha}\right) \\
&+\left(m_c L_0 + m_e d_e + I_2\right)\left(\ddot{d}_b \cos\alpha + 2\Omega \dot{d}_b \sin\alpha - \Omega^2 d_b \cos\alpha + R\Omega^2 \sin\alpha\right) \\
&+\mu \int_0^{L_0} \frac{\rho(s) s \left(d_b \cos\alpha - R\sin\alpha\right)}{\left(R^2 + d_b^2 + s^2 + 2Rs\cos\alpha + 2d_b s \sin\alpha\right)^{\frac{3}{2}}} ds \\
&+\frac{\mu m_c L_0 \left(d_b \cos\alpha - R\sin\alpha\right)}{\left(R^2 + d_b^2 + L_0^2 + 2RL_0 \cos\alpha + 2d_b L_0 \sin\alpha\right)^{\frac{3}{2}}} \\
&+\frac{\mu m_e d_e \left(d_b \cos\alpha - R\sin\alpha\right)}{\left(R^2 + d_b^2 + d_e^2 + 2Rd_e \cos\alpha + 2d_b d_e \sin\alpha\right)^{\frac{3}{2}}} + k_t \alpha = Q_\alpha . \qquad (3.8)
\end{aligned}
$$

In the equations of motion,

$$I_i = \int_0^{L_0} \rho(s) s^{i-1} ds \,,\; i = 1, 2, 3\ldots \qquad (3.9)$$

and m_{tot} is the total mass of the system, given by

$$m_{tot} = m_b + m_c + m_e + I_1 . \qquad (3.10)$$

The equations of motion contain mainly inertial, centrifugal and gravitational terms. There are also two elastic, one viscous and some mixed terms including the Coriolis force.

For convenience of analysis, these equations are non-dimensionalized. Non-dimensional masses are defined by

$$M_e = m_e / m_{tot},\quad M_b = m_b / m_{tot},\quad M_c = m_c / m_{tot} \text{ and } M_p = \rho_m L_0 / m_{tot} . \qquad (3.11)$$

The distances are also non-dimensionalized, and are defined by

$$D_e = d_e / L_0,\quad D_b = d_b / h \text{ and } \xi = s / L_0 . \qquad (3.12)$$

Here, h is an appropriate scaling factor for the small displacements of the base, to be chosen when doing numerical computations. Other useful distance ratios are given by

$$R_L = R / L_0 \text{ and } h_L = h / L_0 . \tag{3.13}$$

Non-dimensional time τ is defined by

$$\tau = \Omega t . \tag{3.14}$$

The equations of motion can now be written in non-dimensional form as:

$$\begin{aligned}
&D_e'' + h_L D_b'' \sin\alpha - (1+\alpha')^2 D_e - h_L D_b \sin\alpha - \{2h_L D_b' + R_L\}\cos\alpha \\
&+\lambda \frac{\{D_e + R_L \cos\alpha + h_L D_b \sin\alpha\}}{\left[\{(h_L/R_L) D_b \sin\alpha + \cos\alpha + (1/R_L) D_e\}^2 + ((h_L/R_L) D_b \cos\alpha - \sin\alpha)^2\right]^{\frac{3}{2}}} \\
&= Q_{de} / m_e L_0 \Omega^2 ,
\end{aligned} \tag{3.15}$$

$$\begin{aligned}
&D_b'' + \frac{M_e}{h_L} D_e'' \sin\alpha + \frac{1}{h_L}\left(M_p \hat{I}_2 + M_e D_e + M_c\right)\alpha'' \cos\alpha + \frac{2(1+\alpha')}{h_L} M_e D_e' \cos\alpha \\
&- \frac{(1+\alpha')^2}{h_L}\left(M_p \hat{I}_2 + M_e D_e + M_c\right)\sin\alpha - D_b + \lambda M_b \frac{D_b}{\{(h_L/R_L)^2 D_b^2 + 1\}^{\frac{3}{2}}} \\
&+\lambda M_e \frac{\{D_b + (1/h_L) D_e \sin\alpha\}}{\left[\{(h_L/R_L) D_b \sin\alpha + \cos\alpha + (1/R_L) D_e\}^2 + \{(h_L/R_L) D_b \cos\alpha - \sin\alpha\}^2\right]^{\frac{3}{2}}} \\
&+\lambda M_p \int_0^1 \frac{\exp[F(\xi)]\{D_b + (1/h_L)\xi \sin\alpha\}}{\left[\{(h_L/R_L) D_b \sin\alpha + \cos\alpha + (1/R_L)\xi\}^2 + \{(h_L/R_L) D_b \cos\alpha - \sin\alpha\}^2\right]^{\frac{3}{2}}} d\xi \\
&+\lambda M_c \frac{\{D_b + (1/h_L)\sin\alpha\}}{\left[\{(h_L/R_L) D_b \sin\alpha + \cos\alpha + (1/R_L)\}^2 + \{(h_L/R_L) D_b \cos\alpha - \sin\alpha\}^2\right]^{\frac{3}{2}}} \\
&+K_b D_b + C_b D_b' = Q_{db} / m_{tot} \Omega^2 h ,
\end{aligned} \tag{3.16}$$

and

$$
\begin{aligned}
&\left(M_e D_e^2+M_c+M_p\hat{I}_3\right)\alpha''+h_L\left(M_p\hat{I}_2+M_eD_e+M_c\right)D_b''\cos\alpha+2M_e\left(1+\alpha'\right)D_eD_e' \\
&+\left(M_p\hat{I}_2+M_eD_e+M_c\right)\left\{-h_LD_b\cos\alpha+2h_LD_b'\sin\alpha+R_L\sin\alpha\right\} \\
&+\lambda M_e\frac{D_e\left\{h_LD_b\cos\alpha-R_L\sin\alpha\right\}}{\left[\left\{(h_L/R_L)D_b\sin\alpha+\cos\alpha+(1/R_L)D_e\right\}^2+\left\{(h_L/R_L)D_b\cos\alpha-\sin\alpha\right\}^2\right]^{\frac{3}{2}}} \\
&+\lambda M_p\int_0^1\frac{\exp[F(\xi)]\xi\left\{h_LD_b\cos\alpha-R_L\sin\alpha\right\}}{\left[\left\{(h_L/R_L)D_b\sin\alpha+\cos\alpha+(1/R_L)\xi\right\}^2+\left\{(h_L/R_L)D_b\cos\alpha-\sin\alpha\right\}^2\right]^{\frac{3}{2}}}d\xi \\
&+\lambda M_c\frac{\left\{h_LD_b\cos\alpha-R_L\sin\alpha\right\}}{\left[\left\{(h_L/R_L)D_b\sin\alpha+\cos\alpha+(1/R_L)\right\}^2+\left\{(h_L/R_L)D_b\cos\alpha-\sin\alpha\right\}^2\right]^{\frac{3}{2}}} \\
&+K_t\alpha=Q_\alpha\big/m_{tot}\Omega^2L_0^2\,. \qquad (3.17)
\end{aligned}
$$

In Eqs. (3.15), (3.16) and (3.17), prime denotes differentiation with respect to τ. Non-dimensional spring and damper constants are defined as

$$K_b=\frac{k_b}{m_{tot}\Omega^2},\ C_b=\frac{c_b}{m_{tot}\Omega},\ \text{and}\ K_t=\frac{k_t}{m_{tot}\Omega^2L_0^2}\,. \qquad (3.18)$$

The Earth's gravitational constant is scaled to

$$\lambda=\mu\big/\left(\Omega^2R^3\right). \qquad (3.19)$$

Finally, non-dimensional integrals appearing in the equations are

$$\hat{I}_i=\int_0^1\exp[F(\xi)]\xi^{i-1}d\xi\,,\ i=1,2,3, \qquad (3.20)$$

where

$$F(\xi)=\frac{R^2}{\bar{h}R_G\left(1+\varepsilon_0\right)}\left\{\frac{3}{2}-\frac{R_G}{\left[R+\xi\left(1+\varepsilon_0\right)L_0\right]}-\frac{\left[R+\xi\left(1+\varepsilon_0\right)L_0\right]^2}{2R_G^2}\right\}. \qquad (3.21)$$

3.3 Generalized Forces

To complete the problem formulation, the generalized forces Q_i must be expressed in terms of the system's external loads and states. For p differential forces $\mathbf{dF}_j$ acting at a point located a distance $\mathbf{r}_j$ from the origin of the inertial frame, the generalized forces are found using

$$Q_i = \sum_{j=1}^{p} \int \mathbf{dF}_j \cdot \frac{\partial \mathbf{r}_j}{\partial q_i}. \tag{3.22}$$

There are two external forces to examine. The first is the driving force of the motor acting on the climber. The thrust F_T exerted by the climber's motor will act in the direction of its motion so that

$$\mathbf{F_T} = F_T \mathbf{i} = F_T \left(\cos\alpha \mathbf{e_v} + \sin\alpha \mathbf{e_h} \right). \tag{3.23}$$

The other external load is due to aerodynamic effects. Aerodynamic forces act on the ribbon as a distributed force in the vertical and horizontal direction as

$$\mathbf{dF_{air}} = dF_v \mathbf{e_v} + dF_h \mathbf{e_h}. \tag{3.24}$$

The aerodynamic forces acting on the climber itself are not studied in this thesis, as they are not as important to consider as those acting on the ribbon. The ribbon is *always* present in the lower atmosphere of the Earth, where aerodynamic forces are large. The climber will pass through, but probably not rest at ribbon positions of such low altitudes. The position vectors of the point of application of the distributed force on the ribbon and the point force on the climber are listed in Eq. (3.1). The generalized forces can now be found using Eq. (3.22), and are presented in Table 3.1.

Table 3.1 Generalized forces for rigid ribbon, mobile base model

Q_i	From motor thrust on climber	From aerodynamic force on ribbon
Q_{db}	$F_T \sin\alpha$	F_h
Q_α	0	$\int s(\cos\alpha dF_h - \sin\alpha dF_v)$
Q_{de}	F_T	0

3.4 Aerodynamic Forces

The segment of ribbon within the atmosphere of the Earth will experience aerodynamic forces. For this thesis, only the first one hundred kilometres of atmosphere are considered, as the density of air becomes negligible by comparison beyond this point. So, the region of altitude of interest may be defined as $0 \le alt \le h_{atm}$, where h_{atm} = 100 km. In this region, air may be treated as a continuum (Regan *et al*, 1993). The aim is to find accurate expressions for the vertical and horizontal components of the aerodynamic forces, dF_v and dF_h, respectively. In Figure 3.2, $\mathbf{v}_{\mathbf{rel}}$ is the velocity of air relative to that of an arbitrary point P on the ribbon. The velocity of air in the atmosphere is the sum of $\mathbf{v}_{\mathbf{atm}}$, a constant velocity representing the rotating atmosphere and $\mathbf{v}_{\mathbf{wind}}$, the wind velocity, which incorporates any deviations from this. Therefore,

$$\mathbf{v}_{\mathbf{rel}} = \mathbf{v}_{\mathbf{atm}} + \mathbf{v}_{\mathbf{wind}} - \mathbf{v}_{\mathbf{P}}, \tag{3.25}$$

and

$$\mathbf{v}_{\mathbf{atm}} = \mathbf{\Omega} \times \mathbf{r}_{\mathbf{P}}. \tag{3.26}$$

dF_L and dF_D are the lift and drag components of the aerodynamic force applied at point P. The drag acts in the direction of the relative velocity vector, and the lift acts perpendicular to it.

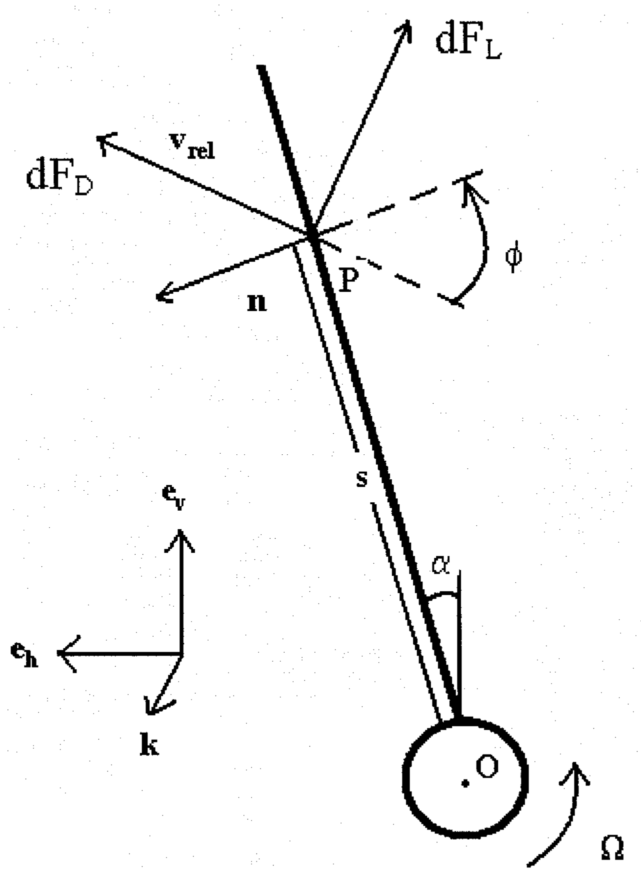

Figure 3.2: Variables for aerodynamic force calculation

In a continuum, a good approximation for the differential lift and drag forces are (Hoerner, 1958)

$$dF_L = C_D q \sin\phi \left|\cos\phi\right| dA\,, \tag{3.27}$$

and

$$dF_D = C_D q \cos\phi \left|\cos\phi\right| dA\,, \tag{3.28}$$

where ϕ is the angle between $\mathbf{v_{rel}}$ and unit normal $\mathbf{n}$. The latter is given by

$$\mathbf{n} = -\sin\alpha \mathbf{e_v} + \cos\alpha \mathbf{e_h}\,. \tag{3.29}$$

The dynamic pressure q is given by

$$q = \left(\tfrac{1}{2}\right)\rho_{air}\left(\mathbf{v}_{\mathbf{rel}} \bullet \mathbf{v}_{\mathbf{rel}}\right). \tag{3.30}$$

Furthermore, C_D is the coefficient of aerodynamic drag, and dA is the infinitesimal surface area exposed to the relative velocity. The cosine and sine of ϕ are obtained from

$$\cos\phi = \frac{\mathbf{v}_{\mathbf{rel}} \bullet \mathbf{n}}{\left|\mathbf{v}_{\mathbf{rel}}\right|} \quad \text{and} \quad (\sin\phi)\mathbf{k} = \frac{\mathbf{v}_{\mathbf{rel}} \times \mathbf{n}}{\left|\mathbf{v}_{\mathbf{rel}}\right|}. \tag{3.31}$$

The lift and drag forces both have components in the local vertical and horizontal directions. Through an appropriate transformation of the lift and drag forces, the vertical and horizontal components of the aerodynamic force, which are required for generalized force computation, may be found:

$$dF_v = C_D q\left|\cos\phi\right| dA\left\{2\sin\phi\cos\phi\cos\alpha + \left(1-2\cos^2\phi\right)\sin\alpha\right\}, \tag{3.32}$$

$$dF_h = C_D q\left|\cos\phi\right| dA\left\{\left(2\cos^2\phi - 1\right)\cos\alpha + 2\sin\phi\cos\phi\sin\alpha\right\}. \tag{3.33}$$

The above expressions are only valid for the rigid ribbon model of the space elevator. The density of air in the atmosphere, ρ_{air}, is a function of altitude, and may be approximated by an exponentially decaying function given by (Regan *et al*, 1993)

$$\rho_{air} = \rho_0 e^{-alt/H}, \tag{3.34}$$

where

$$alt = \left\|\mathbf{r}_{\mathbf{P}}\right\| - R. \tag{3.35}$$

Using atmospheric data for the first 100 km of altitude compiled in (Hanwant, 1995), a best-fit exponential curve yielded $\rho_0 = 1.3$ kg/m^3, $H = 7074$ m.

3.5 Prescribed Motion of the Climber

To examine the effect of the climber on the space elevator system, its motion $D_e(\tau)$ is prescribed. The expression for $D_e(\tau)$ is obtained for a particular type of ascension from its initial non-dimensional altitude D_i to its final one D_f. Like D_e, these values are non-dimensionalized with respect to L_0. The motion that will be used for all numerical simulations, shown in Figure 3.3, has three phases of non-dimensional duration T_a, T_c and T_d, respectively.

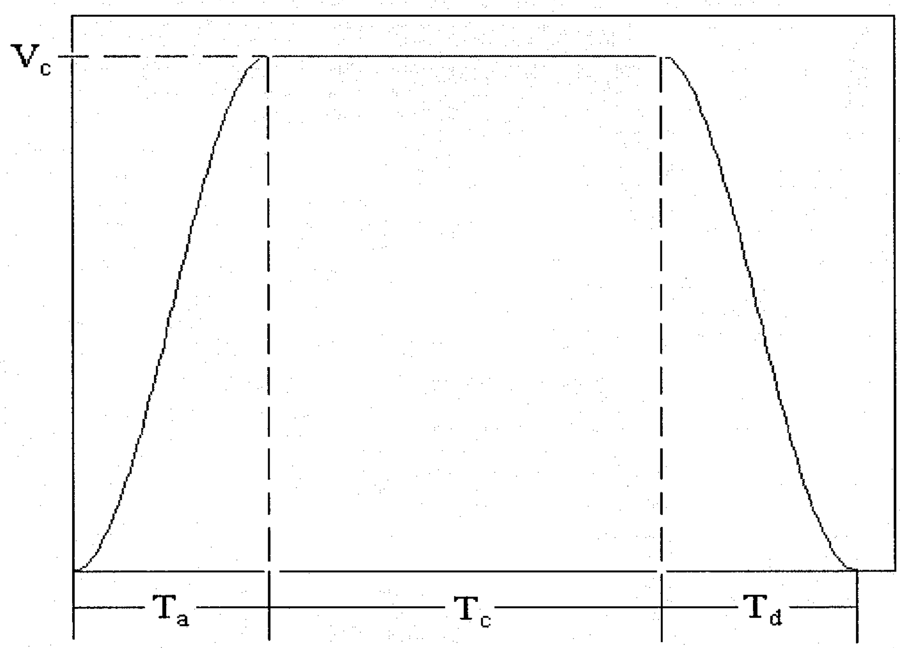

Figure 3.3: Velocity profile of climber, $D_e'(\tau)$

In phase one, the climber accelerates as a half-sinusoid curve from rest to its cruise velocity, which is non-dimensionalized with respect to $L_0\Omega$ to V_c. In phase two, the climber maintains this cruise velocity. In the final phase, the climber decelerates as a half-sinusoid to rest as it reaches D_f. This velocity profile is convenient because the resulting acceleration profile has no discontinuities. $D_e''=0$ initially, at both breakpoints, and at the end of the motion.

For this thesis, the acceleration and deceleration phases are assumed to take equal amounts of time, so that $T_a = T_d$. Then, the prescribed motion is defined by just four parameters: D_i, T_a, T_c and V_c. The motion can be written mathematically in terms of these parameters as

$$D_e(\tau) = \begin{bmatrix} D_i + \frac{V_c}{2}\left\{\tau - \frac{T_a}{\pi}\sin\left(\frac{\pi\tau}{T_a}\right)\right\} & \text{for } 0 \le \tau \le T_a \\ D_i + V_c\left(\tau - \frac{T_a}{2}\right) & \text{for } T_a \le \tau \le T_a + T_c \\ D_i + \frac{V_c}{2}\left\{\tau + T_c - \frac{T_a}{\pi}\sin\left(\frac{\pi(\tau - T_c)}{T_a}\right)\right\} & \text{for } T_a + T_c \le \tau \le 2T_a + T_c \end{bmatrix}. \tag{3.36}$$

Velocity and acceleration expressions can be found through differentiation.

The four motion parameters are useful for expressing the motion, but not useful for conducting a parametric analysis. For this, the parameter $T_R = T_a / T_c$ (time of acceleration to time of cruise ratio) is introduced, and will be referred to as the climbing time ratio. The prescribed motion from one ribbon position to another may now be defined by the four motion parameters: D_i, D_f, V_c and T_R. T_c may be calculated from

$$T_c = \frac{\left(D_f - D_i\right)}{V_c\left(1 + T_R\right)}. \tag{3.37}$$

Chapter 4: Basic Dynamical Behaviour of the Space Elevator

4.1 Equilibrium and Stability

To understand the nature of the dynamics of the space elevator, its equilibrium configurations are first investigated. For this section only, the degree of freedom d_e is non-dimensionalized with respect to the radius of the Earth: $\bar{D}_e = d_e / R$.

First, the simplest case is considered. The base and the ribbon are forced into their nominal positions. The equation of motion for a climber on a vertical ribbon is given by

$$\bar{r}'' = \bar{r} - \frac{\lambda}{\bar{r}^2}. \tag{4.1}$$

In Eq. (4.1), non-dimensional $\bar{r} = \bar{D}_e + 1$, and λ is the non-dimensional gravitational constant defined in Eq. (3.19). Prime denotes differentiation with respect to non-dimensional time τ defined in Eq. (3.14). Of course, the equilibrium position for the climber is at the geostationary altitude, given by

$$\bar{r}_{eq} = \lambda^{1/3} = R_G / R, \tag{4.2}$$

or

$$\bar{D}_{e,eq} = \lambda^{1/3} - 1. \tag{4.3}$$

Equation (4.1) can be integrated to yield

$$\bar{v}^2 = \bar{r}^2 + 2\lambda/\bar{r} + c\,, \tag{4.4}$$

where $\bar{v} = \bar{r}'$ is the non-dimensional velocity of the climber and c is a constant of integration. The interested reader is referred to McInnes (2005) for a discussion of the nature of these trajectories. An important observation is that the equilibrium point is a saddle point and is unstable.

In the second case, the system of a climber *and* a freely rotating ribbon is considered. The two-degree-of-freedom system of $\bar{D}_e$ and α is obtained by setting $D_b = 0$ in Eqs. (3.15) and (3.17), and making the substitution, $D_e = R_L\bar{D}_e$. It is given by

$$\bar{D}_e'' = (1+\alpha')^2\bar{D}_e + \cos\alpha - \lambda\frac{(\bar{D}_e + \cos\alpha)}{\left[1+\left(\bar{D}_e\right)^2 + 2\left(\bar{D}_e\right)\cos\alpha\right]^{\frac{3}{2}}}, \tag{4.5}$$

and

$$\begin{aligned}\left\{M_e R_L^2\bar{D}_e^2 + M_c + M_p\hat{I}_3\right\}\alpha'' &= -R_L\left\{M_p\hat{I}_2 + M_e R_L\bar{D}_e + M_c\right\}\sin\alpha - 2R_L^2(1+\alpha')M_e\bar{D}_e\bar{D}_e' \\ &+ \frac{\lambda M_e R_L^2\bar{D}_e\sin\alpha}{\left[1+\left(\bar{D}_e\right)^2 + 2\left(\bar{D}_e\right)\cos\alpha\right]^{\frac{3}{2}}} + \lambda M_p\sin\alpha R_L\int_0^1\frac{e^{F(\xi)}\xi}{\left[1+(\xi/R_L)^2 + 2(\xi/R_L)\cos\alpha\right]^{\frac{3}{2}}}d\xi \\ &+ \frac{\lambda M_c R_L\sin\alpha}{\left[1+(1/R_L)^2 + (2/R_L)\cos\alpha\right]^{\frac{3}{2}}} - K_t\alpha\,.\end{aligned} \tag{4.6}$$

For this two-degree-of-freedom system to be in equilibrium,

$$\bar{D}_e^{\,2} + 2\bar{D}_e\cos\alpha = \lambda^{2/3} - 1\,, \tag{4.7}$$

must be satisfied, along with

$$M_p \sin\alpha \left\{ \lambda \int_0^1 \frac{\exp[F(\xi)]\xi}{\left[1+(\xi/R_L)^2+2(\xi/R_L)\cos\alpha\right]^{\frac{3}{2}}} d\xi - \hat{I}_2 \right\}$$

$$+M_c \sin\alpha \left\{ \frac{\lambda}{\left[1+(1/R_L)^2+2(1/R_L)\cos\alpha\right]^{\frac{3}{2}}} - 1 \right\} - (1/R_L) K_t \alpha = 0. \tag{4.8}$$

$\bar{D}_e + \cos\alpha = 0$ is another possibility for equilibrium, but it will never be satisfied since $\bar{D}_e \geq 0$, and the expected range for the libration angle is $-5 < \alpha < 5$ degrees. One equilibrium configuration for this system (the one with practical importance) is $\bar{D}_e = \lambda^{1/3} - 1$ (climber at geosynchronous altitude) and $\alpha = 0$ (vertical ribbon). This result was expected from examination of the simpler climber case. Infinite configurations satisfying Eq. (4.7) exist. It would seem that if the design parameters are carefully chosen, Eq. (4.8) could also be satisfied for a variety of α (assuming small α). However, doing so is akin to forcing the libration angle of the space elevator to be neutrally stable. Regardless, for any reasonable values of the ribbon length and taper ratio, Eq. (4.8) cannot be satisfied unless the tower is vertical. As such, practically speaking, the system does not have an equilibrium position other than

$$\mathbf{x_{eq}} = [\bar{D}_e, \alpha]_{eq} = [\lambda^{1/3} - 1, 0]. \tag{4.9}$$

Linearization about $\mathbf{x_{eq}}$ yields the following equations of motion, valid only in its vicinity:

$$\delta\bar{D}_e'' = A\delta\bar{D}_e + B\delta\alpha',$$
$$\delta\alpha'' = C\delta\alpha + D\delta\bar{D}_e',$$

where

$$A = 3,$$

$$B = 2\left(\lambda^{1/3} - 1\right),$$

$$C = \frac{R_L\left[M_p\left\{\lambda\int_0^1 \frac{\exp[F(\xi)]\xi}{\left[1+\xi(1/R_L)\right]^3}d\xi - \hat{I}_2\right\} + M_c\left\{\frac{\lambda}{\left[1+1/R_L\right]^3} - 1\right\} - K_t\right]}{\left\{M_e R_L^2\left(\lambda^{1/3}-1\right)^2 + M_c + M_p\hat{I}_3\right\}},$$

and

$$D = \frac{-2M_e R_L^2\left(\lambda^{1/3}-1\right)}{\left\{M_e R_L^2\left(\lambda^{1/3}-1\right)^2 + M_c + M_p\hat{I}_3\right\}}. \tag{4.10}$$

The coefficient C has a negative value. It is zero only for the limiting case, where the length of the ribbon extends only up to the geosynchronous altitude and $K_t = 0$. For realistic ribbon lengths, say from 75 000 km to 120 000 km, $-0.036 < C < -0.03$. C is negligibly influenced by design parameters m_e and A_m. The coefficient D has a negative value, which resembles the shape of C as L_0 is increased. D is proportional to the mass of the climber m_e and inversely proportional to the maximum cross-sectional area A_m, but is always several orders of magnitude smaller than C, since M_e is much smaller than M_c or M_p. An eigenvalue analysis of the system shows that the equilibrium position $[\bar{D}_e, \alpha]_{eq} = [\lambda^{1/3} - 1, 0]$ is unstable. The four eigenvalues are $E = [\pm E_R, \pm iE_I]$, where $E_R \cong \sqrt{3}$, varying slightly in response to changes in D, and $E_I \cong 0.18$, varying slightly in response to changes in C. The coupled motion of the ribbon libration and climber position is unstable; what this means is that if the climber is given a displacement from its equilibrium position, it will continue to further displace. However, the α motion is stable (the space elevator structure is stable).

4.2 Closed Form Solution for Libration Angle due to Climber Transit

The aim of this section is to obtain a closed-form solution for the libration angle response of the space elevator ribbon due to climber transit. If the translation of the base is ignored in Eq. (3.17), the second order non-linear ordinary differential equation describing the libration angle response to a traversing climber is given by

$$\begin{aligned}
&\left(M_e D_e^2 + M_c + M_p \hat{I}_3\right)\alpha'' = -R_L\left(M_p \hat{I}_2 + M_e D_e + M_c\right)\sin\alpha - 2(1+\alpha')M_e D_e D_e' \\
&+\frac{\lambda M_e R_L D_e \sin\alpha}{\left[1+(D_e/R_L)^2+2(D_e/R_L)\cos\alpha\right]^{\frac{3}{2}}} + \lambda M_p R_L \sin\alpha \int_0^1 \frac{\exp[F(\xi)]\xi}{\left[1+(\xi/R_L)^2+2(\xi/R_L)\cos\alpha\right]^{\frac{3}{2}}} d\xi \\
&+\lambda M_c R_L \frac{\sin\alpha}{\left[1+(1/R_L)^2+2(1/R_L)\cos\alpha\right]^{\frac{3}{2}}} - K_t\alpha .
\end{aligned} \tag{4.11}$$

It is assumed here that the climber position D_e is prescribed as a function of time. Since the libration angle will be less than one degree even in a worst case-excitation scenario (this assumption will be validated later), the equation can be easily linearized by letting $\cos\alpha = 1$ and $\sin\alpha = \alpha$. The linearized equation is given by

$$\begin{aligned}
&\left(M_e D_e^2 + M_c + M_p \hat{I}_3\right)\alpha'' = -R_L\left(M_p \hat{I}_2 + M_e D_e + M_c\right)\alpha - 2(1+\alpha')M_e D_e D_e' \\
&+\lambda M_e R_L^4 \frac{D_e\alpha}{(D_e+R_L)^3} + \lambda M_p R_L^4 \alpha \int_0^1 \frac{\exp[F(\xi)]\xi}{(\xi+R_L)^3} d\xi + \lambda M_c R_L^4 \frac{\alpha}{(1+R_L)^3} - K_t\alpha .
\end{aligned} \tag{4.12}$$

The above equation can be expressed as

$$\alpha'' + g(\tau)\alpha' + h(\tau)\alpha = -g(\tau), \tag{4.13}$$

where

$$h(\tau)=\frac{R_L\left(M_p\hat{I}_2+M_eD_e+M_c\right)-\lambda R_L^4\left\{\frac{M_eD_e}{[D_e+R_L]^3}+M_p\int_0^1\frac{\exp[F(\xi)]\xi}{[\xi+R_L]^3}d\xi+\frac{M_c}{[1+R_L]^3}\right\}+K_t}{M_eD_e^2+M_c+M_p\hat{I}_3},$$

and

$$g(\tau)=\frac{2M_eD_eD_e'}{\left(M_eD_e^2+M_c+M_p\hat{I}_3\right)}. \tag{4.14}$$

Finally, noting that the mass of the ribbon and counterweight are much larger than the mass of the climber, Eq. (4.13) can be well approximated as:

$$\alpha''+g(\tau)\alpha'+W^2\alpha=-g(\tau), \tag{4.15}$$

where W is a constant and is given by

$$W=\sqrt{\frac{\left[R_L\left(M_p\hat{I}_2+M_c\right)-\lambda R_L^4\left\{M_p\int_0^1\frac{\exp[F(\xi)]\xi}{[\xi+R_L]^3}d\xi+\frac{M_c}{[1+R_L]^3}\right\}+K_t\right]}{\left(M_c+M_p\hat{I}_3\right)}}. \tag{4.16}$$

W is the non-dimensional natural frequency of oscillation of the libration angle α. It depends mainly upon the length of the ribbon and its taper ratio. In Figure 4.1, the non-dimensionalized natural frequency of libration for a nominally stretched ribbon measuring 100,000 km is plotted for a wide range of taper ratios. The non-dimensional period of libration is given by $2\pi/W$. Since W is non-dimensionalized with respect to the spin rate of the Earth, the dimensional period of oscillation of α in days is given by $1/W$. For anticipated numerical values of the space elevator ($L\approx 100{,}000$ km and $3<A_m/A_0<10$), this period will be about five days.

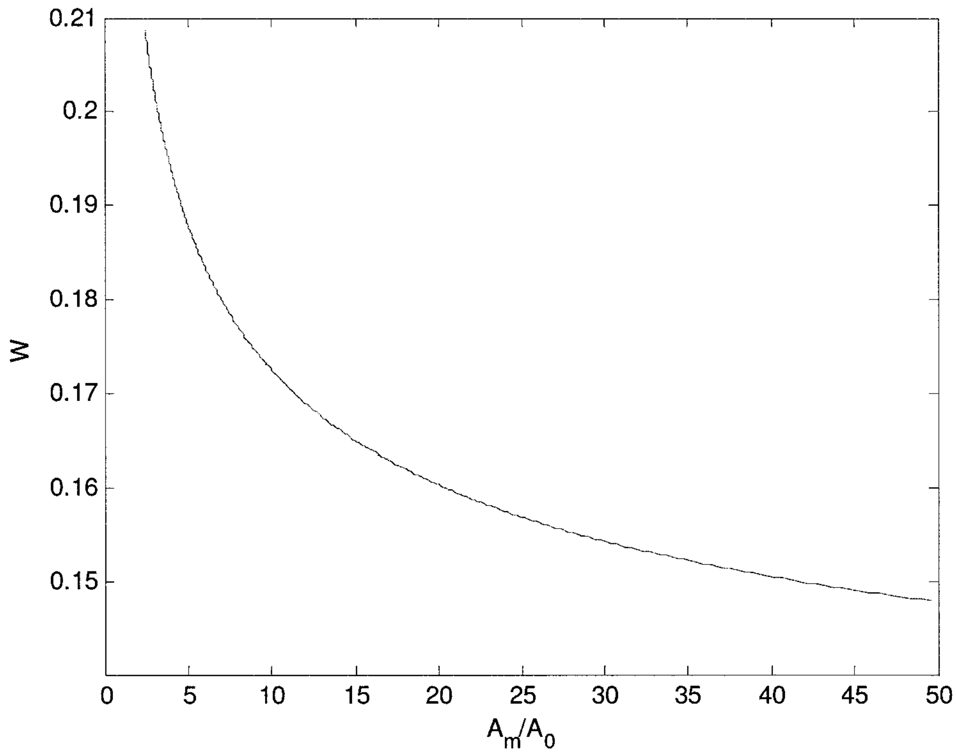

Figure 4.1: Non-dimensional natural frequency of libration (*W*) vs. taper ratio; *L* = 100,000 km

An analytical expression for $\alpha(\tau)$ may be found for a climber transit with constant speed. If the climber goes from D_i to D_f with constant velocity V_c, its position, velocity and acceleration are given by

$$D_e = V_c \tau + D_i$$
$$D_e' = V_c,$$

and

$$D_e'' = 0. \tag{4.17}$$

In reality, the climber will experience some form of ramp up and down in velocity. However, if the climber is to move a long distance, this ramp up and down time will be short in comparison to the cruising time. Thus, to simplify the analysis, climber acceleration and deceleration are approximated as being instantaneous for this analysis.

In other words, the time ratio introduced in Section 3.5 is taken as zero. For a climber with uniform motion, Eq. (4.15) has a closed form solution. It may be found using the substitution:

$$\alpha = \frac{z}{M_e D_e^2 + M_c + M_p \hat{I}_3}. \tag{4.18}$$

Then,

$$z'' + f(\tau) z = -2 M_e D_e D_e',$$

where

$$f(\tau) = W^2 + g(\tau)\left(g(\tau) - \frac{D_e'}{D_e} - \frac{D_e''}{D_e'} \right). \tag{4.19}$$

Inputting the prescribed climber velocity and acceleration given in Eq. (4.17), and using the space elevator property that the climber mass is very small compared to that of the ribbon and counterweight,

$$f(\tau) = W^2 + \left(\bar{M}_e V_c D_e\right)^2 - \bar{M}_e V_c^2,$$

where

$$\bar{M}_e = 2M_e \big/ \left(M_c + M_p \hat{I}_3\right). \tag{4.20}$$

The following observations of the values making up $f(\tau)$ are made:

i. $0 \le D_e \le 1$

ii. $\bar{M}_e$ is $O(M_e) = O(10^{-3})$

iii. For a high cruise speed (say, 500 km/hr), non-dimensional $V_c = O(10^{-2})$

iv. $W^2 = O(R_L) = O(10^{-2})$

Based on these observations, $f(\tau) \cong W^2$. The closed form solution to the libration angle excited by constant climber speed may be easily found:

$$\alpha(\tau) = \frac{c_1 \cos(W\tau) + c_2 \sin(W\tau)}{\left\{M_e (V_c\tau + D_i)^2 + M_c + M_p \hat{I}_3\right\}} - \frac{\bar{M}_e V_c}{W^2}(V_c\tau + D_i),$$

where

$$c_1 = \left(M_e D_i^2 + M_c + M_p \hat{I}_3\right)\left(\alpha_0 + \frac{\bar{M}_e V_c D_i}{W^2}\right),$$

and

$$c_2 = \left(M_e D_i^2 + M_c + M_p \hat{I}_3\right)\left(\frac{\alpha_0'}{W} + \frac{\bar{M}_e V_c^2}{W^3}\right) + \frac{2M_e D_i V_c}{W}\left(\alpha_0 + \frac{\bar{M}_e V_c D_i}{W^2}\right). \tag{4.21}$$

α_0 and α_0' are the initial libration angle and rate, respectively. From Eq. (4.21), the libration angle is the sum of oscillatory terms and a linear term in time. The oscillatory terms decay when the climber ascends, but grow when it descends. This result is due to the rate-dependent term that is present in the equation of motion (4.15). However, because this term is small, the decay/growth of the oscillations that occur during a climber's ascent/descent is also small; the fractional decay/growth is of the order of M_e. This is small enough to be neglected. It may be concluded that the space elevator dynamics due to an ascending *or* descending climber are well behaved. This good behaviour is attributed to the fact that the climber mass is small with respect to the rest of the space elevator structure and that the ribbon itself is not actually being deployed or retrieved.

Equation (4.21) may be well approximated by

$$\alpha(\tau) \cong \alpha_0 \cos(W\tau) + \frac{\alpha_0'}{W}\sin(W\tau) + \frac{\bar{M}_e V_c}{W^2}\left[D_i\left\{\cos(W\tau) - 1\right\} + V_c\left\{\frac{\sin(W\tau)}{W} - \tau\right\}\right]. \tag{4.22}$$

The above expression is useful for devising climbing procedures. It may be noted that the additional libration introduced by a climber is of the order of $\bar{M}_e V_c\left(D_f - D_i\right)/W^2$

radians, which, based on earlier observations, is on the order of 10^{-3} radians. In general, this additional libration is proportional to the climber mass, the cruising velocity and the distance traveled. It is important to note that all three of these parameters have upper bounds. Even if all three of them approach their respective maximum values, the libration induced by climber transit will still be of the order of milliradians. Still, in general, minimizing the climber mass and cruise velocity serves as a general guideline for minimizing climber transit effects.

When the climber is stationary, the libration angle is excited only by the initial conditions. It then behaves much like a pendulum, oscillating about its vertical equilibrium position. If $\alpha(\tau_f) = \alpha_f$ and $\alpha'(\tau_f) = \alpha'_f$ at the moment a climber arrives at its destination, the libration that would ensue is given by:

$$\alpha(\tau) = \alpha_{res} \cos\left(W\tau - \psi\right), \text{ where}$$
$$\alpha_{res} = \sqrt{\alpha_f^2 + \left(\alpha'_f / W\right)^2}, \text{ and}$$
$$\psi = \tan^{-1}\left(\alpha'_f / W\alpha_f\right). \tag{4.23}$$

It is important to note that in the absence of aerodynamic forces, the oscillatory motion of the ribbon is entirely undamped.

The complete closed-form solution for the response of the libration angle to climber transit can be shown by considering both Eqs. (4.22) and (4.23). Let $\tau_f = \left(D_f - D_i\right)/V_c$. Then, the response to a climber having constant speed V_c, beginning its motion at D_i when $\tau = 0$, and arriving at D_f when $\tau = \tau_f$, is well approximated by:

$$\alpha(\tau)=\alpha_0\cos(W\tau)+\frac{\alpha_0'}{W}\sin(W\tau)$$
$$+\frac{\bar{M}_e V_c}{W^2}\left\{D_i\left(\cos(W\tau)-1\right)+V_c\left(\frac{\sin(W\tau)}{W}-\tau\right)\right\} \qquad 0\le\tau<\tau_f$$
$$\alpha(\tau)=\alpha_{res}\cos\left[W\left(\tau-\tau_f\right)-\psi\right] \qquad \tau_f\le\tau \qquad (4.24)$$

Figure 4.2 shows the effect of a climber's ascent from the surface of the Earth to the tip of the ribbon on the libration of the ribbon. The analytical results are compared with those from a numerical simulation. The numerical simulation was run using the Matlab software. The ode45 function was used to integrate Eqs. (3.16) and (3.17) using a relative tolerance of 10^{-5}. The absolute tolerance for the libration angle and rate were 10^{-7} rad and 10^{-10} rad/s, respectively. The absolute tolerance of the base position and velocity were 10^{-3} m and 10^{-6} m/s, respectively. The base position scaling factor, h, was set to 10 m. The design components of the space elevator that were used are L_0 = 100,000 km, σ_0 =35 GPa, γ = 1300 kg/m^3, E = 1 TPa and A_m = 10 mm^2. The climber mass was 800 kg. As a result, $\bar{M}_e = 0.0013$ and W = 0.183. The mass of the base was set to 50,000 tons (an approximate value for an oil tanker). At the beginning of the simulation, the space elevator was in its nominal configuration (zero initial conditions). The motion parameters of the climber were set to D_i = 0, D_f = 1, V_c = 0.0111 (280 km/hr), and T_R = 0.1. The torsional spring constant is many orders of magnitude too small to have much effect. Also, the spring and damper constants to hold the base in place were set to zero (no anchor).

Once the climber begins its ascent, Coriolis effects excite the libration angle by a sum of oscillatory terms and a first order polynomial. The Earth spins towards the east.

Since the libration angle is negative (against the spin of Earth) during transit, it can be concluded that the Coriolis effects push the ribbon westward. Upon climber arrest, the residual libration (libration amplitude) is a function of the final libration state. Here, the residual libration is about 0.81 mrad. Clearly, the ensuing oscillatory motion with this amplitude is undamped.

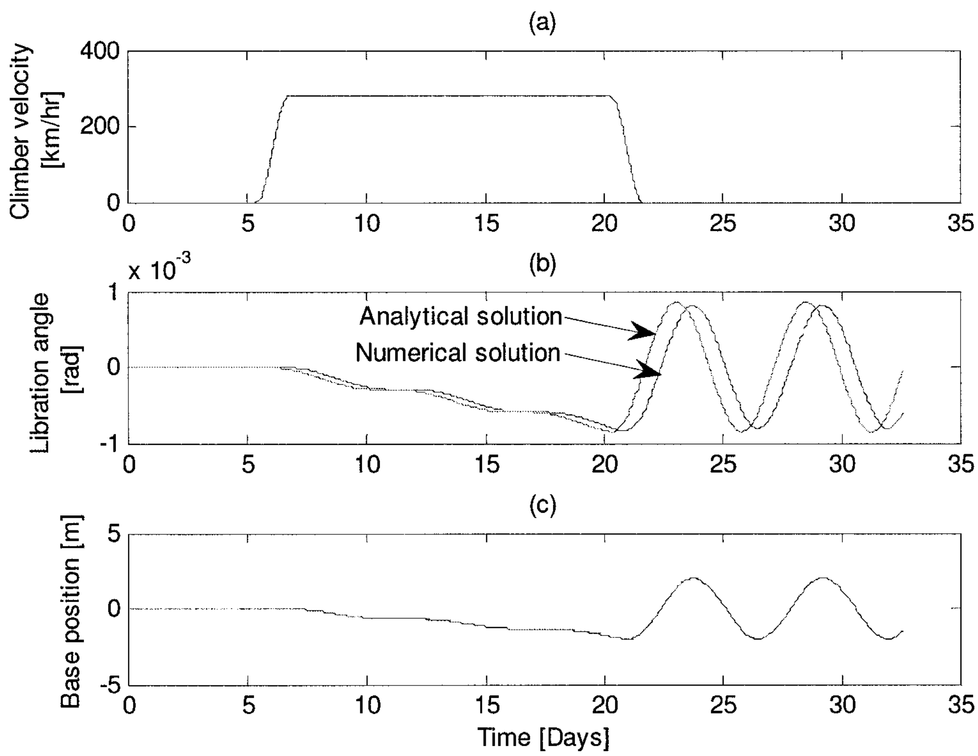

Figure 4.2: The effect of a climber ascending from the bottom of the ribbon to the top on the space elevator: (a) Climber velocity; (b) Libration angle obtained numerically and analytically; (c) Base position

In Figure 4.2-b, the analytical solution shown in Eq. (4.24) is plotted alongside the numerical ones. There is some phase error in the analytical solutions, but the amplitudes are similar. The phase error comes from assuming the acceleration and deceleration of the climber to be instantaneous for the analytical solution; both processes took 32 hours in this simulation. Thus, there is approximately a one-day shift in the in-transit solutions, and a two-day shift in the steady-state solutions. Also, the numerical solutions, which correspond to a high climbing ratio, have a lower residual libration than that which the analytical one, having a zero time ratio, predicts. The reason for this is explained in Section 4.3.1. If a numerical simulation is run with a much lower value of T_R, the analytical solutions are practically indecipherable from the numerical ones.

In Figure 4.2-c, it is observed that the base motion in response to an ascending climber is similar to that of the libration angle. However, even without an anchor, the displacement of the base is only a few meters. It can thus be concluded that climber transit has little effect on generalized coordinate d_b.

The libration response for climber descent is different than that for climber ascent. Figure 4.3 shows the libration response from a numerical simulation where a climber descends from the top of the ribbon to the bottom (in the same manner with which it ascended in the previous example). Coriolis effects act in the opposite direction, pushing the ribbon eastward. However, as the climber moves downward, its force causes a smaller moment about the base, allowing the ribbon to return west. Greater libration oscillations are experienced *during* climber transit for descent than for ascent.

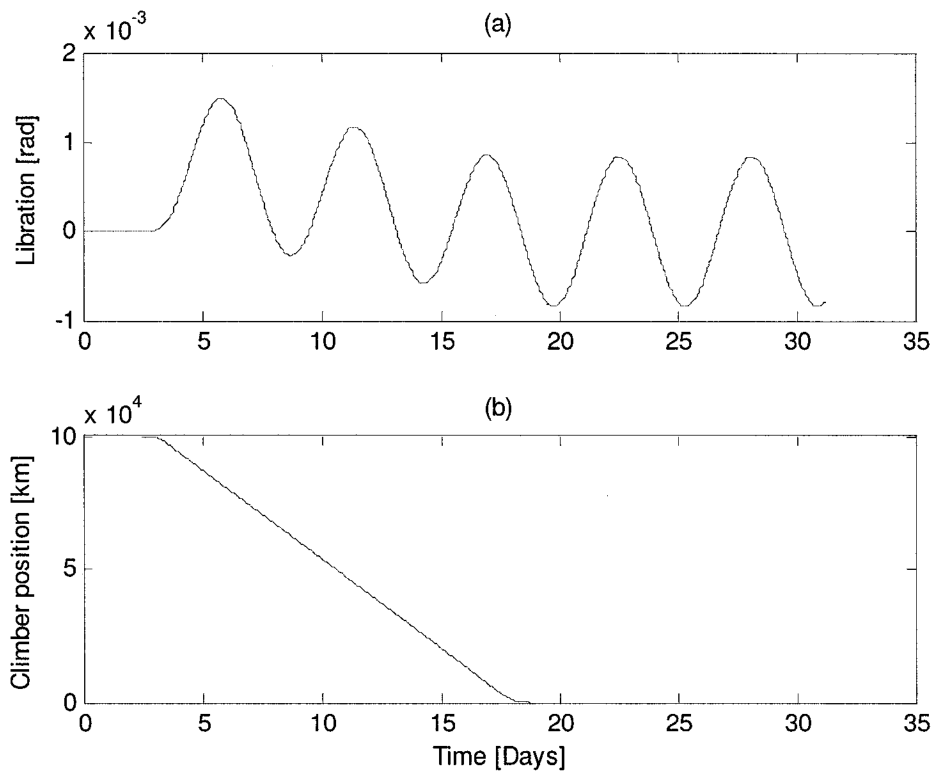

Figure 4.3: The effect of a climber descending from the top of the ribbon to the bottom on its libration:
(a) Libration angle obtained numerically; (b) Climber position

It can be shown that a single ascending or descending climber having constant cruise speed will always induce a residual libration angle into a static ribbon. In order for a single climber to induce no libration angle, *both* the libration angle and rate must be zero when the climber reaches its destination. The response to a constant rate of climb is given by

$$\alpha(\tau) = \alpha_0 \cos(W\tau) + \frac{\alpha_0'}{W}\sin(W\tau) + \frac{\bar{M}_e V_c}{W^2}\left[D_i\{\cos(W\tau)-1\} + V_c\left\{\frac{\sin(W\tau)}{W} - \tau\right\}\right],$$

$$\alpha'(\tau) = -W\alpha_0 \sin(W\tau) + \alpha_0' \cos(W\tau) + \frac{\bar{M}_e V_c}{W^2}\left[-WD_i \sin(W\tau) + V_c\{\cos(W\tau)-1\}\right]. \quad (4.25)$$

An initially static ribbon has an initial libration angle and rate of zero. It is not difficult to ensure that $\alpha'(\tau_f)=0$. This may be accomplished by choosing a value of cruise speed such that the trigonometric components are in phase with each other. However, for an ascending climber, it is impossible to ensure that $\alpha(\tau_f)=0$. For a climber ascending an initially static ribbon,

$$\alpha(\tau)=\frac{\bar{M}_e V_c}{W^2}\left[D_i\left\{\cos(W\tau)-1\right\}+\frac{V_c}{W}\left\{\sin(W\tau)-W\tau\right\}\right]. \tag{4.26}$$

The excitation to the libration angle caused by the climber is clearly the sum of two terms: the first is ≤ 0, and the second is <0 because $W\tau>\sin(W\tau)$ for all time. Since $\alpha(\tau_f)<0$, a climber ascending at a constant rate will always induce a residual libration angle.

For a descending climber, $D_i>0$, and V_c can be rewritten as $-|V_c|$, and so the closed-form solution becomes

$$\alpha(\tau)=-\frac{\bar{M}_e|V_c|}{W^2}\left[D_i\left\{\cos(W\tau)-1\right\}-|V_c|\left\{\frac{\sin(W\tau)}{W}-\tau\right\}\right],$$

$$\alpha'(\tau)=-\frac{\bar{M}_e|V_c|}{W^2}\left[-WD_i\sin(W\tau)-|V_c|\left\{\cos(W\tau)-1\right\}\right]. \tag{4.27}$$

To make both the libration angle and rate equal zero at $\tau=\tau_f$, the following two conditions must be satisfied:

$$\left(\frac{1-\cos x}{\sin x}\right)=\frac{x}{2}, \tag{4.28}$$

where $x=W\tau_f$, and

$$|V_c|=2D_i/\tau_f. \tag{4.29}$$

If Eq. (4.29) is satisfied, $D_f = D_i - |V_c|\tau_f = -D_i$. Since $0 \le D_e(\tau) \le 1$, $D_f = -D_i$ may only be satisfied if both D_i and D_f are zero. Therefore, as is the case with an ascending climber, descent at a constant rate will always induce a residual libration angle.

4.3 Recommended Climbing Procedures

In general, reducing climber mass and cruise velocity reduces the libration angle upon arrival. Still, it has been shown that a single climber ascending or descending the ribbon at a constant cruise speed will introduce non-zero libration that will cause undamped oscillations on the order of milliradians. It is thus desirable to minimize the effects of a climber transit on the libration angle. In this section, three climbing procedures are proposed. The first procedure is a means of passive control through choosing an appropriate time ratio. The second procedure involves *using* the Coriolis effect of the climber to bring an oscillating ribbon to rest. The third and most general climbing procedure involves the proper phasing of multiple climbers so that a static ribbon is returned to equilibrium after all of the climber transits are complete.

4.3.1 Increasing the Time Ratio to Minimize Transit Effects

The analytical results have been obtained by taking the acceleration and deceleration of the climber to be instantaneous. However, varying the time ratio has a profound effect on the residual libration of the ribbon that is induced through climber transit. This can be shown by running numerical simulations. The time ratio used for the simulation in Section 4.2 was 0.1. These simulations have been repeated varying only the time ratio of the climber, keeping V_c fixed. As a result, the total time of the transits vary as well. In Figure 4.4, the residual libration due to climber transit is plotted against time ratio values ranging from 0.001 to 1.5. Clearly, the residual libration is lower for climber transits having larger time ratios. Using a time ratio of 1.5 instead of 0.001 decreases the residual libration upon arrival by 30 times. The increase in the time ratio adds only 9 days to the transit, which, for T_R = 0.001, would be a lengthy 15 days anyway.

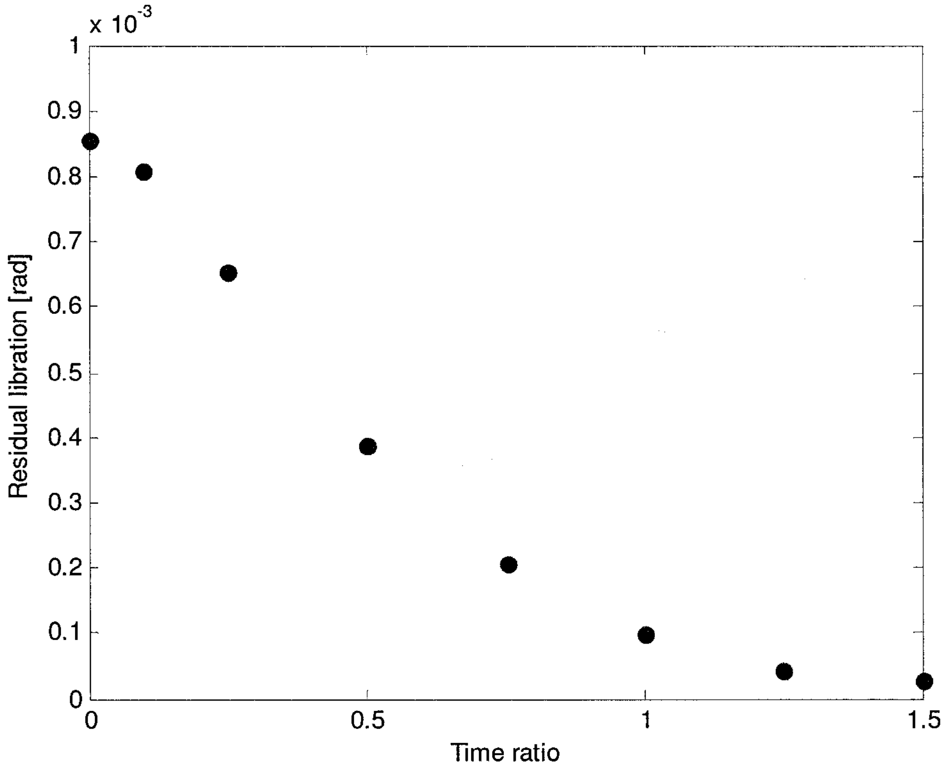

Figure 4.4: Residual libration of ribbon for Earth to tip transit for various time ratios; transit at 280 km/hr

The reason for the decrease in residual libration for a high time ratio is not intuitive. A quick ramp up and down in velocity does not cause a sudden growth in libration. The decrease in residual libration is accomplished through gradual deceleration of the climber (and its corresponding decrease in applied Coriolis force), which allows the libration angle to return slowly back towards zero as the climber undergoes the deceleration phase of its motion. So, the rate of climber deceleration is significant as far as libration is concerned, whereas that of acceleration is not.

4.3.2 Eliminating Residual Libration with a Single Climber

A single climber, going from D_i to D_f can be used to eliminate an existing residual libration angle, α_{res}, as long as a specific cruise speed and corresponding climber mass is chosen. α_{res} may have been originally induced by a previous climber, but also by aerodynamic forces, or another form of excitation.

If $\alpha_{res} \neq 0$, and a climber is sent from D_i to D_f at the moment when $\alpha = +\alpha_{res}$ (i.e. maximum eastward displacement), the state equations are:

$$\begin{aligned} \alpha(\tau) &= \alpha_{res}\cos(W\tau) + \frac{\bar{M}_e V_c}{W^2}\left[D_i\{\cos(W\tau)-1\} + V_c\left\{\frac{\sin(W\tau)}{W} - \tau\right\}\right], \\ \alpha'(\tau) &= -W\alpha_{res}\sin(W\tau) + \frac{\bar{M}_e V_c}{W^2}\left[-WD_i\sin(W\tau) + V_c\{\cos(W\tau)-1\}\right]. \end{aligned} \tag{4.30}$$

Forcing $\tau_f = 2\pi n/W$, $n = 1, 2, 3\ldots$, results in the final libration state:

$$\alpha(\tau_f) = \alpha_{res} - \frac{\bar{M}_e V_c^2}{W^2}\tau_f \quad \text{and} \quad \alpha'(\tau_f) = 0. \tag{4.31}$$

For a constant cruise speed given by

$$V_c = \frac{D_f - D_i}{\tau_f} = \frac{W\left(D_f - D_i\right)}{2\pi n}, \text{ where } n = 1, 2, 3\ldots \tag{4.32}$$

zero residual libration occurs if

$$\alpha_{res} = \frac{\bar{M}_e\left(D_f - D_i\right)^2}{2\pi n W}. \tag{4.33}$$

Substituting for $\bar{M}_e$ using Eq. (4.20), and then for each mass ratio, the appropriate climber mass, expressed in terms of α_{res}, is given by

$$m_e = \frac{\pi\left(m_c + \rho_m L_0 \hat{I}_3\right)W}{\left(D_f - D_i\right)^2} n\alpha_{res}, \text{ where } n = 1, 2, 3\ldots \tag{4.34}$$

Therefore, if a climber going from D_i to D_f is released at the moment when the ribbon, oscillating with amplitude α_{res}, has libration $\alpha = +\alpha_{res}$, there are several climber mass and velocity pairings one can choose to ensure that the ribbon returns to equilibrium upon its arrival. These pairings, given by Eqs. (4.32) and (4.34), are dependent on which value of n is chosen. Since the climber mass has an upper bound, large values for n (corresponding to slower transits) may not be available. Similarly, a maximum allowable cruise velocity may limit the available values of n.

The appropriate climber mass/velocity pairings detailed above may be useful whenever a single climber is sent from one position on the ribbon to another. It applies for both climber ascent and descent.

4.3.3 Not Introducing Libration into a Static Ribbon Using Multiple Climbers

Multiple climbers undergoing the same prescribed motion can induce no oscillatory libration angle into a static ribbon if they begin their respective trajectories a specific number of days apart.

Let p climbers go from one point to another on the ribbon in the same fashion. Regardless of what kind of prescribed motion is taken in the climbing phase, each approximately independent equation will yield its own nearly identical residual libration angle, α_{res}, and phase shift, ψ, causing the ribbon to oscillate upon its arrival. There is a simple method to ensure that the net residual libration angle is zero.

For p climbers having the same prescribed motion (not limited to constant speed trajectory), but leaving some time, $\hat{\tau}_i$ after $\tau = 0$, the libration after the final climber comes to rest is found using Eq. (4.23) and is given by

$$\alpha(\tau) = \alpha_{res} \sum_{i=1}^{p} \left[\cos\left\{ W\left(\tau - \tau_f - \hat{\tau}_i\right) - \psi \right\} \right]. \tag{4.35}$$

Again, τ_f is the time it takes for each climber to complete its transit. Forcing $\alpha(\tau) = 0$, the appropriate times for the i^{th} climber to begin its respective ascent (or descent) in order to force a net residual libration of zero, $\hat{\tau}_i^*$, may be determined:

$$\hat{\tau}_i^* = \frac{2\pi(i-1)(pn+1)}{pW} \quad \text{for } n = 0,1,2... \tag{4.36}$$

What this means, is that in order to avoid inducing a residual libration angle in a static ribbon when sending p climbers, one must simply send each climber with the same prescribed motion, $(pn+1)/pW$ days apart, where $n = 0,1,2...$ (noting that the non-dimensional time τ is 2π times the number of days). A desirable consequence of this motion guideline is that for the case where $n = 0$, all of the oscillatory behaviour of the ribbon vanishes for the period of time when all p climbers are in transit. So, for this case, if there are only a few climbers climbing a long stretch of the ribbon, there is a smooth, linear response to the libration angle for the majority of the transit.

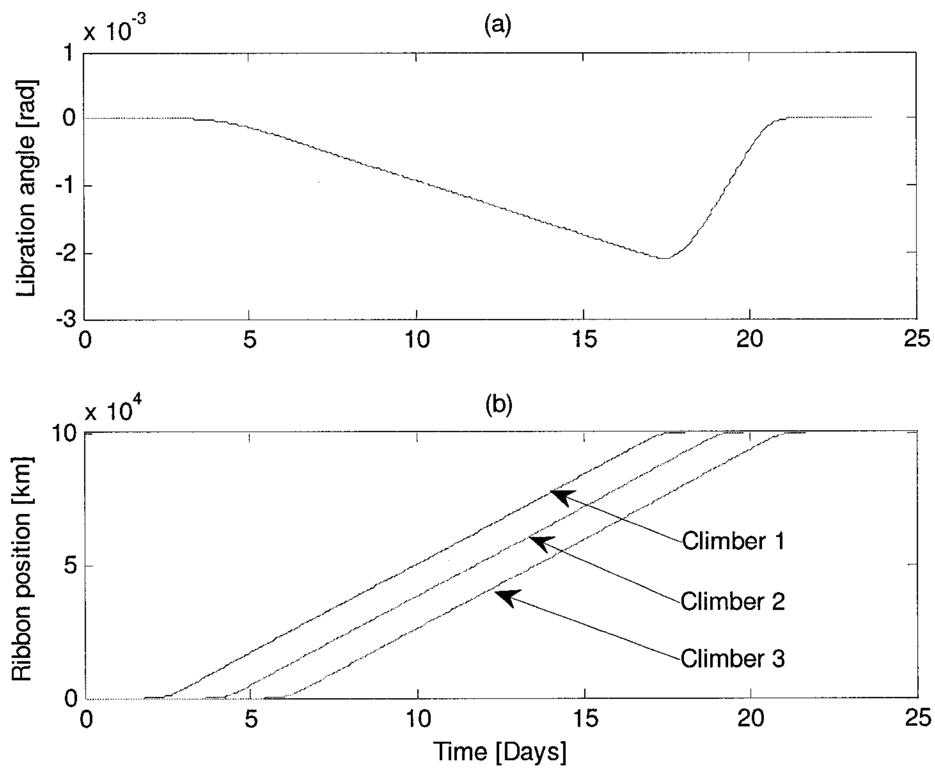

Figure 4.5: The effect of three appropriately spaced climbers ascending from the bottom to the top of the ribbon on the libration angle of the space elevator (a) Libration angle (b) Ribbon position of each climber

For simulations involving more than one climber, the equations of motion change. Any terms containing the climber mass must be replaced by a sum of terms from 1 to p, with climber mass, position, velocity, and acceleration indexed for each individual climber. The multiple climber (with $n = 0$) case is illustrated in Figure 4.5. In this simulation, run in the same fashion as the previous ones, *three* climbers are sent from the Earth to the tip of the space elevator using a time ratio of 0.1. The spacing between the climbers is exactly $1/(pW)$, or about 1.82 days. Due to this proper phasing, the libration angle returns to zero once the final climber reaches its destination, as predicted by the climbing procedure. It is observed that in transit, the maximum libration of the ribbon is nearly three times the residual libration caused by a single climber. That is because the effect of each of the climbers is summed. Also, as predicted, the sinusoidal components of the libration angle vanish once all of the climbers are cruising; since the climbers have constant velocity, the libration angle response varies linearly with time for much of the transit. The progression of the libration angle back to zero appears to be linear as well.

This multiple climber procedure will be particularly useful during the initial phase of the space elevator's operation, when a new climber is sent up the ribbon every so often (hours apart) to thicken it. In the previous literature (Edwards, 2000), the time between climber ascents was determined based only on when the additional ribbon stress due to the additional climber would be acceptable (a climber adds only a small amount of stress to the ribbon once it is sufficiently high). The above conclusion shows that the specific time between sent climbers is crucial in avoiding the induction of a potentially large libration angle. If each climber induces approximately 1 milliradian of libration, the hundreds of climbers that it will take to thicken the ribbon sufficiently could add over 0.1

radians (6 degrees) of libration collectively (if phased improperly), which is unacceptable. Equation (4.36) offers a method of avoiding such an occurrence.

The ability to eliminate any residual libration with one climber, and to not introduce libration into a static ribbon by using multiple climbers, forms a basis for the control of ribbon libration through climber ascent or descent. The methods illustrated here will yield nearly perfect results for a rigid ribbon. Modifications to these climbing procedures due to the fact that the ribbon will undergo elastic deformation are discussed in Chapter 5.

4.4 Rotation of the Ribbon due to Aerodynamic Forces

Another major source of ribbon libration will come from aerodynamic forces in the lower atmosphere of the Earth. This section aims to determine the order of magnitude that such forces will have on the ribbon. Since the libration angle is very small, $\cos\alpha \cong 1$ and $\sin\alpha \cong 0$. The wind is assumed invariant, blowing in the local horizontal direction ($\mathbf{e_h}$), and the relative velocity of air is taken as the wind velocity, v_w. As a result, the angle ϕ becomes zero. The effective width of the ribbon exposed to aerodynamic forces is taken as the constant, b_{eff}. Using Eqs. (3.32) and (3.33), the vertical component of aerodynamic force is zero, and the horizontal one is given by

$$dF_h = C_D q dA = C_D \left(\frac{1}{2}\right) \rho_{air} v_w^2 b_{eff} ds . \tag{4.37}$$

Inputting the air density function derived in Section 3.4,

$$dF_h = \left(\tfrac{1}{2}\right) C_D b_{eff} \rho_0 e^{-s/H} v_w^2 ds. \tag{4.38}$$

The generalized moment due to aerodynamics applied on the generalized coordinate α is then given by

$$\begin{aligned} Q_\alpha &= \int_0^{h_{atm}} s\,dF_h = \left(\tfrac{1}{2}\right) C_D b_{eff} \rho_0 v_w^2 \int_0^{h_{atm}} s e^{-s/H} ds \\ &= \left(\tfrac{1}{2}\right) C_D \rho_0 \left[H^2 - H\left(H + h_{atm}\right)\exp\left(-h_{atm}/H\right)\right] b_{eff} v_w^2. \end{aligned} \tag{4.39}$$

Since $H \ll h_{atm}$,

$$Q_\alpha \cong \left(\tfrac{1}{2}\right) C_D \rho_0 H^2 b_{eff} v_w^2. \tag{4.40}$$

The simplified, non-dimensionalized second order differential equation describing the libration angle of the rigid tether in response to aerodynamic loading is given by

$$\alpha'' + W^2 \alpha = \frac{Q_\alpha}{m_{tot}\Omega^2 L_0^2 W^2 \left(M_c + M_p \hat{I}_3\right)}. \tag{4.41}$$

Thus, the libration response to an invariant horizontal wind can be approximated by

$$\alpha(\tau) = \left[\frac{\left(\tfrac{1}{2}\right) C_D \rho_0 H^2 b_{eff} v_w^2}{\Omega^2 L_0^2 W^2 \left(m_c + \rho_m L_0 \hat{I}_3\right)} \right] \left[1 - \cos\left(W\tau\right)\right]. \tag{4.42}$$

As one would expect, the libration response is proportional to the effective width of the ribbon and the square of the wind velocity. The ribbon is modeled as a thin flat plate here, so the coefficient of aerodynamic drag, C_D, is set to 1.18 (Hoerner, 1958). The atmospheric constants are $\rho_0 = 1.3$ kg/m^3 and H = 7074 m. Substituting the space elevator parameters $\gamma = 1{,}300$ kg/m^3, E = 1 TPa, $\sigma_0 = 35$ GPa, A_m = 10 mm^2, and L = 100,000 km, the response becomes

$$\alpha(\tau) \approx 8 \cdot 10^{-5} b_{eff} v_{wind}^2 \left\{1 - \cos\left(W\tau\right)\right\}. \tag{4.43}$$

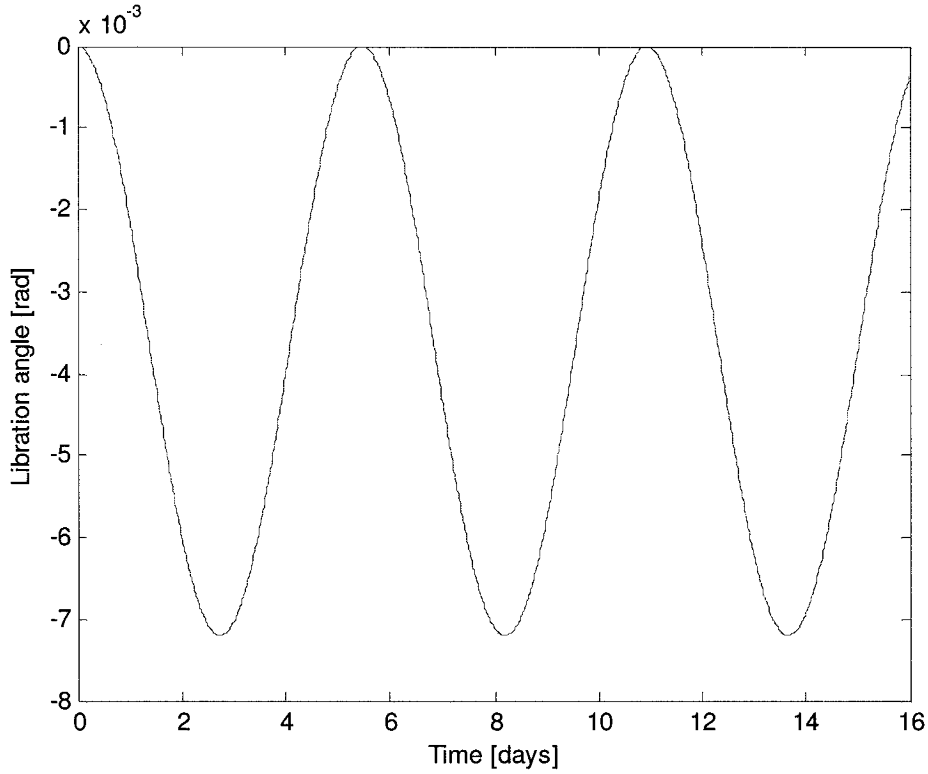

Figure 4.6: Libration response to worst-case-scenario wind loading;
b_{eff} = 5 cm, v_w = 30 m/s

Finally, a worst-case-scenario is examined for the libration response to aerodynamic loading. Although the cross-sectional area of the ribbon is of the order of mm^2, one of its rectangular dimensions will be of the order of centimetres. Thus, in this example, the effective width is set to 5 cm. The constant wind is taken as 30 m/s, blowing westward, which is an *extremely* high wind, especially since the space elevator will likely be stationed in a location where high winds are uncommon. Figure 4.6 shows the libration response to this worst-case-scenario for wind loading. The amplitude of oscillations in libration is of the order of milliradians. It can thus be concluded that aerodynamic effects on libration will only be as great as climber transit effects in a worst-case-scenario. Winds of such high magnitudes are unlikely to arise, and would certainly not remain constant for a period of days. Aerodynamic effects may be decreased if a cord-like cross-section, were used for the portion of ribbon in the lower atmosphere of the Earth, rather than a rectangular one. Then, the effective width would be of the order of millimetres at most.

The aerodynamic analysis in this section was done in an order of magnitude sense. To get a more accurate depiction of the effect of aerodynamic loading on the ribbon, its structural deformation must be taken into account.

Chapter 5: Elastic Tether, Stationary Base Model

5.1 Description of the System

The space elevator model studied in this chapter differs from the one considered in Chapter 3 in two ways: the ribbon has a finite modulus of elasticity such that it may now undergo structural deformation, and the base is fixed in place to simplify the model. The motion of the base was found to be negligible in Chapter 4, and has little effect on the rest of the system; hence it is ignored here for simplicity.

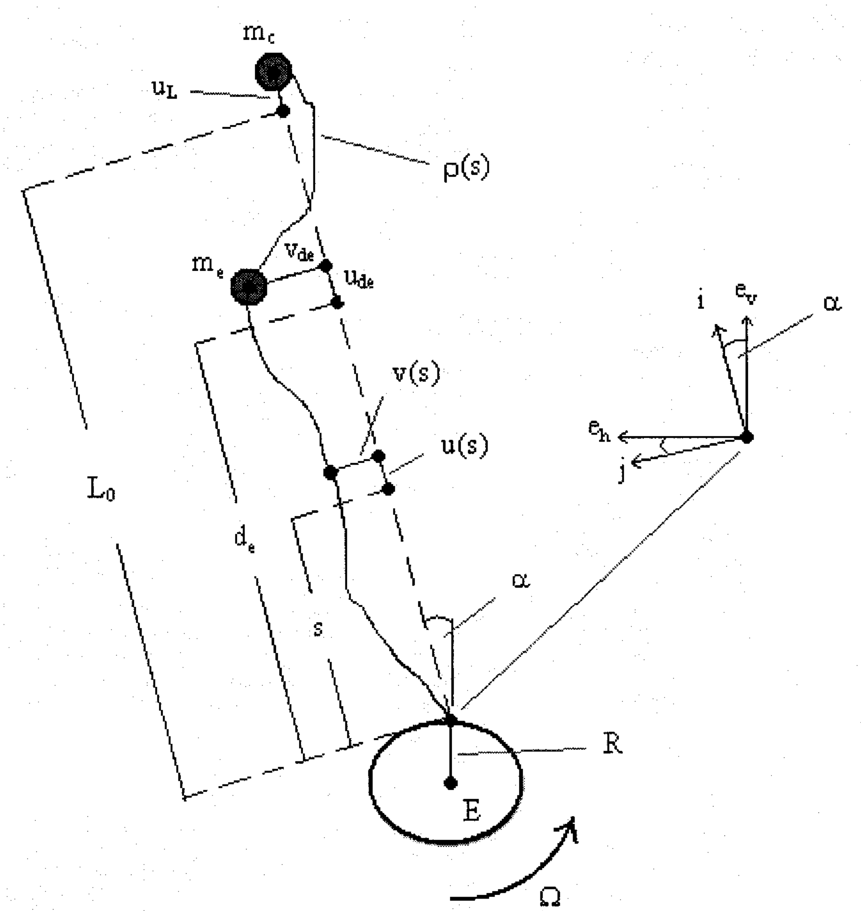

Figure 5.1: Dynamics model of the space elevator with an elastic ribbon

Figure 5.1 shows the dynamics model considered in this chapter. The generalized coordinates d_e and α are as previously defined in Chapter 3. Generalized coordinate d_b vanishes in this model. The longitudinal and lateral displacements of the ribbon are denoted by u and v, respectively, as functions of the position on the ribbon. The assumed modes method (Meirovitch, 1997) is used to describe these displacements: both u and v are discretized as products of generalized coordinates and spatial basis functions. The longitudinal extension is assumed to be a polynomial of s as follows:

$$u = \sum_{i=1}^{N} a_i(t) s^i \, . \tag{5.1}$$

N generalized coordinates, a_i, are used to describe this extension. The basis function s^0 is not used so that the boundary condition, $u = 0$ for $s = 0$, is satisfied at all times. Polynomials are particularly good basis functions as their integration is not computation intensive. The lateral displacement is assumed to be a sum of sinusoidal terms of s as

$$v = \sum_{i=1}^{M} b_i(t) \sin\left(\frac{i\pi s}{L_0}\right). \tag{5.2}$$

M generalized coordinates, b_i, are used to describe this displacement. The sinusoidal basis functions satisfy the boundary conditions: $v(0,t) = v(L_0,t) = 0$. Generalized coordinates d_e, α, a_i and b_i fully define this N+M+2 degree-of-freedom system.

5.2 Additional Lateral Extension Term for Aerodynamic Loading

As observed from the aerodynamic study conducted by Lang (2005b), sinusoidal modes alone cannot fully describe the lateral displacement of the ribbon due to aerodynamic loading. The distributed force caused by the atmosphere of the Earth causes pronounced lateral displacement in the lower portion of the ribbon. As a result, if the lateral displacement of the ribbon in the presence of aerodynamic forces is to be well-modelled, an additional generalized coordinate and corresponding basis function need to be used. The basis function may be chosen by examining the governing equation of the lateral displacement of a ribbon, and neglecting all other generalized coordinates. For a ribbon having a constant cross-sectional area, the lateral extension v of a ribbon element at time t and space coordinate s is governed approximately by

$$\frac{\partial^2 v}{\partial t^2} = k\frac{\partial^2 v}{\partial s^2} + f, \tag{5.3}$$

where f is an applied force and k is a constant. The cross-sectional area of the ribbon varies very little across the region where the aerodynamic forces are considered. Since a basis function is a function of s alone, the *steady state* ($\partial^2 v/\partial t^2 = 0$) solution of Eq. (5.3) to aerodynamic loading is sufficient. The forcing function for constant wind loading is proportional to $\exp(-s/H)$ (Section 3.4). Since the *shape* of the basis function is all that is of interest (not the constants attached to it), it may be found using

$$\frac{\partial^2 v_a}{\partial s^2} = \exp(-s/H). \tag{5.4}$$

Applying the boundary conditions that $v_a = 0$ for $s = 0$ and $s = L_0$, the solution to Eq. (5.4) is

$$v_a = H^2\left[\exp(-s/H) - 1 - \frac{s}{L_0}\{\exp(-L_0/H) - 1\}\right]. \tag{5.5}$$

Again, the H^2 multiplier is irrelevant because only the shape of the basis function is important. Since $\exp(-L_0/H) << 1$, the additional spatial basis function that will be used to describe the lateral extension response of the space elevator is given by

$$v_a = \exp(-s/H) - 1 + \frac{s}{L_0}. \tag{5.6}$$

As seen in Figure 5.2, the basis function given by Eq. (5.6) has a bubble. After the bubble, the function moves back to a value of zero at the tip in a quasi-linear fashion. This basis function is very useful because it allows for near-horizontal ribbon departure angles, which are predicted by the ribbon snapshots obtained numerically by Lang (2005b). The maximum value of this basis function occurs at the ribbon position

$$s^* = -H \ln(H/L_0), \tag{5.7}$$

and is given by

$$|v_a|_{\max} = \frac{H}{L_0}\left[1 - \ln\left(\frac{H}{L_0}\right)\right] - 1. \tag{5.8}$$

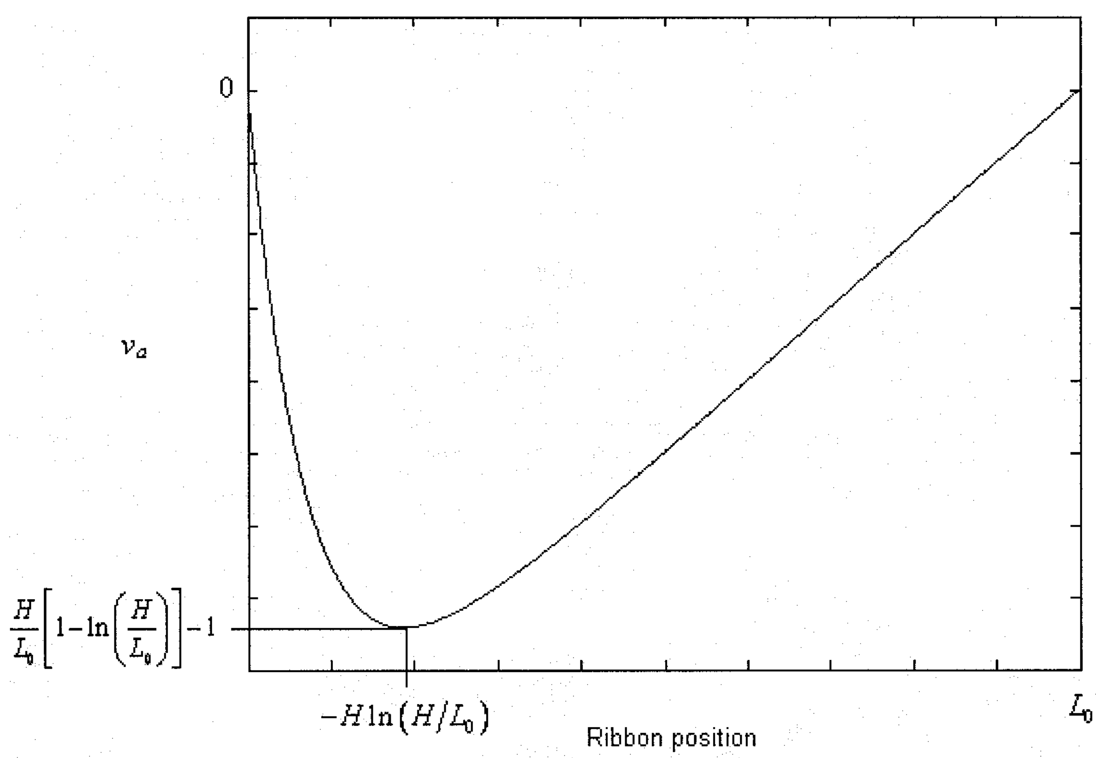

Figure 5.2: Shape of the aerodynamic lateral basis function v_a with ribbon position

H is four orders of magnitude smaller than L_0. As a result, $s^* \leq 0.001L_0$. The bubble will thus occur at a much lower ribbon position than indicated by Figure 5.2.

For numerical simulations involving non-zero aerodynamics, the lateral displacement of the system will be defined by

$$v = \sum_{i=1}^{M} b_i(t)\sin\left(\frac{i\pi s}{L_0}\right) + c(t)v_a, \tag{5.9}$$

where c is another generalized coordinate. As such, the dynamics model describing the space elevator in such a situation will have N+M+3 degrees of freedom.

5.3 Energy Expressions and Equations of Motion

The same method as that employed in Section 3.2 is used to obtain the equations of motion of this more complex system. The radial positions of the various system components are now given by

$$\begin{aligned}
&\mathbf{r_E} = (R\cos\alpha + d_e + u_{de})\mathbf{i} + (v_{de} - R\sin\alpha)\mathbf{j}, \\
&\mathbf{r_R}(s) = (R\cos\alpha + s + u)\mathbf{i} + (v - R\sin\alpha)\mathbf{j}, \text{ and} \\
&\mathbf{r_C} = (R\cos\alpha + L_0 + u_L)\mathbf{i} - R\sin\alpha\mathbf{j}.
\end{aligned} \tag{5.10}$$

The velocity components are given by

$$\begin{aligned}
&\mathbf{v_E} = \{R\Omega\sin\alpha + \dot{d}_e + \dot{u}_{de} - (\Omega + \dot{\alpha})v_{de}\}\mathbf{i} + \{R\Omega\cos\alpha + \dot{v}_{de} + (\Omega + \dot{\alpha})(d_e + u_{de})\}\mathbf{j}, \\
&\mathbf{v_R}(s) = \{R\Omega\sin\alpha + \dot{u} - (\Omega + \dot{\alpha})v\}\mathbf{i} + \{R\Omega\cos\alpha + \dot{v} + (\Omega + \dot{\alpha})(s + u)\}\mathbf{j}, \text{ and} \\
&\mathbf{v_C} = \{R\Omega\sin\alpha + \dot{u}_L\}\mathbf{i} + \{R\Omega\cos\alpha + (\Omega + \dot{\alpha})(L_0 + u_L)\}\mathbf{j}.
\end{aligned} \tag{5.11}$$

In Eq. (5.11),

$$\dot{u} = \sum_{i=1}^{N} \dot{a}_i s^i \,, \tag{5.12}$$

and

$$\dot{v} = \sum_{i=1}^{M} \dot{b}_i \sin\left(\frac{i\pi s}{L_0}\right) + \dot{c} v_a \,. \tag{5.13}$$

Expressions for the kinetic and potential energy functions are obtained as in Section 3.2, with one exception: the elastic potential energy term is now given by

$$P_{EL} = \frac{1}{2} E \int_0^{L_0} A(s) \left[\left(\frac{\partial u}{\partial s}\right)^2 + \frac{\partial u}{\partial s}\left(\frac{\partial v}{\partial s}\right)^2 + \frac{1}{2}\left(\frac{\partial v}{\partial s}\right)^4 - \left(\frac{\partial u}{\partial s}\right)^2 \left(\frac{\partial v}{\partial s}\right)^2 \right] ds + \frac{1}{2} k_t \alpha^2 \,. \tag{5.14}$$

A spring and damper, previously used to model the effects of an anchor restricting the motion of the base, are no longer required. However, because the system may now undergo structural deformation, Eq. (5.14) contains a strain energy term. The strain energy expression, which omits fifth order terms and higher, is derived in (Min *et al*, 1999). A linear stress-strain relation was assumed in deriving it. Since the longitudinal expression includes the nominal extension caused by the nominal strain in the ribbon, the general strain energy term incorporates the nominal strain energy.

The N+M+3 equations of motion are obtained using the Lagrange equation. For the generalized coordinates d_e, α, a_k (k = 1…N), b_k (k = 1…M) and c, the equations of motion are, respectively,

$$
\begin{aligned}
&\ddot{d}_e + \ddot{u}_{de} - \ddot{\alpha} v_{de} \\
&= (\Omega + \dot{\alpha}) \dot{v}_{de} - R\Omega\dot{\alpha}\cos\alpha + \left\{ R\Omega\sin\alpha + \dot{u}_{de} - (\Omega + \dot{\alpha}) v_{de} \right\} \left\{ \dot{u}^* - (\Omega + \dot{\alpha}) v^* \right\} \\
&+ \left\{ R\Omega\cos\alpha + \dot{v}_{de} + (\Omega + \dot{\alpha})(d_e + u_{de}) \right\} \left\{ \dot{v}^* + (\Omega + \dot{\alpha})(1 + u^*) \right\} \\
&- \mu \frac{(R\cos\alpha + d_e + u_{de})(1 + u^*) + (v_{de} - R\sin\alpha) v^*}{\left[(R\cos\alpha + d_e + u_{de})^2 + (v_{de} - R\sin\alpha)^2 \right]^{3/2}} + \frac{Q_{de}}{m_e},
\end{aligned} \tag{5.15}
$$

$$
\begin{aligned}
&\ddot{\alpha} \left[m_e \left\{ (d_e + u_{de})^2 + v_{de}^2 \right\} + \int_0^{L_0} \rho(s) \left\{ (s+u)^2 + v^2 \right\} ds + m_c (L_0 + u_L)^2 \right] \\
&+ m_e \left\{ \ddot{v}_{de} (d_e + u_{de}) - v_{de} \ddot{d}_e - v_{de} \ddot{u}_{de} \right\} + \int_0^{L_0} \rho(s)(s+u)\ddot{v}\, ds - \int_0^{L_0} \rho(s) v \ddot{u}\, ds \\
&= m_e \dot{d}_e \left[\begin{array}{l} v^* \left\{ \dot{d}_e + \dot{u}_{de} - 2(\Omega + \dot{\alpha}) v_{de} + R\Omega\sin\alpha \right\} - \dot{v}^* (d_e + u_{de}) \\ -u^* \left\{ \dot{v}_{de} + 2(\Omega + \dot{\alpha})(d_e + u_{de}) + R\Omega\cos\alpha \right\} + \dot{u}^* v_{de} \end{array} \right] \\
&- 2(\Omega + \dot{\alpha}) \left[m_e \left\{ (d_e + u_{de})(\dot{u}_{de} + \dot{d}_e) + v_{de}\dot{v}_{de} \right\} + \int_0^{L_0} \rho(s) \left\{ (s+u)\dot{u} + v\dot{v} \right\} ds + m_c (L_0 + u_L) \dot{u}_L \right] \\
&- R\Omega^2 \left[\cos\alpha \left\{ m_e v_{de} + \int_0^{L_0} \rho(s) v\, ds \right\} + \sin\alpha \left\{ m_e (d_e + u_{de}) + \int_0^{L_0} \rho(s)(s+u)\, ds + m_c (L_0 + u_L) \right\} \right] \\
&+ \frac{\mu R m_e \left\{ (d_e + u_{de})\sin\alpha + v_{de}\cos\alpha \right\}}{\left\{ (R\cos\alpha + d_e + u_{de})^2 + (v_{de} - R\sin\alpha)^2 \right\}^{\frac{3}{2}}} + \mu R \int_0^{L_0} \frac{\rho(s) \left\{ (s+u)\sin\alpha + v\cos\alpha \right\}}{\left\{ (R\cos\alpha + s + u)^2 + (v - R\sin\alpha)^2 \right\}^{\frac{3}{2}}} ds \\
&+ \mu R m_c \frac{(L_0 + u_L)\sin\alpha}{\left\{ (R\cos\alpha + L_0 + u_L)^2 + (R\sin\alpha)^2 \right\}^{\frac{3}{2}}} - k_t \alpha + Q_\alpha,
\end{aligned} \tag{5.16}
$$

$$
\int_0^{L_0}\left(\rho(s)s^k\sum_{i=1}^{N}\ddot{a}_i s^i\right)ds+\sum_{i=1}^{N}\ddot{a}_i\left(m_e d_e^{i+k}+m_c L_0^{i+k}\right)+m_e d_e^k\ddot{d}_e-\left(m_e d_e^k v_{de}+\int_0^{L_0}\rho(s)s^k v ds\right)\ddot{\alpha}
$$

$$
=-m_e k\dot{d}_e d_e^{k-1}\left\{R\Omega\sin\alpha+\dot{d}_e+\dot{u}_{de}-(\Omega+\dot{\alpha})v_{de}\right\}+m_e\dot{d}_e d_e^k\left\{(\Omega+\dot{\alpha})v^*-\dot{u}^*\right\}
$$

$$
+\int_0^{L_0}\rho(s)s^k\left\{2\dot{v}(\Omega+\dot{\alpha})+(\Omega+\dot{\alpha})^2(s+u)+R\Omega^2\cos\alpha\right\}ds
$$

$$
+m_e\left\{2\dot{v}_{de}(\Omega+\dot{\alpha})+(\Omega+\dot{\alpha})^2(d_e+u_{de})+R\Omega^2\cos\alpha\right\}d_e^k
$$

$$
+m_c\left\{(\Omega+\dot{\alpha})^2(L_0+u_L)+R\Omega^2\cos\alpha\right\}L_0^k
$$

$$
-\frac{\mu m_e(R\cos\alpha+d_e+u_{de})d_e^k}{\left\{(R\cos\alpha+d_e+u_{de})^2+(v_{de}-R\sin\alpha)^2\right\}^{\frac{3}{2}}}-\mu\int_0^{L_0}\frac{\rho(s)(R\cos\alpha+s+u)s^k}{\left\{(R\cos\alpha+s+u)^2+(v-R\sin\alpha)^2\right\}^{\frac{3}{2}}}ds
$$

$$
-\frac{\mu m_c(R\cos\alpha+L_0+u_L)L_0^k}{\left\{(R\cos\alpha+L_0+u_L)^2+(R\sin\alpha)^2\right\}^{\frac{3}{2}}}-kE\int_0^{L_0}A(s)s^{k-1}\left[u_s+\left(\frac{1}{2}-u_s\right)v_s^2\right]ds+Q_{a(k)}, \qquad (5.17)
$$

$$
\int_0^{L_0}\rho(s)\sin\left(\frac{k\pi s}{L_0}\right)\left\{\ddot{v}+\ddot{\alpha}(s+u)\right\}ds+m_e\sin\left(\frac{k\pi d_e}{L_0}\right)\left\{\ddot{v}_{de}+\ddot{\alpha}(d_e+u_{de})\right\}
$$

$$
=-m_e\dot{d}_e\frac{k\pi}{L_0}\cos\left(\frac{k\pi d_e}{L_0}\right)\left\{R\Omega\cos\alpha+\dot{v}_{de}+(\Omega+\dot{\alpha})(d_e+u_{de})\right\}
$$

$$
-m_e\dot{d}_e\sin\left(\frac{k\pi d_e}{L_0}\right)\left\{\dot{v}^*+(\Omega+\dot{\alpha})u^*\right\}
$$

$$
\int_0^{L_0}\rho(s)\sin\left(\frac{k\pi s}{L_0}\right)\left[(\Omega+\dot{\alpha})^2v-2(\Omega+\dot{\alpha})\dot{u}-R\Omega^2\sin\alpha\right]ds
$$

$$
+m_e\sin\left(\frac{k\pi d_e}{L_0}\right)\left\{(\Omega+\dot{\alpha})^2v_{de}-2(\Omega+\dot{\alpha})(\dot{d}_e+\dot{u}_{de})-R\Omega^2\sin\alpha\right\}
$$

$$
-\frac{\mu m_e(v_{de}-R\sin\alpha)\sin\left(\frac{k\pi d_e}{L_0}\right)}{\left\{(R\cos\alpha+d_e+u_{de})^2+(v_{de}-R\sin\alpha)^2\right\}^{\frac{3}{2}}}-\mu\int_0^{L_0}\frac{\rho(s)(v-R\sin\alpha)\sin\left(\frac{k\pi s}{L_0}\right)}{\left\{(R\cos\alpha+s+u)^2+(v-R\sin\alpha)^2\right\}^{\frac{3}{2}}}ds
$$

$$
-\frac{k\pi}{L_0}E\int_0^{L_0}A(s)\cos\left(\frac{k\pi s}{L_0}\right)\left(u_s v_s+v_s^3-u_s^2 v_s\right)ds+Q_{b(k)}, \qquad (5.18)
$$

and

$$\int_0^{L_0} \rho(s) v_a \{\ddot{v} + \ddot{\alpha}(s+u)\} ds + m_e v_a\big|_{de} \{\ddot{v}_{de} + \ddot{\alpha}(d_e + u_{de})\}$$

$$= -m_e \dot{d}_e \left.\frac{\partial v_a}{\partial s}\right|_{de} \{R\Omega\cos\alpha + \dot{v}_{de} + (\Omega+\dot{\alpha})(d_e + u_{de})\} - m_e \dot{d}_e v_a\big|_{de} \{\dot{v}^* + (\Omega+\dot{\alpha})u^*\}$$

$$\int_0^{L_0} \rho(s) v_a \left\{(\Omega+\dot{\alpha})^2 v - 2(\Omega+\dot{\alpha})\dot{u} - R\Omega^2 \sin\alpha\right\} ds$$

$$+ m_e v_a\big|_{de} \left\{(\Omega+\dot{\alpha})^2 v_{de} - 2(\Omega+\dot{\alpha})(\dot{d}_e + \dot{u}_{de}) - R\Omega^2 \sin\alpha\right\}$$

$$- \frac{\mu m_e (v_{de} - R\sin\alpha) v_a\big|_{de}}{\left\{(R\cos\alpha + d_e + u_{de})^2 + (v_{de} - R\sin\alpha)^2\right\}^{\frac{3}{2}}} - \mu \int_0^{L_0} \frac{\rho(s)(v - R\sin\alpha) v_a}{\left\{(R\cos\alpha + s + u)^2 + (v - R\sin\alpha)^2\right\}^{\frac{3}{2}}} ds$$

$$-E \int_0^{L_0} A(s) \frac{\partial v_a}{\partial s}\left(u_s v_s + v_s^3 - u_s^2 v_s\right) ds + Q_c. \tag{5.19}$$

In Eqs. (5.15) through (5.19),

$$u_s = \frac{\partial u}{\partial s} = \sum_{i=1}^{N} i a_i s^{i-1},$$

$$v_s = \frac{\partial v}{\partial s} = \frac{\pi}{L_0} \sum_{i=1}^{M} \left\{ i b_i \cos\left(\frac{i\pi s}{L_0}\right)\right\} + c\left(\frac{1}{L_0} - \frac{1}{H} e^{-s/H}\right),$$

$$u^* = \frac{\partial u_{de}}{\partial d_e} = \sum_{i=1}^{N} i a_i d_e^{\,i-1}, \text{ and}$$

$$v^* = \frac{\partial v_{de}}{\partial d_e} = \sum_{i=1}^{M} \frac{i\pi}{L_0} b_i \cos\left(\frac{i\pi d_e}{L_0}\right) + c\left(\frac{1}{L_0} - \frac{1}{H} e^{-d_e/H}\right). \tag{5.20}$$

Similarly,

$$\dot{u}^* = \sum_{i=1}^{N} i \dot{a}_i d_e^{\,i-1}, \text{ and}$$

$$\dot{v}^* = \sum_{i=1}^{M} \frac{i\pi}{L_0} \dot{b}_i \cos\left(\frac{i\pi d_e}{L_0}\right) + \dot{c}\left(\frac{1}{L_0} - \frac{1}{H} e^{-d_e/H}\right). \tag{5.21}$$

Also, the total mass, m_{tot}, no longer includes the mass of the base, as it not part of the dynamics system.

Again, for convenience, the equations describing the elastic tether space elevator are non-dimensionalized. All non-dimensional lengths introduced in Chapter 3 remain valid. In addition to those,

$$U = \sum_{i=1}^{N} A_i \xi^i = u/L_0 , \tag{5.22}$$

where

$$A_i = a_i L_0^{i-1} . \tag{5.23}$$

Also,

$$V = \sum_{i=1}^{M} B_i \sin(i\pi\xi) + CV_a = v/L_0 , \tag{5.24}$$

where

$$B_i = b_i/L_0 , \; C = c/L_0 , \tag{5.25}$$

and

$$V_a = \exp\left[-\left(L_0/H\right)\xi\right] - 1 + \xi . \tag{5.26}$$

In non-dimensional form, the equations of motion are given by

$$\begin{aligned}
&D_e'' + U_{De}'' - V_{De}\alpha'' \\
&= (1+\alpha')V_{De}' - R_L\alpha'\cos\alpha + \left\{R_L\sin\alpha + U_{De}' - (1+\alpha')V_{De}\right\}\left\{U'^{*} - (1+\alpha')V^{*}\right\} \\
&+ \left\{R_L\cos\alpha + V_{De}' + (1+\alpha')(D_e + U_{De})\right\}\left\{V'^{*} + (1+\alpha')(1+U^{*})\right\} \\
&-\lambda \frac{(D_e + R_L\cos\alpha + U_{De})(1+U^{*}) + (V_{De} - R_L\sin\alpha)V^{*}}{\left[\left\{\cos\alpha + (1/R_L)(D_e + U_{De})\right\}^2 + \left\{(1/R_L)V_{De} - \sin\alpha\right\}^2\right]^{\frac{3}{2}}} + \frac{Q_{de}}{m_e\Omega^2 L_0} ,
\end{aligned} \tag{5.27}$$

$$
\begin{aligned}
&\left[\begin{array}{l} M_e\left\{\left(D_e+U_{De}\right)^2+V_{De}^2\right\}+M_c\left(1+U_1\right)^2 \\ +M_p\left(\hat{I}_3+2\sum_{i=1}^{N}A_i\hat{I}_{i+2}+\sum_{i=1}^{N}\sum_{j=1}^{N}A_iA_j\hat{I}_{i+j+1}+\sum_{i=1}^{M}\sum_{j=1}^{M}B_iB_j\hat{K}_{i,j}\right)\end{array}\right]\alpha''-M_eV_{De}D_e'' \\
&+M_p\sum_{i=1}^{M}B_i''\left(\hat{J}_{2,i}+\sum_{j=1}^{N}A_j\hat{J}_{j+1,i}\right)-M_p\sum_{i=1}^{N}A_i''\left(\sum_{j=1}^{M}B_j\hat{J}_{i+1,j}\right)+M_e\left(D_e+U_{De}\right)V_{De}''-M_eV_{De}U_{De}'' \\
&=M_eD_e'\left[\begin{array}{l} V^*\left\{D_e'+U_{De}'-2\left(1+\alpha'\right)V_{De}+R_L\sin\alpha\right\}-V'^*\left(D_e+U_{De}\right) \\ -U^*\left\{V_{De}'+2\left(1+\alpha'\right)\left(D_e+U_{De}\right)+R_L\cos\alpha\right\}+U'^*V_{De}\end{array}\right] \\
&-R_L\left\{M_p\hat{I}_2+M_p\sum_{i=1}^{N}A_i\hat{I}_{i+1}+M_e\left(D_e+U_{De}\right)+M_c\left(1+U_1\right)\right\}\sin\alpha \\
&-R_L\left(M_eV_{De}+M_p\sum_{i=1}^{M}B_i\hat{J}_{1,i}\right)\cos\alpha \\
&-2\left(1+\alpha'\right)\left\{\begin{array}{l} M_e\left(D_e+U_{De}\right)\left(D_e'+U_{De}'\right)+M_eV_{De}V_{De}'+M_c\left(1+U_1\right)U_1' \\ +M_p\left(\sum_{i=1}^{N}A_i'\hat{I}_{i+2}+\sum_{i=1}^{N}\sum_{j=1}^{N}A_iA_j'\hat{I}_{i+j+1}+\sum_{i=1}^{M}\sum_{j=1}^{M}B_iB_j'\hat{K}_{i,j}\right)\end{array}\right\} \\
&+\lambda M_eR_L\frac{\left\{\left(D_e+U_{De}\right)\sin\alpha+V_{De}\cos\alpha\right\}}{\left[\left\{\cos\alpha+\left(1/R_L\right)\left(D_e+U_{De}\right)\right\}^2+\left(\left(1/R_L\right)V_{De}-\sin\alpha\right)^2\right]^{\frac{3}{2}}} \\
&+\lambda M_pR_L\int_0^1\frac{\exp\left[F(\xi)\right]\left\{\left(\xi+U\right)\sin\alpha+V\cos\alpha\right\}}{\left[\left\{\cos\alpha+\left(1/R_L\right)\left(\xi+U\right)\right\}^2+\left(\left(1/R_L\right)V-\sin\alpha\right)^2\right]^{\frac{3}{2}}}d\xi \\
&+\lambda M_cR_L\frac{\left(1+U_1\right)\sin\alpha}{\left[\left\{\cos\alpha+\left(1/R_L\right)\left(1+U_1\right)\right\}^2+\sin^2\alpha\right]^{\frac{3}{2}}}-K_t\alpha+\frac{Q_\alpha}{m_{tot}\Omega^2L_0^2},
\end{aligned}
\tag{5.28}
$$

$$
\begin{aligned}
&M_p \sum_{i=1}^{N} A_i'' \hat{I}_{i+k+1} + \sum_{i=1}^{N} A_i'' \left(M_e D_e^{i+k} + M_c \right) + M_e D_e^k D_e'' - \left(M_e D_e^k V_{De} + M_p \sum_{i=1}^{M} B_i \hat{J}_{k+1,i} \right) \alpha'' \\
&= 2M_p \left(1+\alpha'\right) \sum_{i=1}^{M} B_i' \hat{J}_{k+1,i} + M_p \left(1+\alpha'\right)^2 \left(\hat{I}_{k+2} + \sum_{i=1}^{N} A_i \hat{I}_{i+k+1} \right) \\
&+ R_L \left(M_p \hat{I}_{k+1} + M_e D_e^k + M_c \right) \cos\alpha \\
&+ M_e \left\{ 2V_{De}' \left(1+\alpha'\right) + \left(1+\alpha'\right)^2 \left(D_e + U_{De}\right) \right\} D_e^k + M_e D_e' D_e^k \left\{ \left(1+\alpha'\right) V^* - U'^* \right\} \\
&- k M_e D_e' D_e^{k-1} \left\{ R_L \sin\alpha + D_e' + U_{De}' - \left(1+\alpha'\right) V_{De} \right\} + M_c \left(1+\alpha'\right)^2 \left(1+U_1\right) \\
&- \lambda M_e \frac{\left(R_L \cos\alpha + D_e + U_{De} \right) D_e^k}{\left[\left\{ \cos\alpha + \left(1/R_L\right)\left(D_e + U_{De}\right) \right\}^2 + \left\{ \left(1/R_L\right) V_{De} - \sin\alpha \right\}^2 \right]^{\frac{3}{2}}} \\
&- \lambda M_p \int_0^1 \frac{\exp\left[F(\xi)\right] \left(R_L \cos\alpha + \xi + U \right) \xi^k}{\left[\left\{ \cos\alpha + \left(1/R_L\right)\left(\xi + U\right) \right\}^2 + \left\{ \left(1/R_L\right) V - \sin\alpha \right\}^2 \right]^{\frac{3}{2}}} d\xi \\
&- \lambda M_c \frac{\left(R_L \cos\alpha + 1 + U_1 \right)}{\left[\left\{ \cos\alpha + \left(1/R_L\right)\left(1 + U_1\right) \right\}^2 + \sin^2\alpha \right]^{\frac{3}{2}}} \\
&- k \bar{\Omega}_a^2 \int_0^1 \exp\left[F(\xi)\right] \xi^{k-1} \left[U_\xi + \left(\frac{1}{2} - U_\xi \right) V_\xi^2 \right] d\xi \\
&+ \frac{Q_{a(k)}}{m_{tot} \Omega^2 L_0^{k+1}}, \qquad (5.29)
\end{aligned}
$$

$$M_p\int_0^1 \exp[F(\xi)]\sin(k\pi\xi)\{V''+\alpha''(\xi+U)\}d\xi+M_e\sin(k\pi D_e)\{V''_{De}+(D_e+U_{De})\alpha''\}$$

$$=M_p\int_0^1 \exp[F(\xi)]\sin(k\pi\xi)\left\{(1+\alpha')^2V-2(1+\alpha')U'-R_L\sin\alpha\right\}d\xi$$

$$+M_e\sin(k\pi D_e)\left\{(1+\alpha')^2V_{De}-2(1+\alpha')(D'_e+U'_{De})-R_L\sin\alpha\right\}$$

$$-M_eD'_e\left[k\pi\cos(k\pi D_e)\{R_L\cos\alpha+V'_{De}+(1+\alpha')(D_e+U_{De})\}+\sin(k\pi D_e)\{V'^*+(1+\alpha')U^*\}\right]$$

$$+\lambda M_e\frac{(R_L\sin\alpha-V_{De})\sin(k\pi D_e)}{\left[\{\cos\alpha+(1/R_L)(D_e+U_{De})\}^2+((1/R_L)V_{De}-\sin\alpha)^2\right]^{\frac{3}{2}}}$$

$$+\lambda M_p\int_0^1\frac{\exp[F(\xi)](R_L\sin\alpha-V)\sin(k\pi\xi)}{\left[\{\cos\alpha+(1/R_L)(\xi+U)\}^2+((1/R_L)V-\sin\alpha)^2\right]^{\frac{3}{2}}}d\xi$$

$$-k\pi\bar{\Omega}_a^2\int_0^1\exp[F(\xi)]\cos(k\pi\xi)\left(U_\xi V_\xi+V_\xi^3-U_\xi^2V_\xi\right)d\xi+\frac{Q_{b(k)}}{m_{tot}\Omega^2L_0}, \tag{5.30}$$

and

$$M_p\int_0^1 \exp[F(\xi)]V_a\{V''+\alpha''(\xi+U)\}d\xi+M_eV_a|_{De}\{V''_{De}+(D_e+U_{De})\alpha''\}$$

$$=M_p\int_0^1 \exp[F(\xi)]V_a\left\{(1+\alpha')^2V-2(1+\alpha')U'-R_L\sin\alpha\right\}d\xi$$

$$+M_eV_a|_{De}\left\{(1+\alpha')^2V_{De}-2(1+\alpha')(D'_e+U'_{De})-R_L\sin\alpha\right\}$$

$$-M_eD'_e\left[\left.\frac{\partial V_a}{\partial\xi}\right|_{De}\{R_L\cos\alpha+V'_{De}+(1+\alpha')(D_e+U_{De})\}+V_a|_{De}\{V'^*+(1+\alpha')U^*\}\right]$$

$$+\lambda M_e\frac{(R_L\sin\alpha-V_{De})V_a|_{De}}{\left[\{\cos\alpha+(1/R_L)(D_e+U_{De})\}^2+((1/R_L)V_{De}-\sin\alpha)^2\right]^{\frac{3}{2}}}$$

$$+\lambda M_p\int_0^1\frac{\exp[F(\xi)](R_L\sin\alpha-V)V_a}{\left[\{\cos\alpha+(1/R_L)(\xi+U)\}^2+((1/R_L)V-\sin\alpha)^2\right]^{\frac{3}{2}}}d\xi$$

$$-\bar{\Omega}_a^2\int_0^1\exp[F(\xi)]\frac{\partial V_a}{\partial\xi}\left(U_\xi V_\xi+V_\xi^3-U_\xi^2V_\xi\right)d\xi+\frac{Q_c}{m_{tot}\Omega^2L_0}. \tag{5.31}$$

In Eqs. (5.27) through (5.31),

$$
\begin{aligned}
U_\xi &= \frac{\partial U}{\partial \xi} = \sum_{i=1}^{N} iA_i \xi^{i-1}, \\
V_\xi &= \frac{\partial V}{\partial \xi} = \pi \sum_{i=1}^{M} \left\{ iB_i \cos(i\pi\xi) \right\} + C\left(1 - \frac{L_0}{H} e^{-L_0\xi/H}\right), \\
U^* &= \frac{\partial U_{De}}{\partial D_e} = \sum_{i=1}^{N} iA_i D_e^{\,i-1}, \text{ and} \\
V^* &= \frac{\partial V_{De}}{\partial D_e} = \sum_{i=1}^{M} i\pi B_i \cos(i\pi D_e) + C\left(1 - \frac{L_0}{H} \exp\left[-(L_0/H) D_e\right]\right).
\end{aligned} \tag{5.32}
$$

Similarly,

$$
\begin{aligned}
U'^* &= \sum_{i=1}^{N} iA_i' D_e^{\,i-1}, \text{ and} \\
V'^* &= \sum_{i=1}^{M} i\pi B_i' \cos(i\pi D_e) + C'\left(1 - \frac{L_0}{H} \exp\left[-(L_0/H) D_e\right]\right).
\end{aligned} \tag{5.33}
$$

The frequency ratio associated with axial elongation is defined as

$$
\bar{\Omega}_a = \frac{\sqrt{EA_m/(m_{tot}L_0)}}{\Omega}. \tag{5.34}
$$

Non-dimensional integrals $\hat{I}_i$ are as defined in Eq. (3.20). Other non-dimensional integrals are given by

$$
\begin{aligned}
\hat{J}_{i,j} &= \int_0^1 \exp[F(\xi)] \xi^{i-1} \sin(j\pi\xi)\, d\xi, \text{ and} \\
\hat{K}_{i,j} &= \int_0^1 \exp[F(\xi)] \sin(i\pi\xi) \sin(j\pi\xi)\, d\xi.
\end{aligned} \tag{5.35}
$$

5.4 Generalized Forces

The generalized forces coming from the motor thrust acting on the climber and aerodynamic forces acting on the ribbon are shown in Table 5.1. They are computed as they were in Chapter 3. However, some new generalized coordinates have been added, and one has been removed compared to Chapter 3. Also, the position vectors (locations of applied forces) are now given by Eq. (5.10).

Table 5.1: Generalized forces for elastic ribbon, stationary base model

Q_i	From motor thrust on climber	From aerodynamic force on ribbon
Q_α	$F_t v_{de}$	$\int \begin{bmatrix} -\{(s+u)\sin\alpha + v\cos\alpha\} dF_v \\ +\{(s+u)\cos\alpha - v\sin\alpha\} dF_h \end{bmatrix}$
Q_{de}	$F_t\left(1+u^*\right)$	0
$Q_{a(k)}$	$F_t d_e^k$	$\int s^k\left(\cos\alpha dF_v + \sin\alpha dF_h\right)$
$Q_{b(k)}$	0	$\int \sin\left(\frac{k\pi s}{L_0}\right)\left(\cos\alpha dF_h - \sin\alpha dF_v\right)$
Q_c	0	$\int v_a\left(\cos\alpha dF_h - \sin\alpha dF_v\right)$

5.5 Analytical Results

5.5.1 Equilibrium and Stability

As already shown, the ribbon is nominally stretched by the nominal strain ε_0 when in equilibrium. The equilibrium position of the space elevator (nominally stretched vertical ribbon, climber at the geosynchronous altitude) expressed in terms of its generalized coordinates is given by

$$x_{eq} = \left[D_e,\ \alpha,\ A\{1,\ 2,\ 3...\},\ B\{1,\ 2,\ 3...\},\ C\right]_{eq}$$
$$= \left[R_L\left(\lambda^{1/3} - 1\right)\Big/(1+\varepsilon_0),\ 0,\ A\{\varepsilon_0,\ 0,\ 0...\},\ B\{0,\ 0,\ 0...\},\ 0\right]. \tag{5.36}$$

Equations (5.27) through (5.31) are satisfied if the generalized coordinates are given by Eq. (5.36), and all their derivatives are set to zero. As with the rigid tether system, the climber sits at a saddle point. If the climber's position is fixed, this equilibrium position is stable.

5.5.2 Modal Analysis for the Longitudinal Extension of the Ribbon

The longitudinal extension of the ribbon is now examined by neglecting its lateral displacement and libration. Climber effects are also omitted from the analysis. If this is done, Eq. (5.29), which governs generalized coordinates A_k, becomes

$$M_p \sum_{i=1}^{N} A_i'' \hat{I}_{i+k+1} + \sum_{i=1}^{N} A_i''(M_c)$$
$$= M_p\left(\hat{I}_{k+2} + \sum_{i=1}^{N} A_i \hat{I}_{i+k+1}\right) + R_L\left(M_p \hat{I}_{k+1} + M_c\right) + M_c\left(1 + \sum_{i=1}^{N} A_i\right) - \lambda M_p R_L^3 \int_0^1 \frac{\exp[F(\xi)]\xi^k}{(R_L + \xi + U)^2} d\xi$$
$$-\lambda M_c R_L^3 \frac{1}{(R_L + 1 + U_1)^2} - k\bar{\Omega}_a^2 \int_0^1 \exp[F(\xi)]\xi^{k-1} U_\xi d\xi. \tag{5.37}$$

For the analysis, it is useful to transform generalized coordinate A_i to a new generalized coordinate, $\bar{A}_i$, using the following substitution:

$$A_i = A_{i,eq} + \bar{A}_i. \tag{5.38}$$

From Section 5.5.1, $A_{1,eq} = \varepsilon_0$ and $A_{i,eq} = 0$, for i = 2, 3, 4…. As a result,

$$U = \bar{U} + \varepsilon_0 \xi, \tag{5.39}$$

where

$$\bar{U} = \sum_{i=1}^{N} \bar{A}_i \xi^i . \tag{5.40}$$

If the terms associated with the gravitational force are expanded binomially ignoring second order terms and above, the equations describing the longitudinal extension of the ribbon may be expressed as

$$M_{k,i}^A \bar{A}_k'' + K_{k,i}^A \bar{A}_k = \mathbf{0}, \tag{5.41}$$

where

$$M_{k,i}^A = M_p \hat{I}_{i+k+1} + M_c ,$$

and

$$K_{k,i}^A = ik\bar{\Omega}_a^2 \int_0^1 \exp\left[F(\xi)\right]\xi^{i+k-2} d\xi - \left(M_p \hat{I}_{i+k+1} + M_c\right)$$
$$-2\lambda R_L^3 \left\{ M_p \int_0^1 \frac{\exp\left[F(\xi)\right]\xi^{i+k}}{\left[R_L + \xi\left(1+\varepsilon_0\right)\right]^3} d\xi + M_c \frac{1}{\left(R_L + 1 + \varepsilon_0\right)^3} \right\}. \tag{5.42}$$

The general eigenvalue problem in Eq. (5.41) is solved using Matlab, for a 100,000 km ribbon having a taper ratio of six. Table 5.2 shows the non-dimensional frequencies of the longitudinal modes for $N = 3$, 4 and 5. The frequencies are non-dimensionalized with respect to Ω. For values of N (number of longitudinal modes) greater than five, some of the eigenvalues are negative. This result occurs because matrices M^A and K^A become very ill-conditioned as the value of N increases. The matrices become ill-conditioned because, as will be observed, the polynomial basis functions differ greatly from the actual modes. The results for the longitudinal modal analysis are reliable only for $N < 6$.

From Table 5.2, the first mode of longitudinal extension has a frequency of 4.41, i.e., a period of approximately five and a half hours. The frequencies of mode 2 through mode 5 increase in a quasi-linear fashion. It can be seen in Table 5.2 that the frequencies converge fairly well when N is increased.

Table 5.2: Frequencies of longitudinal modes

Mode #	1	2	3	4	5
Non-dimensional frequency ($N = 3$)	4.52	12.85	24.76	N/A	N/A
Non-dimensional frequency ($N = 4$)	4.45	12.82	24.43	38.04	N/A
Non-dimensional frequency ($N = 5$)	4.41	12.73	24.36	37.70	57.80

For the $N = 5$ system, the corresponding matrix of normalized eigenvectors (along the columns) is given by

$$\begin{matrix} -0.11 & -0.12 & -0.22 & -0.06 & 0.02 \\ 0.34 & 0.38 & 0.67 & 0.36 & -0.21 \\ -0.67 & -0.64 & -0.21 & -0.73 & 0.61 \\ 0.61 & 0.62 & -0.59 & 0.56 & -0.71 \\ -0.21 & -0.23 & 0.34 & -0.13 & 0.29 \end{matrix} \;.$$

Clearly, the basis functions (powers of ξ) chosen to approximate the longitudinal extension, or, assumed modes, do *not* correspond to the actual modes. Oddly, the first two modes are quite similar.

5.5.3 Modal Analysis for the Lateral Displacement of the Ribbon

The lateral extension of the ribbon is now examined by neglecting its longitudinal extension (other than its nominal amount given by $U = \varepsilon_0 \xi$), and again, ignoring climber effects. The generalized coordinate associated with aerodynamic loads is also neglected. However, the libration of the ribbon must be included in the analysis. This is because it represents the zeroth mode of lateral motion. If this is done, and higher order terms and damping terms are neglected, the coupled system of equations governing the libration (Eq. (5.28)) and generalized coordinates B_k (Eq. (5.30)) may be written as

$$\mathbf{M}^{\mathbf{B}}\mathbf{B}'' + \mathbf{K}^{\mathbf{B}}\mathbf{B} = \mathbf{0}, \tag{5.43}$$

where

$$\mathbf{B} = [\alpha, B_1, B_2, \ldots B_k]^T,$$

$$\mathbf{M}^{\mathbf{B}} = \left[\begin{array}{c|c} m_{1,1} & m_{1,i+1} \\ \hline m_{k+1,1} & m_{k+1,i+1} \end{array}\right] \quad \text{and} \quad \mathbf{K}^{\mathbf{B}} = \left[\begin{array}{c|c} k_{1,1} & k_{1,i+1} \\ \hline k_{k+1,1} & k_{k+1,i+1} \end{array}\right]$$

where both indexes i and k = 1, 2, 3…M, and

$$m_{1,1} = (1+\varepsilon_0)^2\left(M_p\hat{I}_3 + M_c\right),\; m_{k,1} = M_p(1+\varepsilon_0)\hat{J}_{2,k},$$

$$m_{1,i} = M_p(1+\varepsilon_0)\hat{J}_{2,i},$$

$$m_{k,i} = M_p\hat{K}_{k,i},$$

$$k_{1,1} = (1+\varepsilon_0)\left[R_L\left(M_p\hat{I}_2 + M_c\right) - \lambda R_L^4\left\{M_p\int_0^1 \frac{\exp[F(\xi)]\xi}{\left[R_L + \xi(1+\varepsilon_0)\right]^3}d\xi + M_c\frac{1}{(R_L+1+\varepsilon_0)^3}\right\}\right],$$

$$k_{k,1} = M_p\left[R_L\hat{J}_{1,k} - \lambda R_L^4\int_0^1 \frac{\exp[F(\xi)]\sin(k\pi\xi)}{\left[R_L + \xi(1+\varepsilon_0)\right]^3}d\xi\right],$$

$$k_{1,i} = M_p\left[R_L\hat{J}_{1,i} - \lambda R_L^4\int_0^1 \frac{\exp[F(\xi)]\sin(i\pi\xi)}{\left[R_L + \xi(1+\varepsilon_0)\right]^3}d\xi\right],$$

and

$$k_{k,i} = \pi^2\left(\varepsilon_0 - \varepsilon_0^2\right)ik\bar{\Omega}_a^2\int_0^1 \exp[F(\xi)]\cos(i\pi\xi)\cos(k\pi\xi)\,d\xi$$
$$+M_p\left[\lambda R_L^3\int_0^1 \frac{\exp[F(\xi)]\sin(i\pi\xi)\sin(k\pi\xi)}{\left[R_L + \xi(1+\varepsilon_0)\right]^3}d\xi - \hat{K}_{k,i}\right]. \tag{5.44}$$

Again, the generalized eigenvalue problem in Eq. (5.43) may be solved using Matlab. This time, the results seem reliable for a high number of modes. Table 5.3 contains the non-dimensional natural frequencies for the first one hundred modes of the lateral extension of the ribbon.

Table 5.3: Non-dimensional frequencies of lateral modes

Mode #	Frequency	Mode #	Frequency	Mode #	Frequency
0	0.16	33	72.77	66	148.28
1	2.32	34	73.17	67	150.22
2	4.66	35	78.19	68	155.17
3	6.93	36	86.26	69	161.50
4	9.20	37	88.60	70	170.12
5	11.48	38	89.12	71	172.98
6	13.75	39	91.09	72	174.73
7	16.02	40	91.36	73	176.09
8	18.30	41	92.28	74	177.85
9	20.57	42	93.89	75	180.41
10	22.85	43	95.75	76	182.44
11	25.12	44	97.97	77	183.91
12	27.40	45	101.77	78	186.93
13	29.67	46	102.61	79	188.97
14	30.53	47	104.82	80	189.20
15	31.96	48	107.12	81	191.36
16	34.23	49	109.37	82	191.53
17	36.51	50	111.61	83	193.73
18	38.78	51	111.79	84	196.28
19	41.06	52	113.75	85	198.30
20	43.33	53	114.15	86	202.39
21	45.60	54	114.57	87	207.41
22	47.88	55	115.87	88	209.73
23	50.11	56	118.82	89	210.58
24	51.86	57	120.23	90	211.98
25	52.50	58	122.09	91	214.26
26	54.61	59	123.13	92	216.55
27	55.67	60	126.25	93	218.83
28	57.17	61	130.69	94	221.12
29	59.35	62	136.36	95	223.99
30	61.87	63	142.24	96	225.69
31	63.90	64	144.70	97	229.76
32	67.67	65	145.15	98	231.21
				99	232.57

The first frequency (zeroth mode) is that of the libration (α). It has a value of about 0.16. This is reasonably close to the value of $W = 0.18$ obtained in Chapter 4, when the ribbon was assumed to be rigid. The corresponding difference in the period of libration for the rigid and elastic ribbon is nearly 20 hours (the elastic ribbon has the longer period). The first sinusoidal mode of transverse vibration has a period of about ten hours. The frequencies of the sinusoidal modes increase in a quasi-linear fashion. The deviations from the linear relationship may be due to the taper function of the ribbon.

The modal matrix consisting of normalized eigenvectors is approximately equivalent to the identity matrix. This means that the assumed sinusoidal modes for the lateral extension are approximately the actual modes for the lateral motion of the ribbon. Patamia (2005a, 2005b) discusses the sinusoidal mode shapes associated with the lateral displacement of the ribbon. His results for transverse mode shapes are $\sin(i\pi\xi)$, where $i \cong 1,2,3...$, as the results of this study suggest. Strangely, the frequency of the libration mode, or pendulum mode of the ribbon in his study was found to be about one day. This study (and that of Lang (2005a)) has found the librational frequency to be around five days.

5.5.4 Steady State Lateral Displacement due to Aerodynamic Loading

The effect of wind on the lateral extension of the ribbon is now considered. If all other generalized coordinates assume their respective equilibrium values, Eq. (5.31) becomes

$$M_p C'' \int_0^1 \exp[F(\xi)] V_a^2 d\xi$$
$$= M_p C \int_0^1 \exp[F(\xi)] V_a^2 d\xi - \lambda R_L^3 M_p C \int_0^1 \frac{\exp[F(\xi)] V_a^2}{\left[\left\{R_L + \xi(1+\varepsilon_0)\right\}^2 + (CV_a)^2\right]^{\frac{3}{2}}} d\xi$$
$$-\bar{\Omega}_a^2 C \int_0^1 \exp[F(\xi)] \left(\frac{\partial V_a}{\partial \xi}\right)^2 \left\{\varepsilon_0 - \varepsilon_0^2 + C^2 \left(\frac{\partial V_a}{\partial \xi}\right)^2\right\} d\xi + \frac{Q_c}{m_{tot}\Omega^2 L_0}. \tag{5.45}$$

The approximate steady state solution to the effect of wind on the lateral extension of the ribbon, C_{ss}, may be found by setting $C''=0$ and inputting (from Table 5.1)

$$Q_c = \int v_a (\cos\alpha dF_h - \sin\alpha dF_v) \cong \int v_a dF_h. \tag{5.46}$$

Then, assuming $C_{ss} \ll R_L$, and retaining only first order strain energy terms,

$$C_{ss} = \frac{\int v_a dF_h}{m_{tot}\Omega^2 L_0 W_C^2}, \tag{5.47}$$

where

$$W_C = \sqrt{\int_0^1 \exp[F(\xi)] \left[\varepsilon_0 \bar{\Omega}_a^2 \left(\frac{\partial V_a}{\partial \xi}\right)^2 + \frac{\lambda R_L^3 M_p V_a^2}{\left\{R_L + \xi(1+\varepsilon_0)\right\}^3} - M_p V_a^2\right] d\xi}. \tag{5.48}$$

Since it is assumed that the wind acts in the horizontal direction, the differential horizontal component of the aerodynamic force is simply the drag force, which is given in Eq. (3.28). Assuming very small libration, and setting b_{eff} to be the effective width exposed to aerodynamic winds, and v_w to be the uniform horizontal wind,

$$dF_h = -C_D b_{eff} \rho_0 v_w^2 \exp(-s/H) \cos^2\phi ds. \tag{5.49}$$

The negative sign appears because the wind is assumed to point westward ($-\mathbf{e_h}$ direction).

The flight path angle of the horizontal wind, ϕ, varies along the ribbon because of the non-linear aerodynamic basis function. It is observed from Figure 5.3 that ϕ is highest in the lower atmosphere, where air density is the highest. This phenomenon should result in lower lateral displacement. Due to the horizontal wind, $\tan\phi$ is simply the derivative of the lateral displacement:

$$\tan\phi = c_{ss}\frac{\partial v_a}{\partial s} = c_{ss}\left(\frac{1}{L_0} - \frac{1}{H}\exp(-s/H)\right) \cong C_{ss}\left[1 - \frac{L_0}{H}\exp(-s/H)\right]. \tag{5.50}$$

$|\cos\phi|$ is obtained by using the trigonometric identity:

$$|\cos\phi| = \frac{1}{\sqrt{1+\tan^2\phi}} = \frac{1}{\sqrt{1+C_{ss}^2\left[1-\frac{L_0}{H}\exp(-s/H)\right]^2}}. \tag{5.51}$$

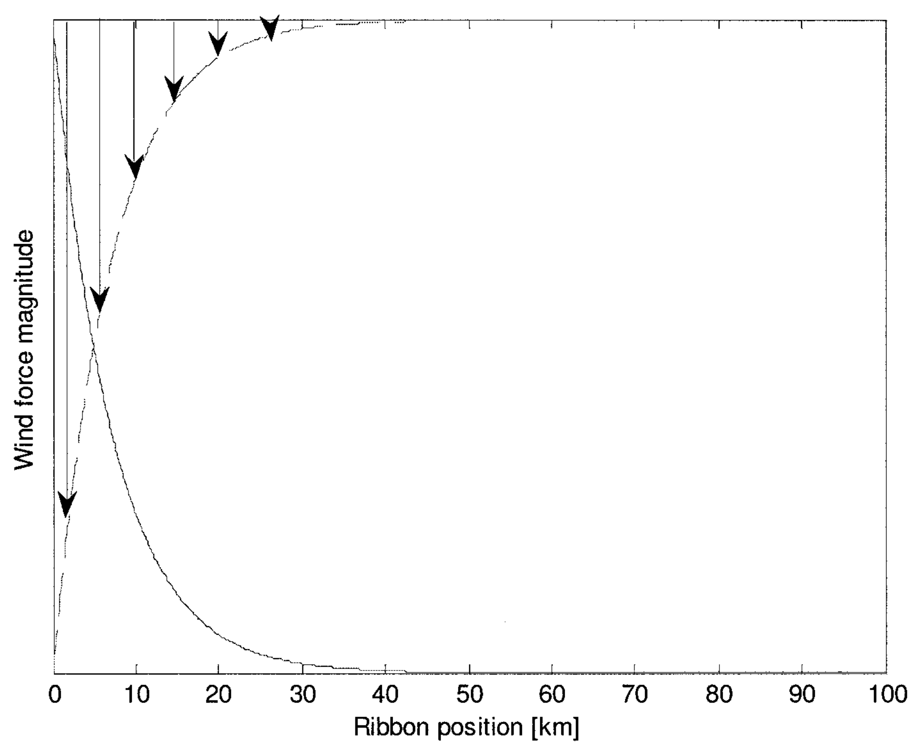

Figure 5.3: Aerodynamic basis function and wind force variation vs. ribbon position

The approximate steady state solution for the lateral extension of the ribbon may be found by solving the following implicit equation:

$$C_{ss} + \frac{C_D b_{eff} \rho_0 v_w^2}{m_{tot} \Omega^2 L_0 W_C^2} \int_0^{h_{atm}} v_a \exp(-s/H) \cos^2 \phi ds = 0. \tag{5.52}$$

Equation (5.52) is implicit because the flight path angle of the wind depends on C_{ss}. The equation does not have an analytical solution, but it may be solved numerically. Using space elevator parameters assumed earlier, standard atmospheric values, and an effective width of 5 cm, the steady state value for the generalized coordinate associated with aerodynamic loads may be determined for a range of wind velocity values. Their relationship is plotted in Figure 5.4.

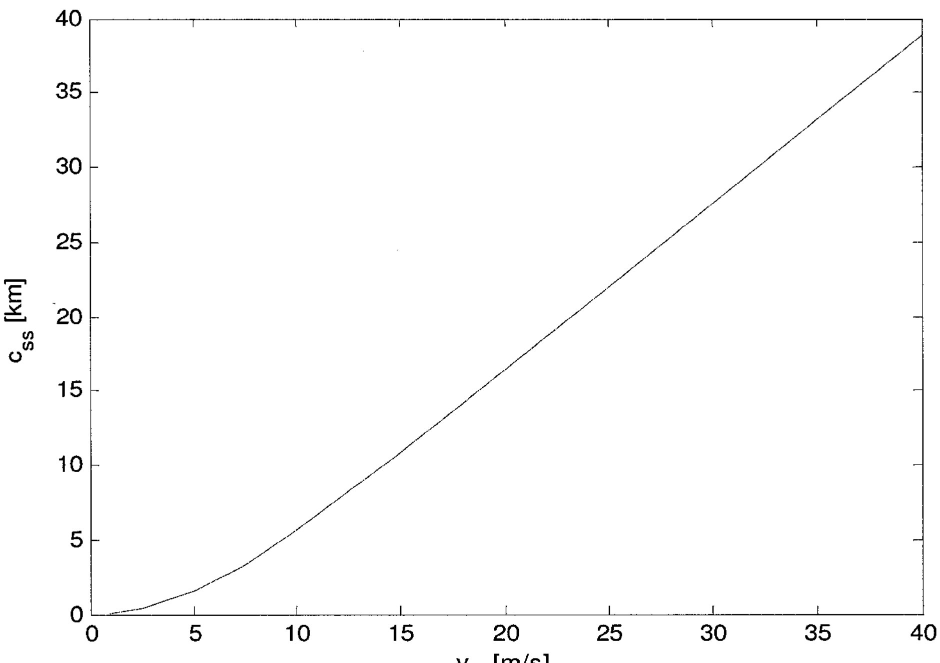

Figure 5.4: Steady state value for generalized coordinate associated with basis function v_a vs. wind velocity

In Figure 5.4, the standard quadratic relationship exists for small winds. However, since C_{ss} appears in the denominator of $|\cos\phi|$, the plot becomes quasi-linear for high winds. In general, high winds will cause tens of kilometres of lateral displacement in the ribbon in the first one hundred kilometres of its length.

5.6 Effect of the Climber on the Elastic Ribbon Model

In this section, Matlab is used to simulate the effect of a climber transit on the ribbon of the space elevator. Its effect on the libration of the ribbon is compared to the results obtained in Chapter 4, when the ribbon was assumed to be rigid. Equations (5.28) through (5.30) are solved using ode45. Aerodynamic loads are ignored, and so Eq. (5.31) is not used. The motion of the climber is prescribed, and so Eq. (5.27) is only used to calculate the required force or thrust of the climber. Again, the space elevator parameters used here are L = 100,000 km, $\sigma_0 = 35$ GPa, $\gamma = 1300$ kg/m^3, E = 1 TPa and A_m = 10 mm^2. The climber has a mass of 800 kg. The ribbon begins in its equilibrium configuration. The climber proceeds from the bottom of the ribbon to the top with a cruising velocity of 280 km/hr, and has a time ratio of 0.1. Three basis functions (or assumed modes) are used to approximate each of the longitudinal and lateral motion of the ribbon ($N = M = 3$). Therefore, along with the libration, the system being simulated is represented by seven coupled second-order equations. A relative tolerance of 10^{-3} is used for the ode45 solver. The absolute tolerance for α, α', A_k, A'_k, B_k and B'_k is 10^{-6}.

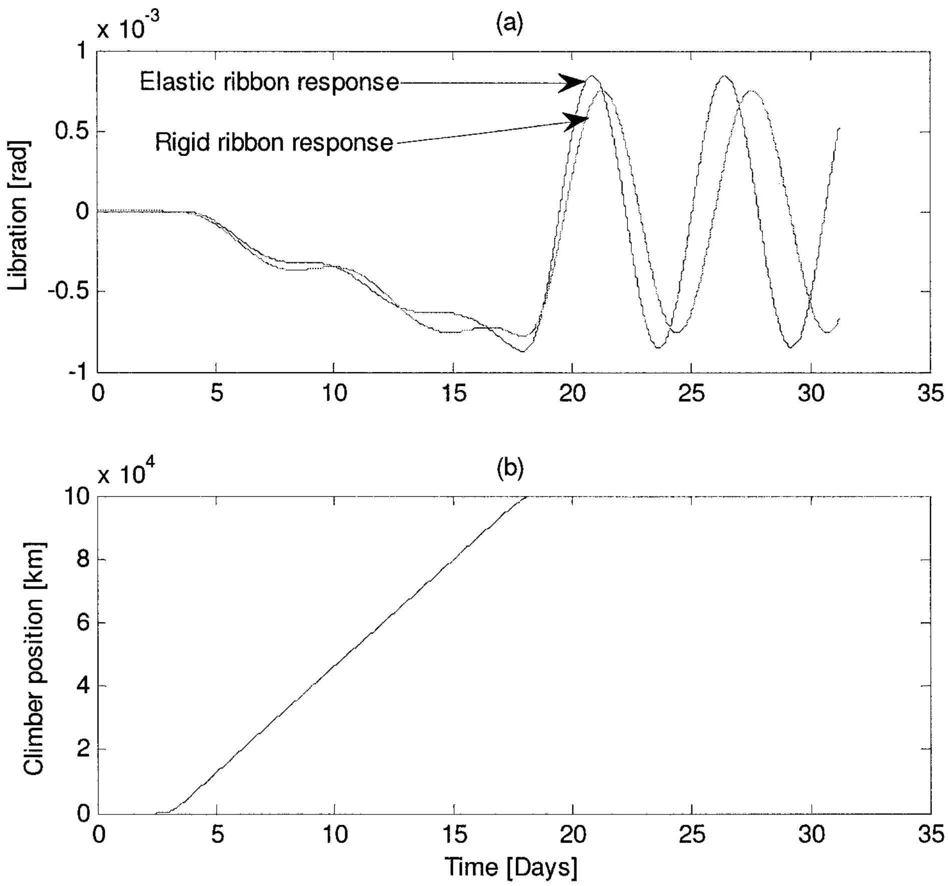

Figure 5.5: Libration response vs. time for (a) elastic and rigid ribbon models to (b) prescribed climber transit

Figure 5.5 compares the libration response of the elastic ribbon model to the rigid one. Clearly, the responses are quite similar. One notable difference between the two is in the frequency. The elastic ribbon clearly has a longer period, which is expected from the observation made in the modal analysis of the lateral motion of the ribbon. Another difference is that the in-transit response of the elastic ribbon has a greater sinusoidal component than the rigid one, causing slightly greater fluctuations in libration. To know the particular reason for this, one must find a closed form solution to the equations of motion for the libration of the elastic ribbon; this has not been attempted in this thesis.

For this particular case, the elastic model experiences less residual libration. However, the elastic model could just as easily experience more residual libration than that predicted by the rigid one for a different prescribed motion.

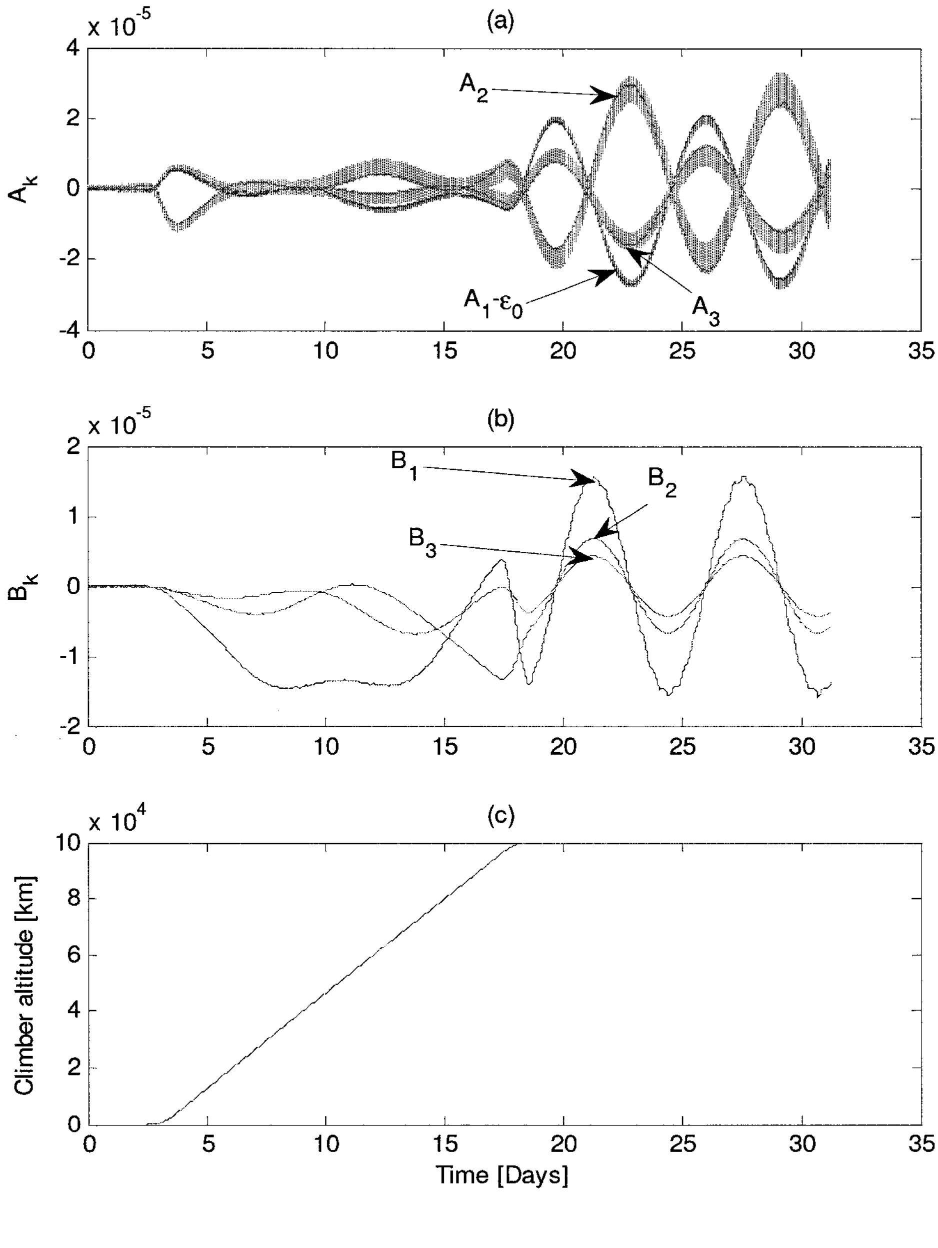

Figure 5.6: Ribbon extension vs. time
(a) Longitudinal extension generalized coordinates;
(b) Lateral displacement generalized coordinates; (c) Prescribed climber transit

Figure 5.6 shows how the aforementioned climber transit will influence the longitudinal and lateral extension of the ribbon. The three non-dimensionalized generalized coordinates for longitudinal extension (A_k) and lateral motion (B_k) are plotted against time. The effect of climber transit at constant speed on these generalized coordinates is minimal. Since the assumed sinusoidal modes for the lateral displacement of the ribbon correspond roughly to the actual modes, the response of B_1 is greater than that of B_2, and the response of B_2 is greater than that of B_3. As the assumed modes attached to A_k do not correspond to modes, the same may not be said for their responses. It is noted that for all time, the values of all $\overline{A}_k$ (variations from equilibrium) are much less than ε_0, which is about 0.035.

In Chapter 4, climbing procedures to minimize and/or control ribbon libration were derived assuming the ribbon to be rigid. In general, all three of the climbing procedures hold good for the elastic ribbon space elevator. The transverse modal analysis has revealed that the period of libration for the elastic ribbon case is longer than that of the rigid ribbon case. The numerical results in this section confirm that result. As such, when using the climbing procedures, the non-dimensional frequency derived in Chapter 4, W, should be replaced by the non-dimensional frequency of the zeroth mode found from the transverse modal analysis in Section 5.5.3. The multiple-climber climbing procedure should work very well with this modification to the phasing. The procedure where a single climber returns an oscillating ribbon to equilibrium will contain some error due to the additional in-transit ribbon oscillations seen in the elastic ribbon.

Chapter 6: Launch Dynamics

This chapter considers the launch of a payload from a climber. Once a climber reaches a desired launch altitude, d_0, the satellite it contains may be released. If no additional velocity impulse is added to the satellite, it will have used no fuel to arrive in orbit. These orbits will be called 'free Earth orbits'.

At the time of launch, the climber (and the satellite it contains) will have radius r_0, magnitude of velocity v_0, and flight path angle β_0. The values of v_0 and β_0 may be modified by an applied velocity impulse. The semi-major axis and eccentricity of the orbit that the satellite will fall into are given by (Kaplan, 1976)

$$a = 1\Big/\left(\frac{2}{r_0} - \frac{v_0^2}{\mu}\right), \tag{6.1}$$

$$e = \sqrt{\left(\frac{r_0 v_0^2}{\mu} - 1\right)^2 \cos^2\beta_0 + \sin^2\beta_0}\,. \tag{6.2}$$

6.1 Ideal Launch Scenario

Ideally, at the moment of satellite launch, the space elevator will be static, and in its nominal configuration. If this is the case, and no additional impulse is applied to the satellite, then $r_0 = R + d_0$, $v_0 = \Omega(R + d_0)$ and $\beta_0 = 0$. The resulting semi-major axis and eccentricity pairings are plotted in Figure 6.1 with all lengths non-dimensionalized with respect to the radius of the Earth.

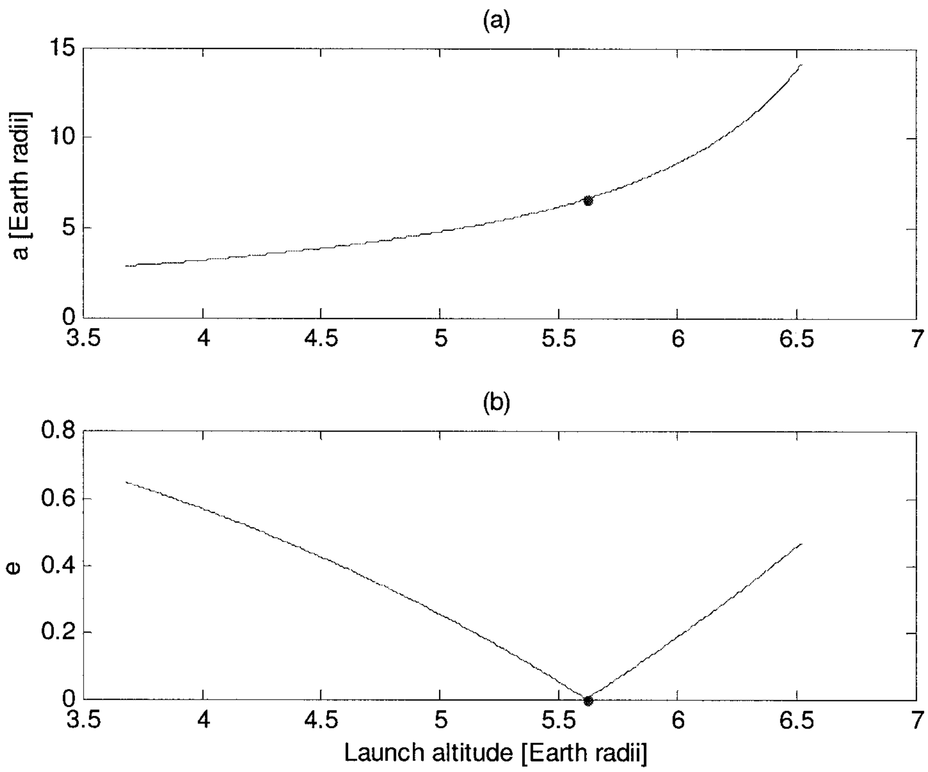

Figure 6.1: Orbit parameters vs. launch altitude: (a) semi-major axis, (b) eccentricity

It is observed that the geosynchronous altitude is the only point on the ribbon that is in a natural circular orbit (shown by a bullet in Figure 6.1). If a mass is released from any other altitude in the range shown above, it will be in an elliptical orbit. The minimum launch altitude considered is 23,500 km, because at any point below this, the perigee of the elliptical orbit of the satellite will be within 100 km from the surface of the Earth. The maximum launch altitude considered here is about 42,000 km, because the semi-major axis of the resulting orbit for launches at altitudes beyond this point is very large. Though not seen from Figure 6.1, $d_0 = 7.345R$, or about 46,850 km, is a critical launch altitude, which places payloads in a parabolic orbit. Therefore, for satellite placement in free Earth orbits, the launch altitude will be in the range given by $23{,}500 < d_0 < 46{,}850$

km. Also, any natural ($\Delta v = 0$) launch in the range given by $46{,}850 \text{ km} < d_0 < L$ will send the payload into a hyperbolic orbit, as it will have a velocity greater than the escape velocity given by $v_{esc} = \sqrt{2\mu/r_0}$. These trajectories are the starting point for planning interplanetary space missions using the space elevator, but are not discussed further, as this discussion is limited to the placement of satellites into Earth orbits.

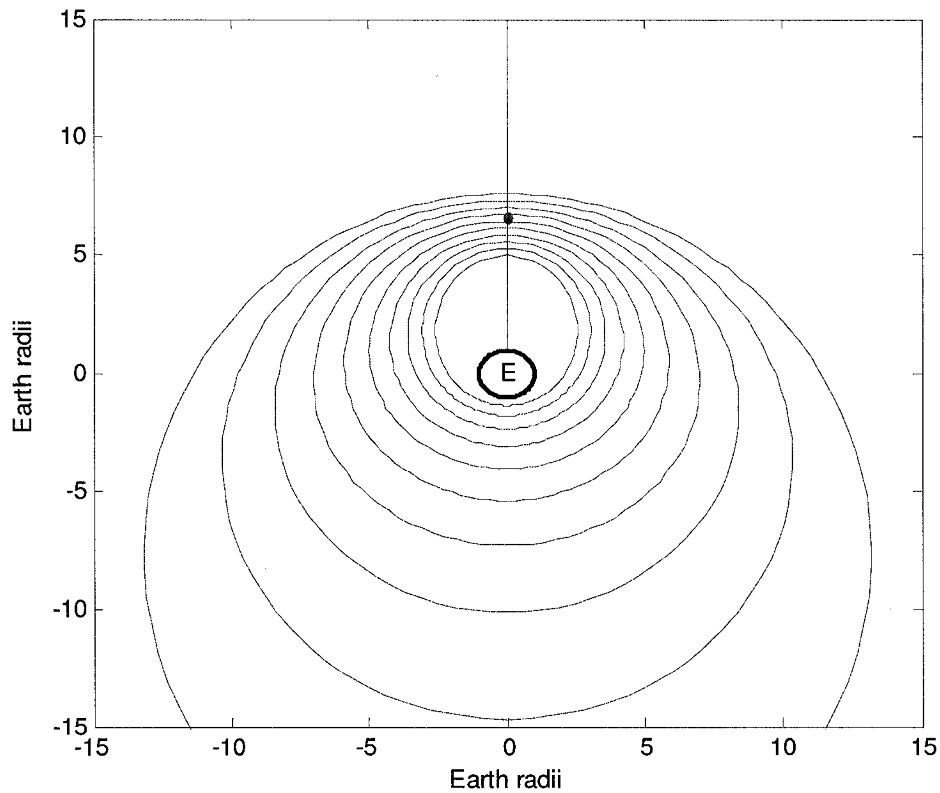

Figure 6.2: Free Earth orbits using the space elevator

A better picture of what has been called the free Earth orbits available to satellites using the space elevator is shown in Figure 6.2. Since the flight path angle of the climber at the time of launch is zero, the point of launch can only be the apogee or the perigee of the orbit. Since the portion of ribbon below the geosynchronous altitude is traveling slower than it would in a natural circular orbit, launches below this altitude commence at the apogee of the orbit. Similarly, for launches above the geosynchronous altitude, the initial radius becomes the perigee of the orbit.

While Figure 6.2 shows the spectrum of free orbits available to Earth satellites, there are a wide range of reasonably low cost orbits that may be reached by transferring from the free orbits with a small impulse, Δv. For example, if a particular circular orbit having $r_c \neq R_G$ is desired, a certain Δv will be required. The most efficient elliptical to circular orbit transfer occurs at the perigee of an elliptical orbit if $r_c < R_G$, and at its apogee if $r_c > R_G$. These transfers are essentially the second impulse of a Hohmann transfer. It is noted that in either case, the impulse takes place at the side of the orbit opposite that which it was originally launched from. In Figure 6.3, the minimum required impulse and the launch altitude of the original elliptical orbit are plotted against a wide range of desired circular orbits. The required impulse for a geosynchronous orbit is zero, as it should be. The only circular orbits that require large impulses are those at low altitudes (altitude in the hundreds of kilometres). The benefits of using the space elevator to reach orbits in this range are diminished; the required impulse using the space elevator as a platform actually exceeds 3 km/s. The space elevator would not be used to transport satellites to circular orbits of such low altitudes, because rockets can accomplish this task rather inexpensively. A more positive result is that every circular orbit having a radius in the range given by $30,300 < r_c < 43,500$ km may be arrived at with an impulse of less than 100 m/s.

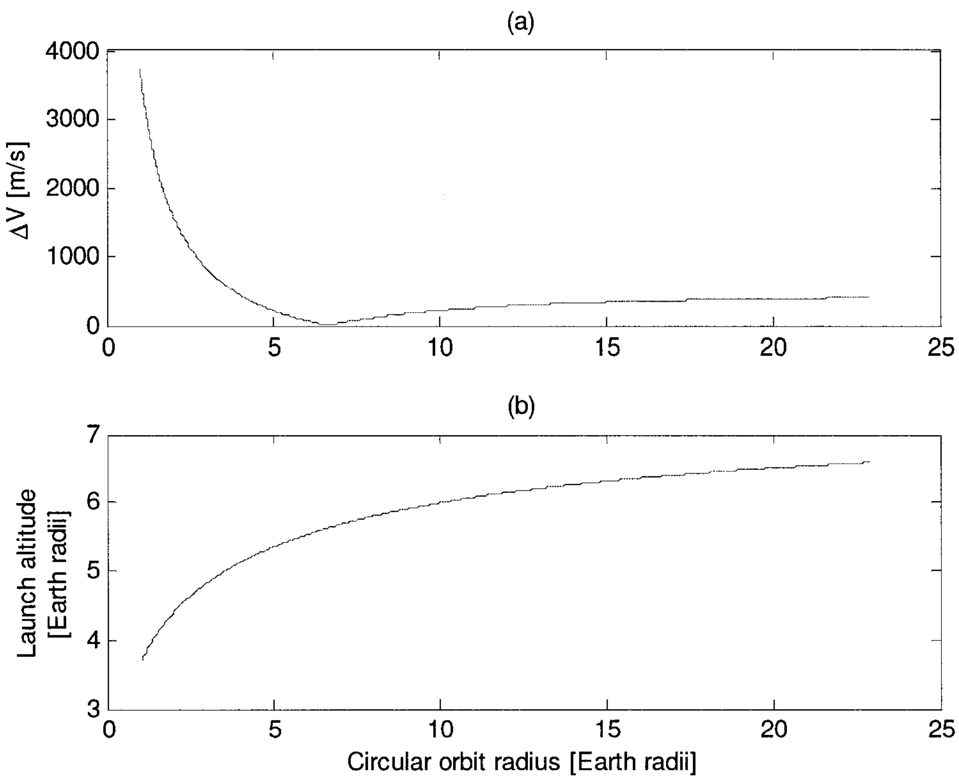

Figure 6.3: Minimum cost (top) and original launch altitude (bottom) to arrive in circular orbits of various radii

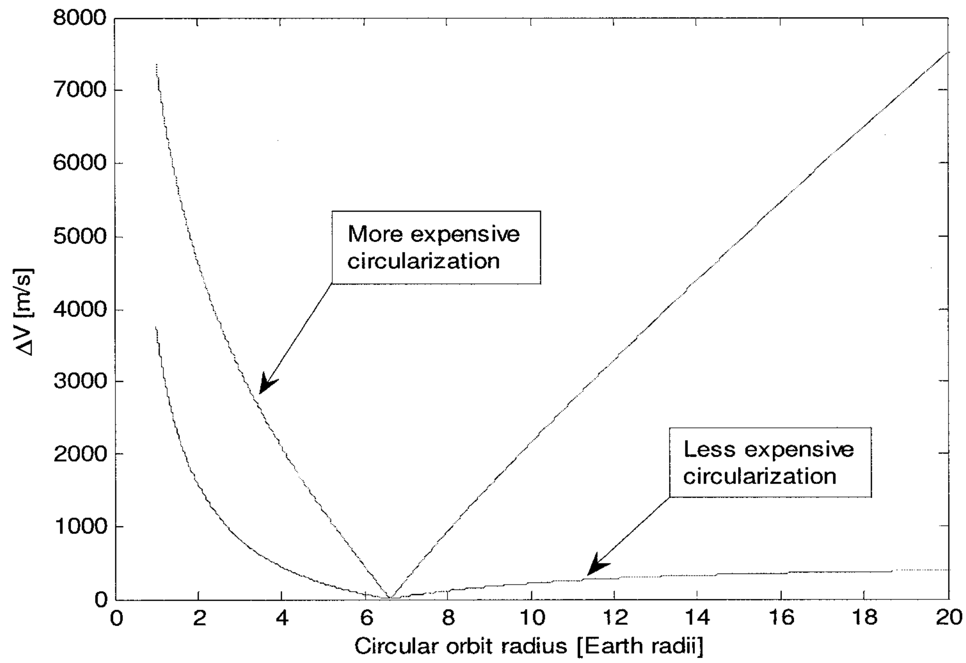

Figure 6.4: Required impulse for two methods of circularizing orbits of various radii

If the orbit of a satellite is circularized at the moment of launch instead of waiting until the other side of the elliptical orbit is reached, the required impulse is much higher. The required impulses associated with both methods are illustrated in Figure 6.4.

6.2 Non-Ideal Launch Scenario

Now, the fact that the space elevator may not be static at the time of launch is taken into account. The required impulse to counter perturbations from the ideal case may be calculated. Also, if these perturbations are not taken into account, their effect on the orbit of a launched satellite is determined.

As shown in Chapter 4, a residual oscillatory libration angle may be introduced to a static space elevator by the Coriolis acceleration of a climber or aerodynamics within the atmosphere. In the case of climber transit, the amplitude of the residual libration, α_{res}, will likely be in the range of milliradians. It is unlikely that any other excitation will cause a residual libration greater than this. Although a method of eliminating such residual oscillations has been proposed, it is prudent to assume $\alpha_{res} \neq 0$ at the time of launch, and devise a method to deal with it. In this section, the structural deformation of the ribbon is ignored. This is a reasonable assumption because the structural deformation of the ribbon will be damped by the material's visco-elastic properties (which will probably be of the order of 1-2% of critical damping). As higher modes tend to experience the most damping, the structural deformation of an excited ribbon will eventually dissipate, leaving libration as the only perturbation of the space elevator from its nominal state. In any case, libration represents the most significant perturbation of the ribbon from equilibrium.

If the ribbon is oscillating, its maximum libration rate occurs when the ribbon is vertical ($\alpha = 0$). This is an ideal moment to launch, because r_0 is unchanged from the ideal case. This libration rate is given by $\dot{\alpha} = \Omega W \alpha_{res}$, where W is the non-dimensional natural frequency of libration, which was derived in Chapter 4. The perturbation velocity caused by this libration rate, which points in the transverse direction and is, of course, equal to the required impulse to counter it, is given by

$$\Delta v = \Omega W \alpha_{res} d_0 . \tag{6.3}$$

ΩW will have a value of about $1.5 \cdot 10^{-5}$. Also, as already mentioned, for satellite placement, $23{,}500 < d_0 < 42{,}000$ km. So, if a satellite is launched from a ribbon that is oscillating with amplitude on the order of milliradians, at the moment when it is vertical, applying the correct impulse on the order of metres per second will eliminate the effect of oscillation. The required impulse is proportional to the amplitude of oscillation. Thus, it has been shown that for amplitudes of libration in the milliradians range, the effect of libration on the orbit of a launched satellite may be zeroed with a reasonably small impulse.

Conversely, the non-zero libration rate may be used to generate two new figures for free Earth orbits; one for when the ribbon is headed westward, and one when it is headed eastward. However, if the libration rate is low, the new figures will not change greatly, and the simplest solution may be to apply the small impulse as suggested above.

Finally, as shown in Figure 6.5, if the effect of libration on the order of milliradians is simply ignored, and a satellite is launched from the geosynchronous altitude at the moment when the ribbon is vertical, the semi-major axis of the orbit of the satellite will change by tens of kilometres, and its eccentricity by the order of 10^{-3}. If the ribbon is not vertical at the time of launch, then in addition to the change in these two orbital parameters, the argument of the perigee of the orbit will be slightly modified, because $\beta_0 \neq 0$.

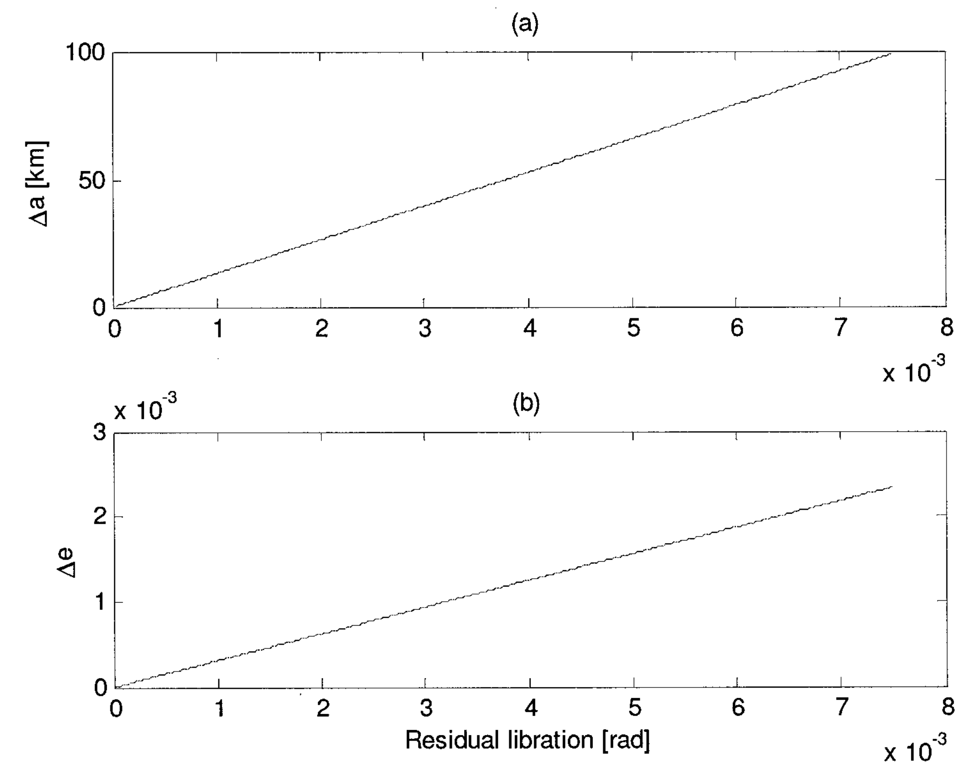

Figure 6.5: Deviation in (a) semi-major axis and (b) eccentricity of the geosynchronous circular orbit due to residual libration angle for launch at moment when the ribbon is vertical

Chapter 7: Conclusions

7.1 Summary of Findings

This thesis has studied several aspects of the dynamics of a space elevator. The most important findings in the thesis are summarized below.

Due to the nominal stretch that the space elevator ribbon will experience, the taper function ensuring uniform stress throughout is slightly different from the one that has been derived in the previous literature. Also, the space elevator must have a counterweight, having a specific mass based on the ribbon's material and design parameters, attached to its free end to satisfy the boundary condition there. The presence of a climber will cause an additional tension gradient across the ribbon. As a result, the mass of a climber has an upper bound.

A dynamics model using a rigid ribbon assumption has been used to study the basic dynamic behaviour of the space elevator. The primary response of the ribbon to ascending climbers is to rotate in the opposite direction as that of the Earth. This westward propagation is due to the Coriolis force on the moving climber. For a climber transit at constant speed, the response is a sum of oscillatory terms (which decay for ascent and grow for descent) and a linear term. However, due to the relatively small mass of the climber and the fact that the ribbon itself is not actually deployed or retrieved, the decay or growth of the oscillatory terms will be negligible. This result distinguishes the dynamics of the space elevator from those of a typical tethered satellite system, where the growth of tether oscillations during constant rate retrieval can be very large. Also, for constant speed transits, the amount of libration induced on the ribbon is proportional to the mass of the climber, its cruise velocity, and the distance it travels. Since all of these values have upper bounds, the ribbon libration they cause is bounded as well; it will be of the order of milliradians at most. Still, the ribbon will experience *undamped* oscillations about its vertical equilibrium position. The period of such oscillations would be about five to six days. Even though the amplitude of these oscillations is small, it is desirable to minimize, and if possible, eliminate it.

Three simple climbing procedures that aim to minimize or eliminate residual oscillation upon climber arrival have been presented. The first procedure is to decelerate the climber very gradually following a half sine function as it approaches its destination. This can reduce (though not entirely eliminate) the residual libration caused by a single climber. The second climbing procedure aims to eliminate ribbon oscillations. It is applicable for the case where a single climber is sent from one point on the ribbon to another at a constant speed. If the climber is sent at the moment when the ribbon reaches its maximum eastward propagation with a specific climber mass and velocity pairing, the ribbon will reach equilibrium at the moment when the climber arrives at its destination; the oscillation can be eliminated by *using* the Coriolis force on the climber. The third climbing procedure, which allows for the ribbon to begin and end in equilibrium, requires that multiple climbers undergo the same transit, and be separated by a specific amount of time. This climbing procedure illustrates the danger of phasing climbers inappropriately:

just as proper phasing can cancel the effect of each climber, improper phasing can add the adverse effect of each climber.

A more realistic dynamics model of the space elevator, one with an elastic ribbon, was also studied. The assumed modes method was used to discretize the space and time variables of the ribbon. The spatial basis functions used to approximate the longitudinal extension of the ribbon were polynomials, whereas sinusoidal functions were used to accomplish this for the lateral displacement. A modal analysis was conducted separately for each of the longitudinal and lateral motion of the ribbon. Due to poor conditioning of the inertia and stiffness matrices associated with the longitudinal extension equations for a high number of basis functions, only the first five modes could be analyzed accurately using numerical techniques. The first five modal natural frequencies were calculated. The same approach was taken for the modal analysis of the lateral motion. The analysis included the libration of the ribbon, as it is the zeroth mode of lateral vibration. The inertia and stiffness matrices for lateral motion were well-conditioned, and the first one hundred modal natural frequencies were calculated. The matrix composed of the eigenvectors along the columns was close to the identity matrix. Thus, it was concluded that after the zeroth mode, all subsequent mode shapes are approximately equal to $\sin(i\pi\xi)$, where ξ is the non-dimensional ribbon material coordinate ranging from 0 to 1 and $i = 1, 2, 3\ldots$

Numerical simulations of the climber ascending the elastic ribbon reveals that the recommended climbing procedures derived using the rigid ribbon model will, in general, hold good for the actual, elastic ribbon case. The main change is that the period of libration that must be used for the climbing procedures corresponds to the period of the zeroth mode obtained from the lateral motion modal analysis, and not the one obtained using the rigid ribbon assumption.

A simplified case of aerodynamic loading was investigated in the thesis: a westward-facing wind, uniform in space and time. The rigid ribbon model was used to gauge the effect that such a wind would have on the libration of the ribbon. It was found that a high velocity wind could cause the ribbon to rotate by several milliradians. An additional lateral motion basis function was derived to study the steady-state effect that such a wind would have on the elastic ribbon model. The basis function allowed for near horizontal ribbon departure angles as observed in the previous literature. It was found that high winds could cause a bubble of lateral displacement tens of kilometres long within the first one hundred kilometres of the ribbon.

The spectrum of free Earth orbits available to satellites released from the climber is quite broad. Impulse manoeuvres will be required to reach any orbit not falling within this spectrum. Such fuel costs will be *very* small compared to what is normally required for a rocket to attain such orbits without the aid of the space elevator. For example, although there is only one free circular Earth orbit (at the geosynchronous altitude), there is a wide range of low-cost (<100 m/s) circular high-altitude orbits. The space elevator will probably not be used for the placement of satellites in circular low Earth orbits, as the additional impulse required to arrive there is of the order of kilometres per second.

The fact that the ribbon will be in motion when the satellites are launched is not likely to play a major role in such launches. The launch from a ribbon experiencing simple pendulum motion has been considered. It has been shown that the steady state motion of the ribbon due to climber transit or aerodynamic excitation will be undamped rotational oscillations of the order of milliradians. The effect of such dynamics may be countered by impulses of the order of metres per second. Even if this ribbon motion were not accounted for in the launch, its effect on the orbit of the launched satellite would be small: the semi-major axis would change by only tens of kilometres, and the eccentricity by the order of 10^{-3}.

In general, all aspects of the dynamics of the space elevator are fairly well-behaved. The system is stable, and no reasonable climber transit or aerodynamic effects will push it undesirably far from equilibrium. No results from this study indicate that space elevator operation will be infeasible.

7.2 Suggestions for Future Work

The analysis in this thesis was limited to the equatorial plane of the Earth. A more complete dynamic analysis could be done by studying the general three-dimensional motion of the space elevator. This would allow certain other aspects of the space elevator's dynamics to be studied. In particular, the way in which the system behaves when the base moves away from the equator could be studied. Off-equator space elevator operation will be very important because the equatorial plane of the Earth is overcrowded with man-made space debris. Out of plane motion of the base will be required to remove the ribbon from the orbital path of any large objects.

A future model of the space elevator should allow for more complex structural deformation. For instance, the twisting of the ribbon could be studied. Also, the visco-elasticity of the ribbon could be included in the dynamic model. Certain basic aspects of control concerning the climber were presented in this thesis, but more complex active control systems for the climber should be analyzed. Control systems for the base as a means of ribbon control should be studied for reasons given above. Also, a more in-depth analysis of the effects of aerodynamics should be performed numerically.

This thesis examined the operational phase of the space elevator. The dynamics governing the *deployment* of the space elevator are more complex. A complete dynamic analysis of this phase should be proposed and optimized.

This thesis discussed the placement of satellites using the space elevator as a platform. The same should be done for interplanetary missions. The almost free escape from the Earth would change the approach to such missions significantly. They could occur much more frequently, and at a much lower cost.

Further study of space elevator dynamics may seem premature, as a material meeting the requirements of the ribbon has yet to be synthesized. However, material technology will be propelled forward because of demand coming from a wide range of terrestrial applications. A carbon nanotube lattice reaching its theoretical strength would be very useful in many industries, from sports to aeronautics. So, as thousands strive to improve the strength of such materials, a handful may continue to study the dynamics of the space elevator.

An operational space elevator will completely alter space travel. It will, quite literally, bridge the gap between man and space.

References

Artsutanov, Y., (1960) "To Space by a Locomotive," *Komsomolskaya Pravda* (Translated from Russian).

Clarke, A. C., (1979) "The Space Elevator – Thought Experiment or Key to the Universe?" Advances in Earth Oriented Applied Science and Technology, Vol. 1, pp. 39.

Clarke, A. C., (1978) *The Fountains of Paradise*, Harcourt Brace Jovanovich, New York, NY.

Edwards, B. C., (2000) "Design and Deployment of a Space Elevator," *Acta Astronautica*. Vol. 47, No. 10, pp. 735-744.

Edwards, B. C. and Westling, E. A., (2003) *The Space Elevator: A Revolutionary Earth-to-Space Transportation System*, BC Edwards.

Hanwant, B. S., (1995) *Composition, Chemistry, and Climate of the Atmosphere*, Van Nostrand Reinhold.

Hoerner, S. F., (1958) *Fluid Dynamic Drag*, Midland Park, NJ.

Iijima S., (1991) "Helical microtubules of graphitic carbon," *Nature*, Vol. 354, pp. 56-58.

Kaplan, M. H., (1976) *Modern Spacecraft Dynamics & Control*, John Wiley & Sons, Inc, U.S.A.

Lang, D., (2005a) "Space Elevator Dynamic Response to In-Transit Climbers," Seattle, WA, http://home.comcast.net/~GTOSS/GTOSS_and_Space_Elev.html.

Lang, D., (2005b) "Approximating Aerodynamic Response of the Space Elevator to Lower Atmospheric Wind," Seattle, WA, http://home.comcast.net/~GTOSS/GTOSS_and_Space_Elev.html.

Misra, A. K., and Modi, V. J., (1986) "A Survey on the Dynamics and Control of Tethered Satellite Systems," *Advances in the Astronautical Sciences*, Vol. 62, pp. 667-719.

McInnes, C. R., (2005) "Dynamics of a Particle Moving Along an Orbital Tower," *Journal of Guidance, Control and Dynamics*, Vol. 28, No. 2, pp. 380-382.

Meirovitch, L., (1997) *Principles and Techniques of Vibrations*, Prentice-Hall, Inc., Upper Saddle River, NJ.

Min, B. No, Misra, A. K., and Modi, V. J., (1999) "Nonlinear Free Vibration of a Spinning Tether," *The Journal of the Astronautical Sciences*, Vol. 47, Nos. 1 and 2, pp. 1-23.

Patamia, S. E. and Campbell, G. G., (2005a) "Dynamic Response of Proposed Space Elevator to Solar Radiation Pressure," *Proceedings of Space Exploration*, Albuquerque, NM.

Patamia, S. E. and Jorgensen, A. M., (2005b) "Analytical Model of Large Scale Transverse Dynamics of Proposed Space Elevator," *56 th International Astronautical Congress of the International Astronautics Federation*, Fukuoka, Japan, Paper No. IAC-05-D4.2.06.

Pearson, J., (1975) "The Orbital Tower: a Spacecraft Launcher Using the Earth's Rotational Energy," *Acta Astronautica*. Vol. 2, pp. 785-799.

Regan, F. J. and Anandakrishnan, S. M., (1993) *Dynamics of Atmospheric Re-Entry*, AIAA Education Series, Washington, DC.

Tsiolkovsky, K.E., (1895) "Speculations Between Earth and Sky," Moscow, Isd-vo AN-SSSR, pp. 35 (In Russian, reprinted in 1959).

Yakobson, B. I. and Smalley, R. E., (1997) "Fullerene nanotubes: C1000,000 and beyond," *American Scientist*, Vol. 85, pp. 324.